ANNUAL TECHNICAL REPORT FOR ROVER PROJECT GR210/11

EL 27292 ROVER NORTH AND EL 27372 ROVER

FOR THE PERIOD 27 MAY 2017 TO 26 MAY 2018

Date:	13 July 2018	
Internal Report No.	AR2018_11	
Compiled by:	Conan Mills	
Title Holder:	Adelaide Exploration Pty Ltd	
	P.O. Box 1210 Unley BC 5061 SA	
Operator:	Andromeda Metals Ltd	
	(same address as above)	
Project Name:	Rover Project	
Target Commodity:	Copper-Gold	
Exploration Permits:	EL 27292 Rover North	
	EL 27372 Rover	
1:250,000 sheets:	SE 53-14 Tennant Creek	
	SE 53-13 Green Swamp Well	
1:100,000 sheets:	5658 Kelly	
	5558 Billiatt	
Distribution:	DPIR	1 Digital
	Andromeda Metals Ltd	1 Digital

Table of Contents

List of Figures

List of Tables

1. Summary

Work on the Rover Project during the current period included an Induced Polarisation (IP) and Magnetotelluric (MT) survey (July 2017) over three prospects in the Rover field, as part of Joint Venture with Emmerson Resources Ltd (Emmerson) using that company's M.I.M Distributed Acquisition System (MIMDAS). Emmerson withdrew from the Joint Venture in September 2017. A trial Ground Electro-Magnetic (EM) survey was completed in May 2018, during the due diligence period of a Heads of Agreement signed with Minotaur Exploration Ltd (Minotaur). Minotaur withdrew from the Heads of Agreement in June 2018.

During the IP and MT survey, nine lines, each 1.1km long for a total of 9.9km, were surveyed over three prospects: Rover 4 (R4), Rover 11 Central (R11C) and Rover 11 East (R11E). The objective of the survey was to determine the efficacy of IP and MT to image ironstone bodies with drilling control, in order to judge the effectiveness of applying the technique to the wider field.

The technique was effective for identifying the cover sequence over the prospects, and defining broad alteration haloes associated with ironstones. Unfortunately, the technique did not generate targets that were directly attributable to mineralisation (as defined by drilling) that could be separated from the alteration haloes, precluding its use as a direct targeting method to sufficiently de-risk follow up drilling.

The May 2018 Ground EM survey was conducted over two prospects; Rover 1 and Rover 4, to determine whether the known mineralization could be resolved using the most advanced ground EM surveys. There was no response over the Western Lode at Rover 1 or from any of the Rover 4 lodes and this was thought to be due to the small size of the lodes, the depth of the mineralization, particularly at Rover 1 and the poor conductance of the targets.

2. Introduction

This report details exploration undertaken on the Rover Project (EL 27292 and EL 27372) between 27 May 2017 and 26 May 2018. During this time, Andromeda Metals Ltd (“Andromeda Metals”; parent company of titleholder Adelaide Exploration Pty Ltd) and Emmerson Resources Ltd (“Emmerson”) entered into a Heads of Agreement (HOA; 11 November 2016) over the Rover Project. Emmerson withdrew from the Heads of Agreement on 28 September 2017, having completed an Induced Polarisation (IP) and Magnetelluric (MT) survey over Rover 4, Rover 11 Central and Rover 11 East prospects.

A Heads of Agreement was subsequently signed with Minotaur Exploration Ltd (“Minotaur”) and a site visit and ground electro-magnetic (EM) survey was completed over Rover 1 and Rover 4 prospects. Minotaur withdrew from the Heads of Agreement on 5 June 2018 after the Ground EM was judged ineffective in resolving the mineralisation at the Rover Project.

3. Location

The two Exploration Lease that comprise the Rover Project are located approximately 75km southwest of the Tennant Creek Township (see Figure 1). The licences fall on the Kelly (5658) and Billiat (5558) 1:100,000 scale map sheets.

The principal access to the Rover Field is south from Tennant Creek along the Stuart Highway for approximately 5km before turning west and utilising dirt, 4x4 and fence line tracks for approximately 85km. However, much of the area is without tracks and difficult to reach, even in a 4x4 vehicle. The unsealed tracks become impassable during the wet season.

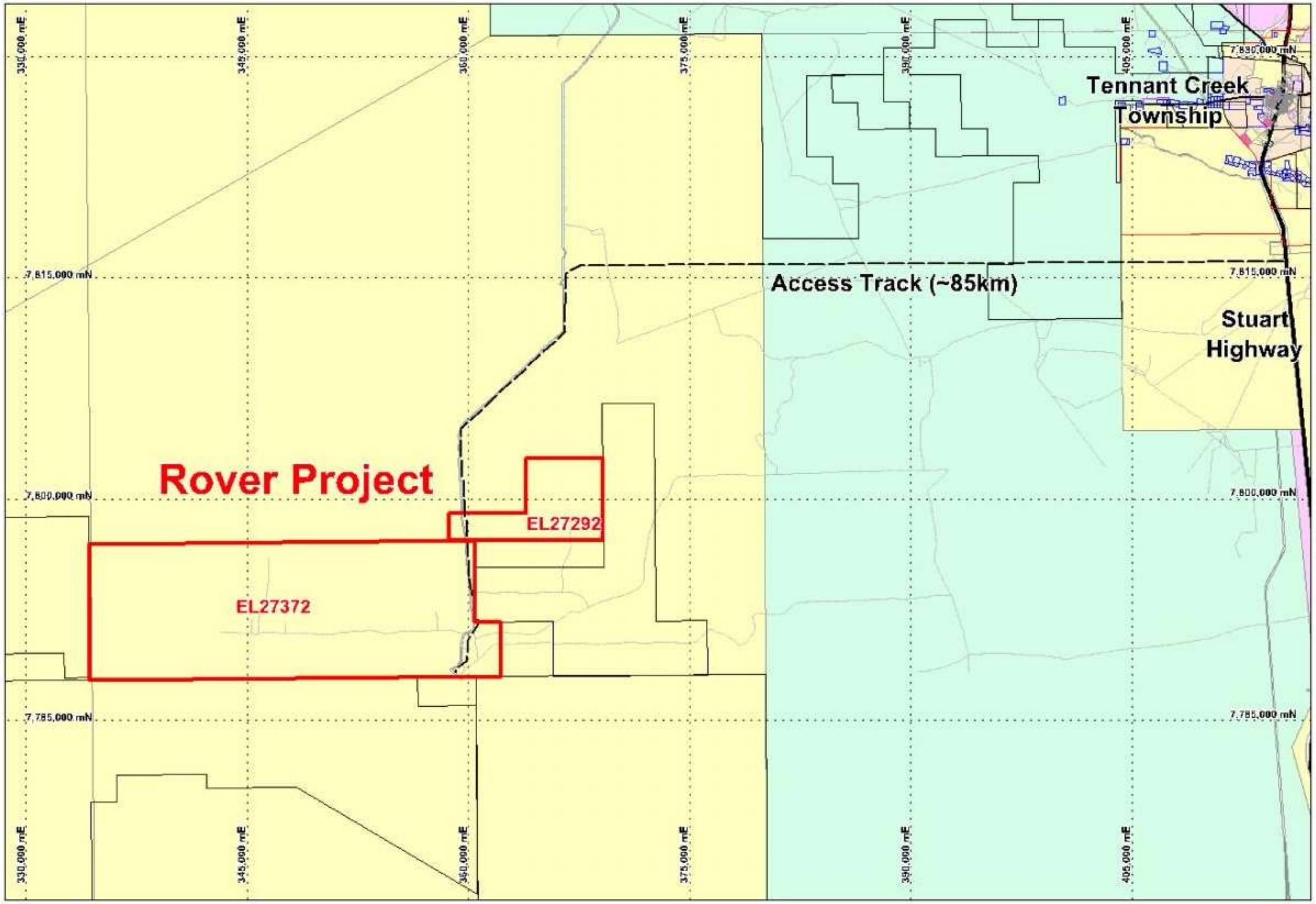

Figure 1. Location of the Rover Project with respect to Tennant Creek Township.

4. Tenure

Rover Project tenure details are shown below in Table 1. Renewal applications for both Exploration Licences were submitted to the Department on 18 May 2018.

Table 1. Rover Project Tenement Details.

Tenement Number	Tenement Name	Titleholder	Interest (%)	Grant Date	Current Expiry Date	Area km²
EL 27292	Rover North	Adelaide Exploration Pty Ltd	100	27/05/2010	26/05/2018	39
EL 27372	Rover	Adelaide Exploration Pty Ltd	100	27/05/2010	26/05/2018	248

5. Geology and Climate[1]

5.1. Regional Geology

The reader is referred to AusIMM Monograph 14 (Geology of the Mineral Deposits of Australia and Papua New Guinea), Volume 1, pp. 829-861, to gain a good introduction to the regional geology and styles of gold-copper mineralisation of the area.

In 1995 the Northern Territory Geological Survey released a geological map and explanatory notes for the Tennant Creek 1:100,000 sheet, which cover the area of the Licences.

The geological terrain of the Tennant Creek region consists of a deformed and complex Lower Proterozoic metasedimentary basement intruded by several generations of Proterozoic granite. This basement terrain is overlain by relatively undeformed and generally flat lying younger sediments of the Middle Cambrian to Devonian Wiso Basin to the west and Late Proterozoic to Devonian Georgina Basin to the east. These basins have subsequently been blanketed by extensive shallow colluvial, alluvial and aeolian cover sediments belonging to the current Holocene landscape regime.

The rocks of the Warramunga Formation host most of the orebodies in the region and are interpreted to underlie the Exploration Licences.

5.2. Geology of the Rover Project

The Proterozoic basement of the Rover Field is concealed by shallow Wiso Basin cover, and basement geology has been interpreted from available drilling and airborne magnetic surveys.

Basement geology in the Rover area is interpreted as being a close analogy of the Tennant Creek Field with Warramunga Formation hosting the ironstone bodies of the Rover Field occupying a well-defined inlier within younger Proterozoic rocks assigned to the Ooradidgee Group (or Flynn

[1] Section 5 is from the 2017 Annual Technical Report for the Rover Project, by A Walters, Emmerson Resources Ltd.

Subgroup) and overlying Hatches Creek Group. The interpreted Warramunga Formation in the Rover Field is therefore contained within a basement inlier of very similar character to that at Tennant Creek, and is of a similar scale and orientation to the so-called 'Central Field' at Tennant Creek.

Lithologies interpreted to be Warramunga Group intersected in drill core at Rover are indistinguishable from Warramunga formation sediments at Tennant Creek. These include sequences of deformed and greenschist facies metamorphosed greywacke, shales, mudstones and minor tuff beds. "Hematite shales" are also recorded in many of the Rover drill holes.

Several historic holes at Rover have failed to intersect Warramunga sediments, instead encountering felsic and mafic volcanic sequences. These may represent possible correlates to the Flynn Subgroup/Ooradidgee Group.

The flat lying Cambrian sediments of the Wiso Basin cover comprise siltstones and carbonates (predominantly dolomite), while a thin basal conglomerate is observed in many drill holes completed in the Rover Field.

Thin Quaternary cover at Rover is dominated by sand considered to be largely aeolian in origin. Weathering is lateritic in nature with a prominent ferruginous layer comprised of iron pisoliths present just a few meters below surface. This ferruginous layer is the likely source to short wavelength low amplitude (~2 nT) "noise" observed in ground magnetic data collected in the field. Weathering persists to approximately 100m below surface.

Ground water is present in the Wiso Basin sediments and significant flows can be obtained from relatively shallow depths (<30m). Narrow porous and permeable zones within carbonate below the base of weathering also contain ground water. Water quality in the Rover Field is verging on potable.

5.3. Climate

The Tennant Creek district lies within the tropics however its distance from the ocean limits the amount of moisture available. The climate is hot in summer and relatively mild in winter. Yearly average rainfall at Tennant Creek is about 459mm falling predominantly in the summer months (December to February). Prevailing winds at the surface are from the southeast. Mean daily temperature maxima range from about 24 C in July to over 37 C in December.

6. Previous Work

NOTE: For previous exploration over the Rover Project the reader is referred to;

Combined Annual Technical Report No. GR210/11, EL 27372 Rover & EL 27292 Rover North, Tennant Creek, Northern Territory, For the period 27th May 2015 to 26th May (2016 2016_07_18 Rover 2016 ATR EL 27372 EL 27292 AR2016_16) and;

Final Report for the Rover Project Joint Venture EL's 27292 & 27372 GR210/11 11 November 2016-28 September 2017

7. Work by JV Partner Emmerson Resources Ltd

Emmerson and Andromeda Metals entered into a Heads of Agreement (HOA) over the Rover Project which incorporates EL 27372 and EL 27292 on the 11 November 2016. Emmerson was the nominated Operator of the Rover project from 20 April 2017 until its withdrawal from the Heads of Agreement in September 2017. Andromeda Metals was subsequently appointed nominated Operator of the project (2 October 2017).

In July 2017 Geophysical Resources and Services Pty Ltd (GRS) were commissioned by Emmerson to run a survey of 3D M.I.M. Distributed Acquisition System (MIMDAS) Induced Polarisation (IP) and Magnetotellurics (MT) covering three blocks over separate prospects R4, R11C and R11E.

Technical work undertaken by Emmerson during their period as Operator of the Rover Project includes is detailed in Appendix I. Final Report for the Rover Project Joint Venture 11 November 2016 – 28 September 2017. Note, work completed by Emmerson which fell into the previous reporting period consisted of a compilation of historic data.

A complete report compiled by GRS; "3D MIMDAS Survey Rover Prospect, Australia; Acquisition and Modelling Report" is included as Appendix II.

8. Work Undertaken During Due Diligence Period with JV Partner Minotaur Exploration Ltd

Minotaur and Andromeda Metals entered into a Heads of Agreement over the Rover Project (again including EL 27372 and EL 27292) on 16 April 2018. Minotaur withdrew from the Agreement within the sixty day due diligence period on 5 June 2018.

A site visit by Minotaur and Andromeda Metals staff was conducted in April 2018 and included a review of drill core from Rover 1, Rover 4 and Rover 12 prospects. A trial Ground EM survey followed over Rover 1 and Rover 4 mineralised bodies in April and May.

In total, 3.7 line km of moving loop ground EM were surveyed along north-south lines using an in-loop and slingram configuration.

> "Surface moving loop EM was conducted over the Rover 1 and Rover 4 mineralised bodies to determine whether these bodies could be detected using ground EM techniques. The survey was conducted in both in-loop and slingram configuration. A total of 3.7 line km of data was collected along 4 north-south lines.
>
> No response was observed in the moving loop data over the Western Lode at Rover 1 and only a weak response in the X Component data at the southern end of the line approaching the Jupiter Load at Rover 1. It should be noted that access over the main Jupiter load at Rover 1 was restricted due to the location of the mineralisation to the south of the tenement boundary.
>
> At Rover 4, no responses were observed over the known mineralised bodies. A weak response was observed in the in-loop X Component data on the northern margin of line

> 360700E. Modelling of this response gives a low conductance body which correlates with a subtle east-west magnetic and gravity feature to the north of the survey line.”

A full report, prepared by Minotaur Chief Geophysicist Andrew Thompson on the Ground EM survey completed during the due diligence period is included as Appendix III. Geophysical Report GPY2018/01 Rover Ground EM Interpretation Report.

9. Expenditure

Allowable expenditure for the reporting period (Year 8) for EL 27292 totalled $41,398. The covenant for the period was $28,000. The Mineral Title Expenditure Report for EL 27292 was submitted to DPIR on 25 June 2018 and is included as Appendix IV.

Allowable expenditure for the reporting period (Year 8) for EL 27372 totalled $282,403. The covenant for the period was $108,000. The Mineral Title Expenditure Report for EL 27372 was submitted to DPIR on 25 June 2018 and is included as Appendix V.

10. Data Submission

Geophysical Data (from the IP, MT and Ground EM surveys) accompanying this report is sent via USB thumb drive, posted to the Department 13/07/2018 in the format supplied to the Operator by its JV partners.

11. References

Adelaide Exploration Pty Ltd, 2016 Exploration Licences EL 27372, EL 27292
Combined Annual Technical Report GR210/11 EL 27372 Rover & EL 27292 Rover North Tennant Creek Northern Territory for the period 27 May 2016 to 26 May 2017
(2016_07_18 Rover 2016 ATR GR210_11 EL 27372 EL 27292 AR2016_16)

Emmerson Resources Ltd, 2017, Exploration Licences EL 27372, EL 27292
Final Report for the Rover Project Joint Venture EL’s 27292 & 27372 GR210/11 11 November 2016-28 September 2017

Monograph 14 - Geology of the Mineral Deposits of Australia and Papua New Guinea, Volume 1.
(1990) Edited by F.E. Hughes

12. Copyright Statement.

13. Appendix I. Final Report for the Rover Project Joint Venture EL’s 27292 & 27372 GR210/11

3 Kimberley Street, West Leederville, WA 6007
PO BOX 1573 West Perth WA 6872
Telephone 08 9381 7838 Facsimile 08 9381 5375
Email: info@emmersonresources.com.au
Website: www.emmersonresources.com.au
ABN 53 117 086 745

FINAL REPORT FOR THE ROVER PROJECT JOINT VENTURE
EL'S 27292 & 27372
GR210/11

11 November 2016 – 28 September 2017

LICENSEE:
Adelaide Exploration Pty Ltd
A.B.N. 29 097 387 918

OPERATOR:
GIANTS REEF EXPLORATION PTY LTD
A.B.C.009 200 346
(A wholly owned subsidiary of Emmerson Resources Ltd)

AUTHOR:
ADAM WALTERS

OCTOBER 2017

DISTRIBUTION:
Andromeda Resources
Emmerson Resources Ltd
Central Land Council

MAP SHEETS:

☐	TENNANT CREEK	SE53-14
☐	GREEN SWAMP WELL	SE53-13
☐		1:250 000
☐	KELLY	5658
☐	BILLIATT	5558
		1:100 000

Table of Contents

FIGURES

1.0 SUMMARY

Emmerson Resources Ltd (Emmerson) and Andromeda Resources (Andromeda; formerly Adelaide Resources Ltd) entered into a Heads of Agreement (HOA) over the Rover Project which incorporates EL's 27372 and 27292 in the Rover Field south west of the Tennant Creek Mineral Field and the township of Tennant Creek on the 11 November 2016. Emmerson withdrew from the Heads of Agreement on 28th September 2017.

The titles were acquired by Adelaide and subsequent interest by Emmerson was to search for Tennant Creek style iron oxide copper-gold deposits (IOCG).

This final report records the exploration work completed on these titles during the HOA period from 11 November 2016 to the 28 September 2017.

Exploration activity during the HOA period included desktop evaluations and interpretations aimed at assessing the structure and geology for the Rover Field and the execution of a 3D MIMDAS survey over Rover 4 (R4), Rover 11 Central (R11C) and Rover 11 East (R11E).

Emmerson Resources Ltd (Emmerson) consultant Grant Osborne (Rocky) was engaged to compile historical geoscientific data over the rover field and use this data to assess the structure and geology, the results of his work are summarised below;

> *Summary*
>
> *Relatively juvenile exploration history*
>
> *Rapid resource drilling employed by AND and MLX at the Rover 1 and 4 targets (± Exp108, Exp142) has resulted in exploration bias toward a select few targets*
>
> *Of the 18 Rover targets defined by GeoPeko, 9 reflect TCMF-style ironstone mineralization hosted in Warramunga Formation and 9 reflect disseminated magnetite in Ooradidgee Group volcaniclastics. The former appear to be controlled by a thrust fault*
>
> *Within the ADN tenements there are a total of 24 magnetic targets only 12 of which have been drill tested, and of these only 6 have >=4 diamond drill holes, the rest being one-hole tests*
>
> *There is no camp scale geological interpretation.*

In July 2017 Geophysical Resources and Services Pty Ltd (GRS) were commissioned by Emmerson to run a survey of 3D M.I.M. Distributed Acquisition System (MIMDAS) Induced Polarisation (IP) and Magnetotellurics (MT) covering three blocks over separate prospects R4, R11C and R11E.

The three blocks all had the same geometry consisting of three, 100m spaced 1100m lines with transmitters extending out of the single middle transmit line by 950m. Receiver spacing was 100m on the outside and 50m on the center line while transmit locations were 50m inside and 100m outside the grid.

The MIMDAS trial was completed over selected target areas to assess the potential of the technique to define targets below significant basin and Ooradidgee cover sequences. The survey at Rover 4 was considered the test case as it represented the area with the shallowest cover (approx.200m) and the best drilling control.

The results for the R4 area were disappointing with the main chargeability response occurring immediately above the copper and gold mineralisation. It appears the chargeability response is associated with the clay alteration above the deposit.

The resistivity data in both the MIMDAS and the MT survey has successfully mapped the base of the Ooradidgee sediments but there is no indication of the sulphide mineralization in the inverted resistivity sections.

This result was repeated to some degree at Rover 11E where the broad chargeability response appears to map alteration rather than ironstone hosted sulphide mineralisation.

It is concluded that the technique will not generate targets with a high enough probability of success to warrant additional work.

2.0 INTRODUCTION

Emmerson Resources Ltd (Emmerson) and Andromeda Resources (Andromeda; formerly Adelaide Resources Ltd) entered into a Heads of Agreement (HOA) over the Rover Project which incorporates EL's 27372 and 27292 in the Rover Field south west of the Tennant Creek Mineral Field and the township of Tennant Creek on the 11 November 2016. Emmerson withdrew from the Heads of Agreement on 28th September 2017.

The titles were acquired by Adelaide and subsequent interest by Emmerson was to search for Tennant Creek style iron oxide copper-gold deposits (IOCG).

This final report records the exploration work completed on these titles during the HOA period from 11 November 2016 to the 28 September 2017.

Figure 1 shows the location of the Rover Project title with respect to the Tennant Creek Township.

3.0 LOCATION

The Rover titles are located approximately 75km southwest of the Tennant Creek Township. The Licence falls on the Kelly (5658) Billiat (5558) 1:100,000 scale map sheets.

The principal access to the Rover Field is south from Tennant Creek along the Stuart Highway for approximately 35km before turning west and utilising dirt, 4X4 and fence line tracks for approximately 60km. However, much of the area is rocky, without tracks and difficult to reach, even in a 4x4 vehicle. The unsealed tracks become impassable during the wet season.

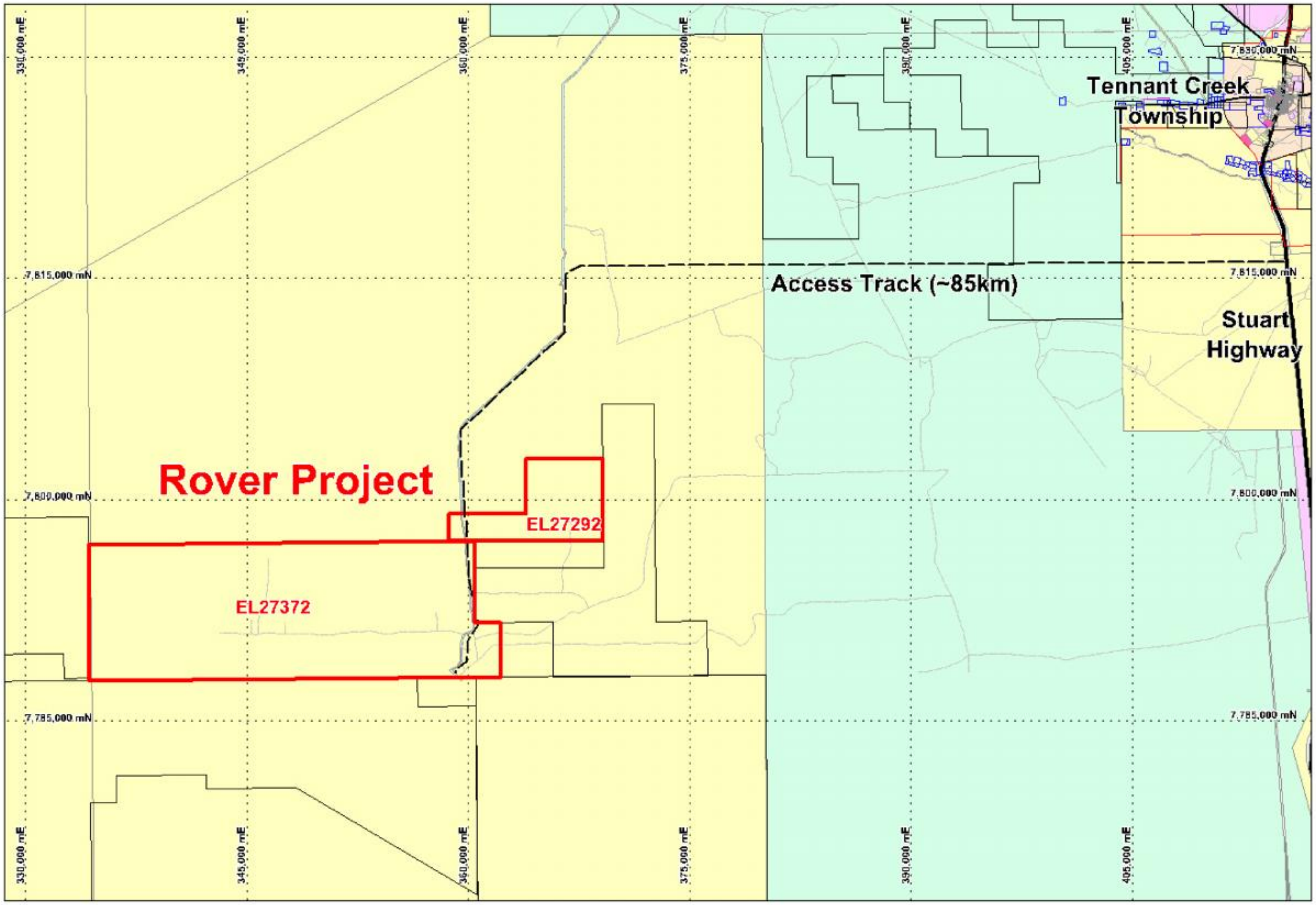

Figure 1: Location of the Rover Project with respect to the Tennant Creek Township

4.0 TENURE

The tenure details of the Rover Project are detailed in the following table;

Tenement ID	Tenement Name	Holder	Interest	Grant Date	Effective Date	Expiry Date	Area (Ha)
EL27292	Rover	ADN	100	27/05/2010	27/05/2016	27/05/2018	3,876
EL27372	Rover	ADN	100	27/05/2010	27/05/2016	26/05/2018	24,859

Table 1: Rover Project Tenure Details

The Rover Project is located on –

- NT Parcel 03556, Aboriginal Freehold Land, held by the Karlantijpa South Aboriginal Land Trust

5.0 GEOLOGY & CLIMATE

5.1 Regional Geology

The reader is referred to AusIMM Monograph 14 (Geology of the Mineral Deposits of Australia and Papua New Guinea), Volume 1, pp. 829-861, to gain a good introduction to the regional geology and styles of gold-copper mineralisation of the area.

In 1995 the Northern Territory Geological Survey released a geological map and explanatory notes for the Tennant Creek 1:100,000 sheet, which cover the area of the Licences.

The geological terrain of the Tennant Creek region consists of a deformed and complex Lower Proterozoic metasedimentary basement intruded by several generations of Proterozoic granite. This basement terrain is overlain by relatively undeformed and generally flat lying younger sediments of the Middle Cambrian to Devonian Wiso Basin to the west and Late Proterozoic to Devonian Georgina Basin to the east. These basins have subsequently been blanketed by extensive shallow colluvial, alluvial and aeolian cover sediments belonging to the current Holocene landscape regime.

The rocks of the Warramunga Formation host most of the orebodies in the region and are interpreted to underlie the Exploration Licences.

5.2 Geology of the Rover Project

The Proterozoic basement of the Rover Field is concealed by shallow Wiso Basin cover, and basement geology has been interpreted from available drilling and airborne magnetic surveys.

Basement geology in the Rover area is interpreted as being a close analogy of the Tennant Creek Field with Warramunga Formation hosting the ironstone bodies of the Rover Field occupying a well-defined inlier within younger Proterozoic rocks assigned to the Ooradidgee Group (or Flynn Subgroup) and overlying Hatches Creek Group. The interpreted Warramunga Formation in the Rover Field is therefore contained within a basement inlier of very similar character to that at Tennant Creek, and is of a similar scale and orientation to the so-called 'Central Field' at Tennant Creek.

Lithologies interpreted to be Warramunga Group intersected in drill core at Rover are indistinguishable from Warramunga formation sediments at Tennant Creek. These include sequences of deformed and greenschist facies metamorphosed greywacke, shales, mudstones and minor tuff beds. "Hematite shales" are also recorded in many of the Rover drill holes.

Several historic holes at Rover have failed to intersect Warramunga sediments, instead encountering felsic and mafic volcanic sequences. These may represent possible correlates to the Flynn Subgroup/Ooradidgee Group.

The flat lying Cambrian sediments of the Wiso Basin cover comprise siltstones and carbonates (predominantly dolomite), while a thin basal conglomerate is observed in many drill holes completed in the Rover Field.

Thin Quaternary cover at Rover is dominated by sand considered to be largely aeolian in origin.

Weathering is lateritic in nature with a prominent ferruginous layer comprised of iron pisoliths present just a few meters below surface. This ferruginous layer is the likely source to short wavelength low amplitude (~2 nT) "noise" observed in ground magnetic data collected in the field. Weathering persists to approximately 100m below surface.

Ground water is present in the Wiso Basin sediments and significant flows can be obtained from relatively shallow depths (<30m). Narrow porous and permeable zones within carbonate below the base of weathering also contain ground water. Water quality in the Rover Field is verging on potable.

5.3 Climate

The Tennant Creek district lies within the tropics however its distance from the ocean limits the amount of moisture available. The climate is hot in summer and relatively mild in winter. Yearly average rainfall at Tennant Creek is about 459mm falling predominantly in the summer months (December to February). Prevailing winds at the surface are from the southeast. Mean daily temperature maxima range from about 24 C in July to over 37 C in December.

6.0 WORK DONE DURING THE REPORT PERIOD

NOTE: For previous exploration over the Rover project the reader is referred to;

Combined Annual Technical Report No. GR210/11, EL 27372 Rover & EL 27292 Rover North, Tennant Creek, Northern Territory, For the period 27th May 2015 to 26th May (2016 2016_07_18 Rover 2016 ATR EL 27372 EL 27292 AR2016_16).

Exploration activity during the HOA period included desktop evaluations and interpretations aimed at assessing the structure and geology for the Rover Field and the execution of a 3D MIMDAS survey over Rover 4 (R4), Rover 11 Central (R11C) and Rover 11 East (R11E).

Initial review of historical exploration included the selection of intervals from 12 diamond drill holes, these were retrieved from the Rover Core laydown area and transported back to Tennant Creek for relogging. Holes and depths are summarised in the below table;

Prospect	HoleID	mFrom	mTo	Interval
R1	R1ARD30	330	560	230
R1N	R1NARD22	370	450	80
R2	R2ARD17	270	360	90
R4	R4ARD34	310	410	100
R4	R4ARD40	160	240	80
R11	R11ARD19	270	305	35
R11	R11ARD65	250	300	50
R12	R12ARD59-2	400	510	110
R12	R12ARD01	450	550	100
R14	R14ARD08	200	240	40
R20	R20ARD23	100	175	75
R27	R27ARD18	250	350	100

Table 2: Drillhole Intervals Details

Fire breaks were cleared around the core laydown area and infrastructure, while on site.

Emmerson Resources Ltd (Emmerson) consultant Grant Osborne (Rocky) was engaged to compile historical geoscientific data over the rover field and use this data to assess the structure and geology, the results of his work are summarised below;

Summary

Relatively juvenile exploration history

Rapid resource drilling employed by AND and MLX at the Rover 1 and 4 targets (± Exp108, Exp142) has resulted in exploration bias toward a select few targets

Of the 18 Rover targets defined by GeoPeko, 9 reflect TCMF-style ironstone mineralization hosted in Warramunga Formation and 9 reflect disseminated magnetite in Ooradidgee Group volcaniclastics. The former appear to be controlled by a thrust fault

Within the ADN tenements there are a total of 24 magnetic targets only 12 of which have been drill tested, and of these only 6 have >=4 diamond drill holes, the rest being one-hole tests

There is no camp scale geological interpretation

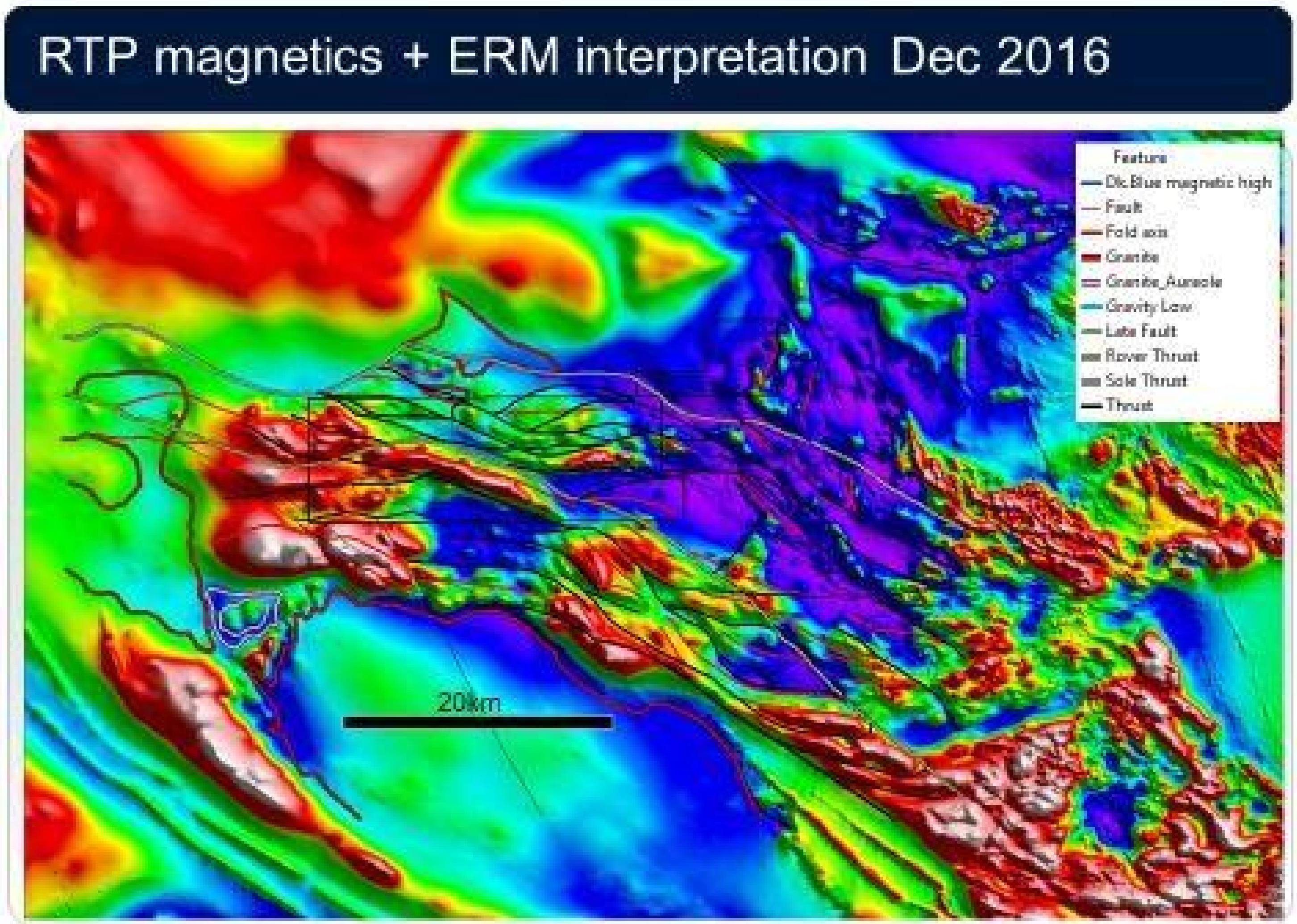

Figure 2: Rover Project vs. RTP Magnetics & ERM Interp

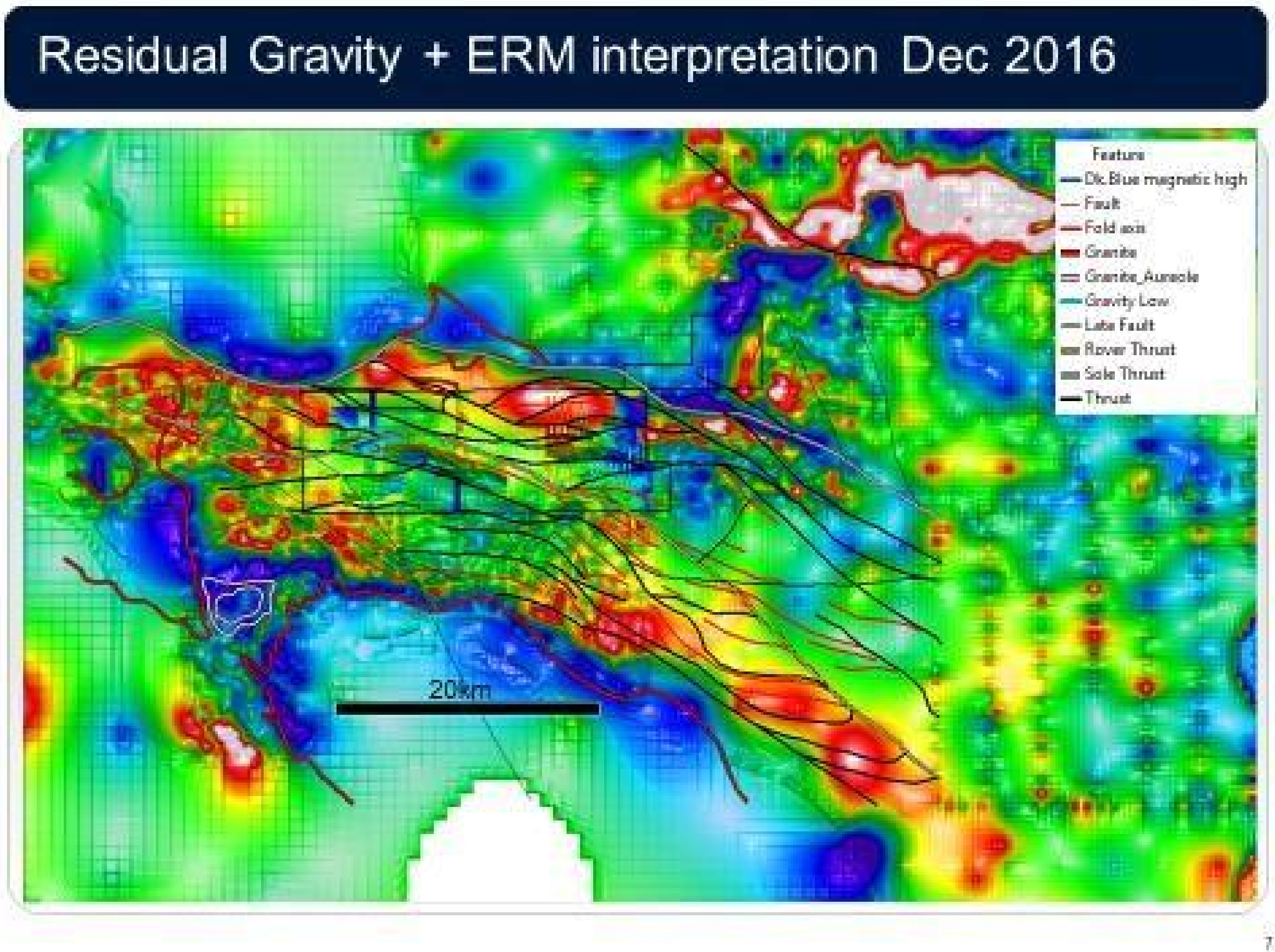

Figure 3: Rover Project vs Residual Gravity & ERM Interp.

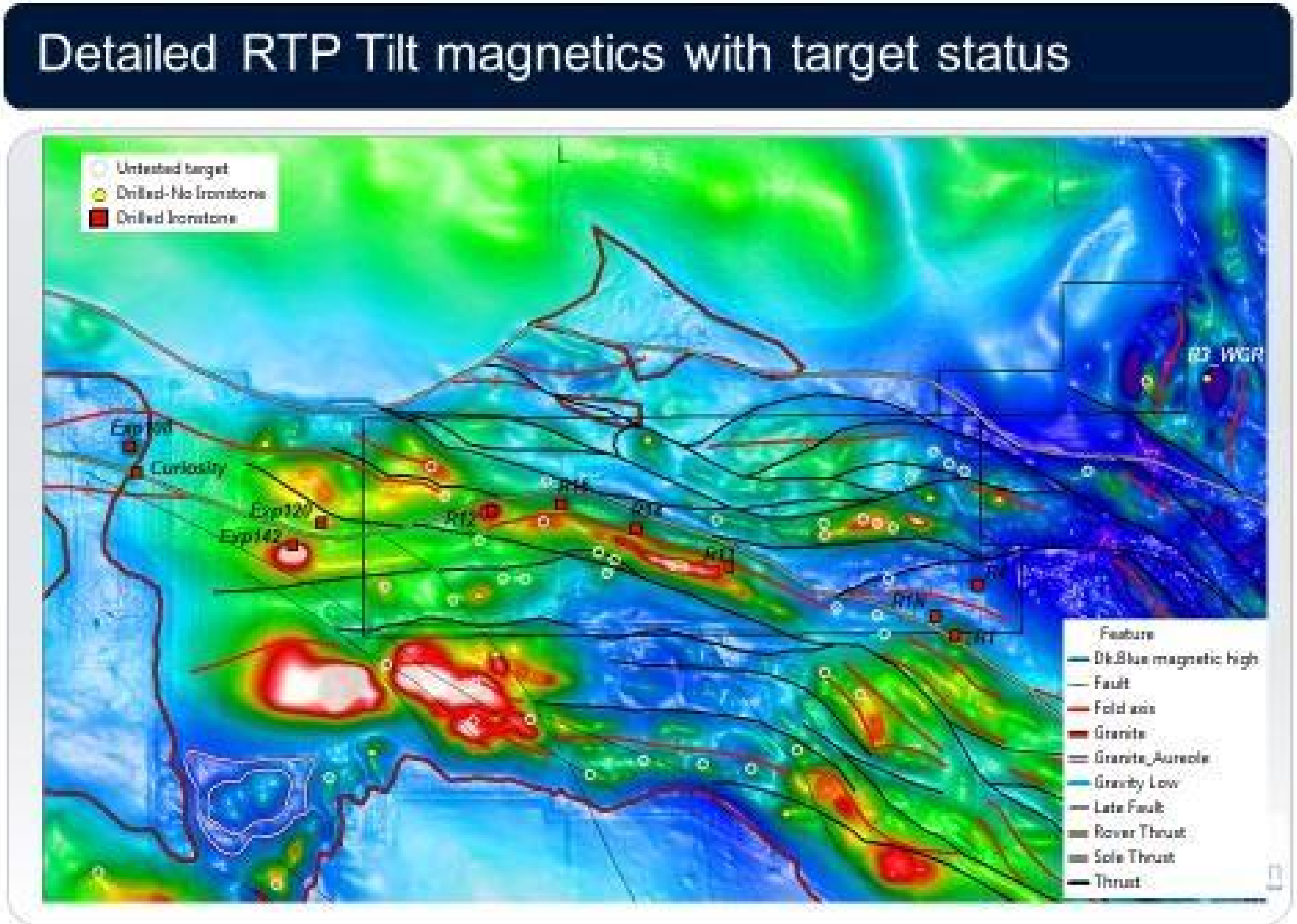

Figure 4: Rover Project vs. Detailed RTP Tilt Magnetics & Target Status

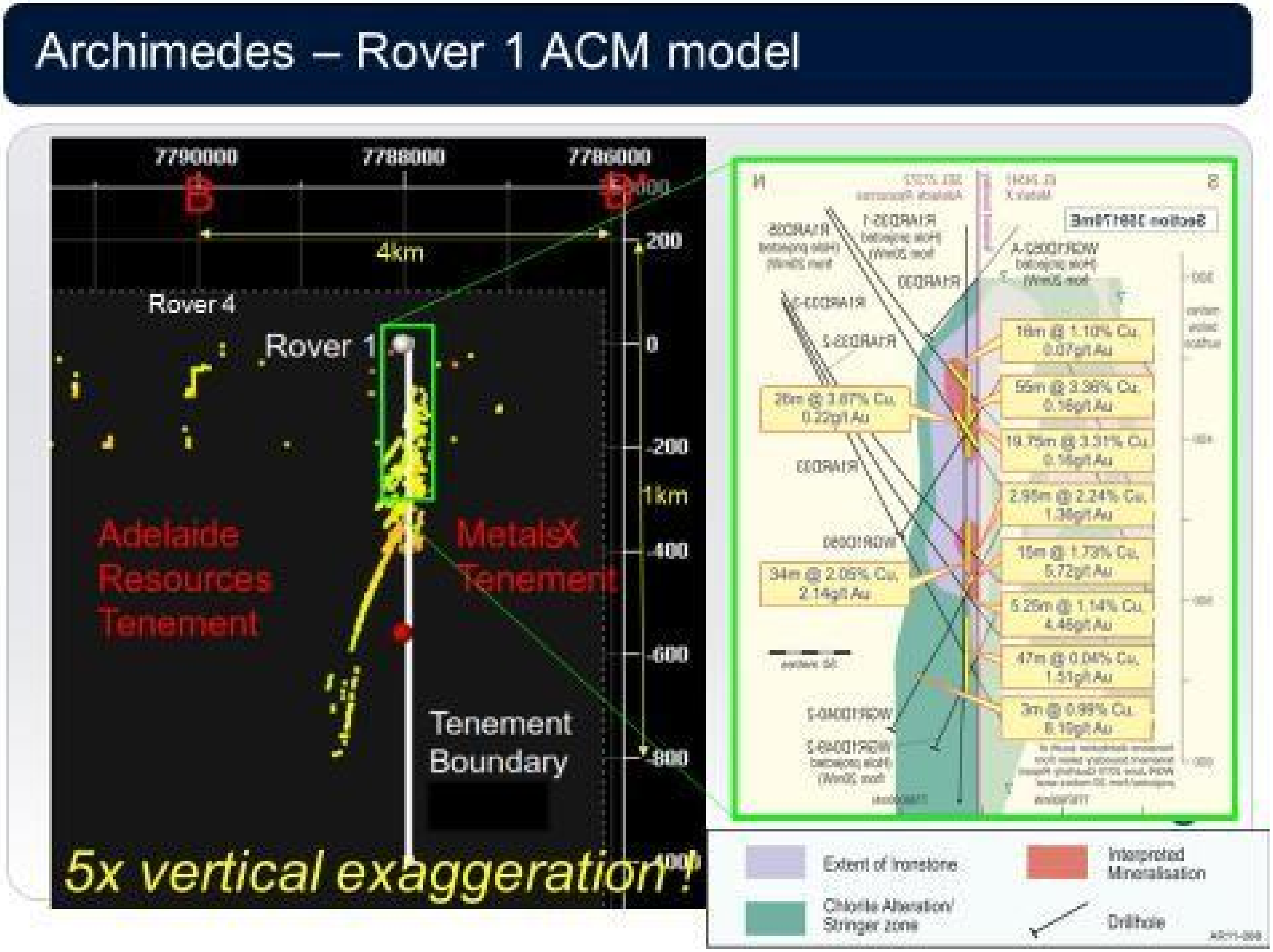

Figure 5: Rover 1 Archimedes ACM model and Rover 1 Schematic from MTX ASX Release

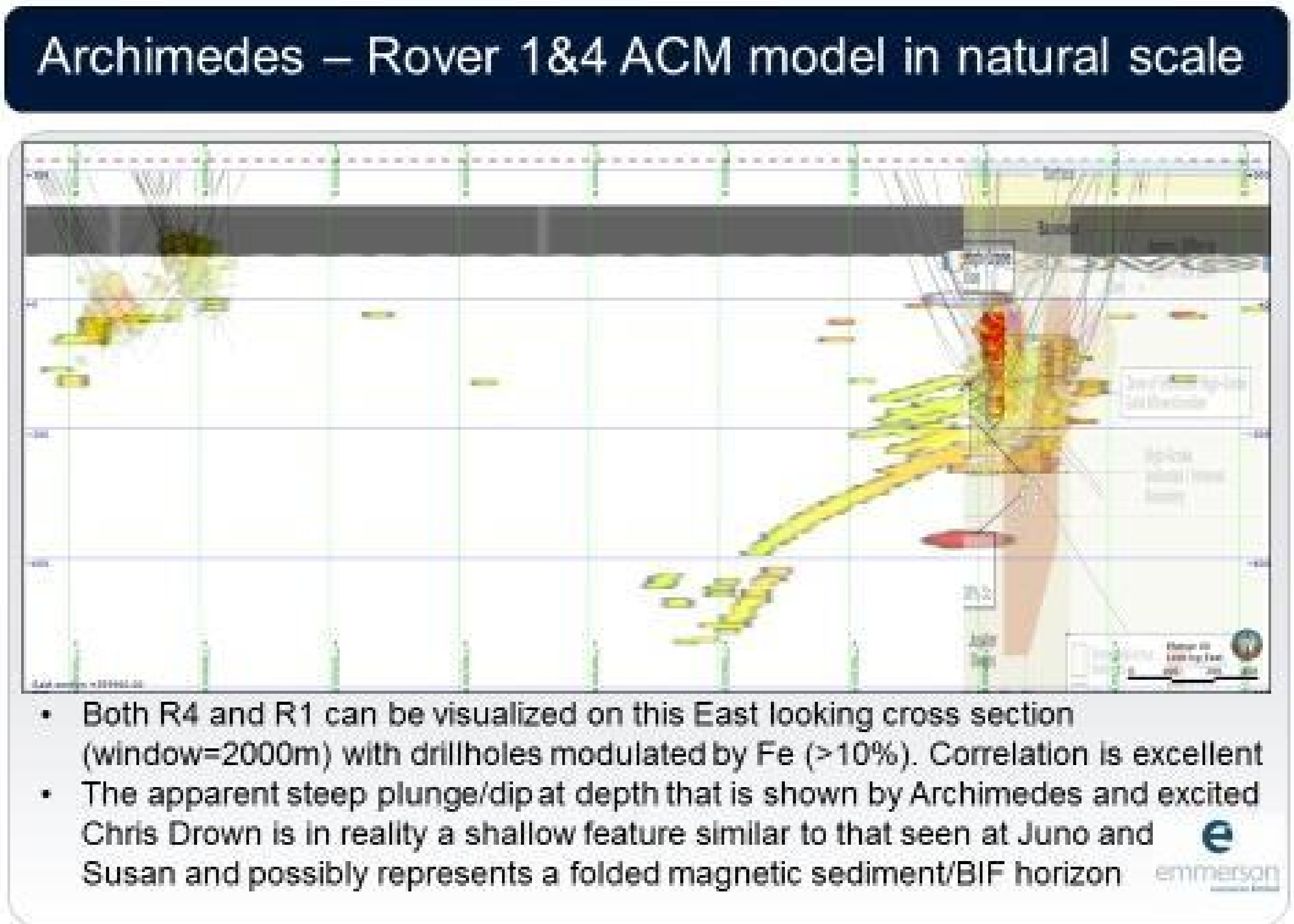

Figure 6: Rover 1 ACM model adjusted by ERM.

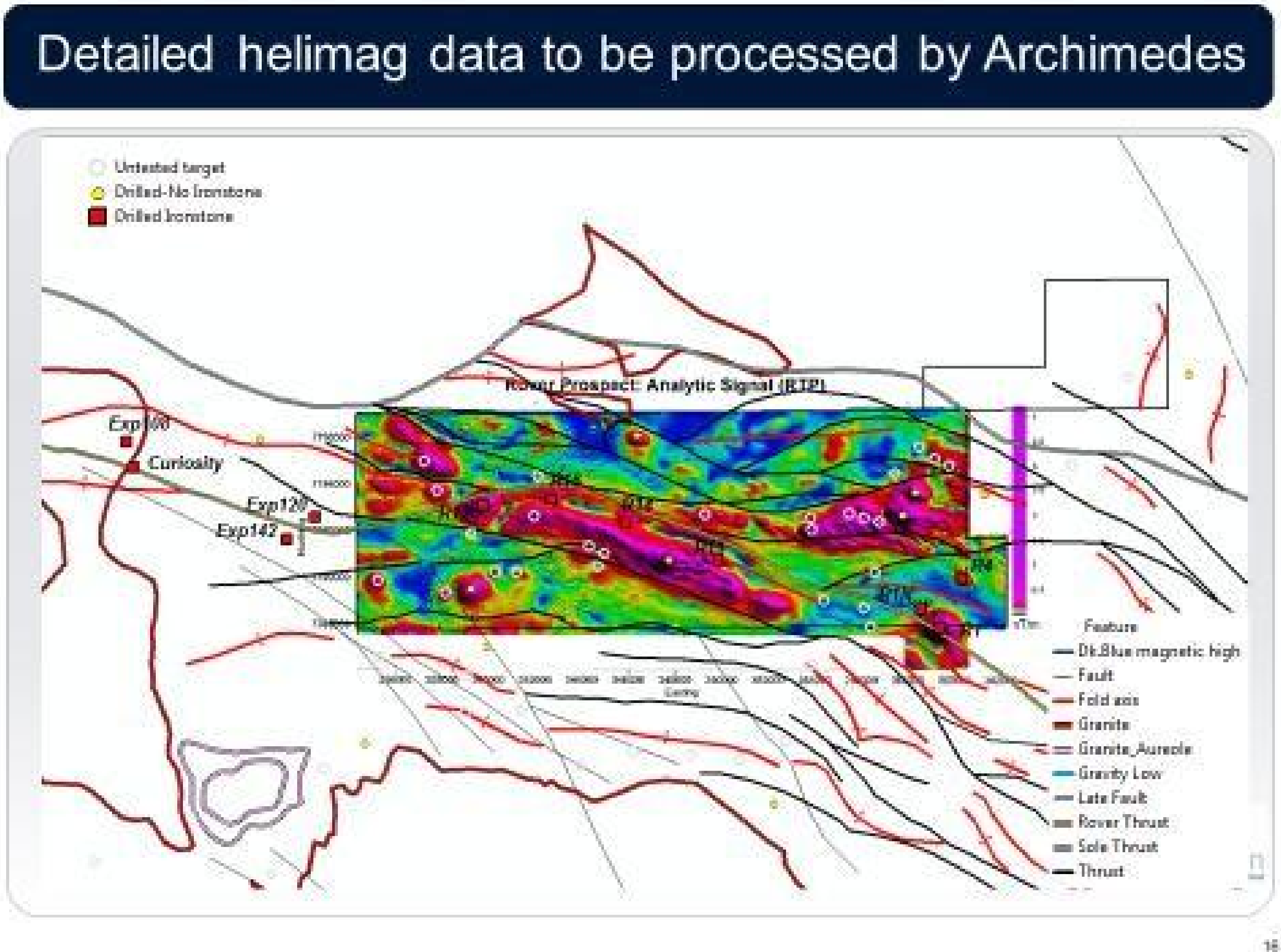

Figure 7: Rover Project vs. Helimag

The Rover IOCG Camp comprises one major ironstone–hosted Cu-Au deposit (Rover 1), five smaller ironstone–hosted occurrences of Cu-Au (Rover 4, Rover 11, Rover 12, Rover 14, Explorer 142), one barren ironstone (Rover 16) and a Ag-Pb-Zn occurrence (Explorer 108-Curiosity) all located along, or adjacent to, what is interpreted to be a ~40km long EW thrust fault.

Deposits in within Metals X Limited (now WGR) tenements with the exception of the down-plunge continuation of the western lode at Rover 1 which is held by Adelaide Resources Limited (ADN) and forms part of the Rover JV with Emmerson.

The total quoted Indicated and Inferred resources for the Rover 1 deposit (=sum of resources in both the ADN and MLX ASX releases) are of the order of 7.01Mt @ 1.71g/t Au, 1.22% Cu (with accessory Ag, Bi, Co) equivalent to ~386,500oz contained Au and 85,520t contained Cu proportioned approximately 97% : 3% between WGR and ADN (Rover JV).

In terms of combined contained Au and Cu metal the Rover 1 deposit is closely comparable to the Peko deposit (3.16Mt @ 3.5g/t Au, 4.00% Cu, 14g/t Ag, 0.2% Bi equivalent to 240, 518oz contained Au and 118,884t contained Cu) which is the third biggest Au deposit in the TCMF.

The Rover 4 ironstone is shallow (top varies from 139m-275m BGL) and its horizontal attitude suggests this orebody may be located on a flat thrust plane? Good gold grades exist under the ironstone in feeders.

Ag-Pb-Zn mineralization at Explorer 108/Curiosity is hosted within intense carbonate alteration and may be related to shearing (Burke, 2013). Indicated and Inferred Resource estimate (Explorer 108) of 11.87 million tonnes at 3.24% Zn, 2.0% Pb, 0.36% Cu and 11.1g/t Ag. It is not known whether this target has been tested at depth for Cu-Bi-Au zonation.

No data is available for the Exp142 deposit.

In July 2017 Geophysical Resources and Services Pty Ltd (GRS) were commissioned by Emmerson to run a survey of 3D M.I.M. Distributed Acquisition System (MIMDAS) Induced Polarisation (IP) and Magnetotellurics (MT) covering three blocks over separate prospects R4, R11C and R11E, locations are displayed in figure 9 below.

The three blocks all had the same geometry consisting of three, 100m spaced 1100m lines with transmitters extending out of the single middle transmit line by 950m. Receiver spacing was 100m on the outside and 50m on the center line while transmit locations were 50m inside and 100m outside the grid as show in Figure 9. A summary of the survey specifications are provided in Table 3 below.

Exploration Maturity – ADN tenements

Target	# Drill holes	Ironstone	Magnetic Sed/Volc
R1	67	Y	
R4	48	Y	
R12	13	Y	
R11E/W	9	Y	
R14	4	Y	
R16	4	Y	
R2	1		Y
R8	1		Y
R13	1		Y
R20	1		Y
R27	1		Y
R1n	1	IOCG alteration	
12 targets	6 one hole tests	5 have >1g/t Au	

21

Figure 8: Rover Project target prospects maturity

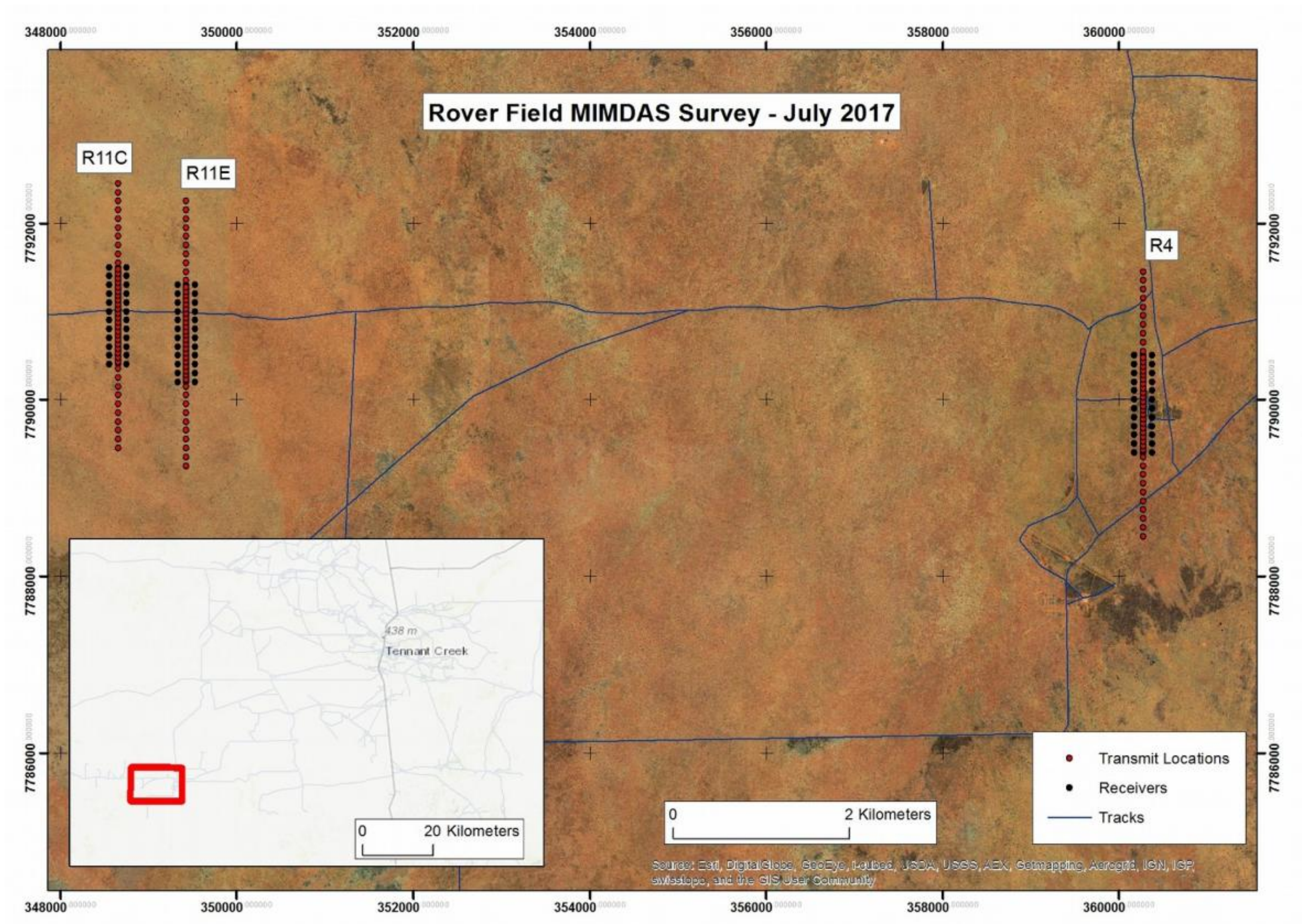

Figure 9: Location of the Rover Project 3D MIMM surveys.

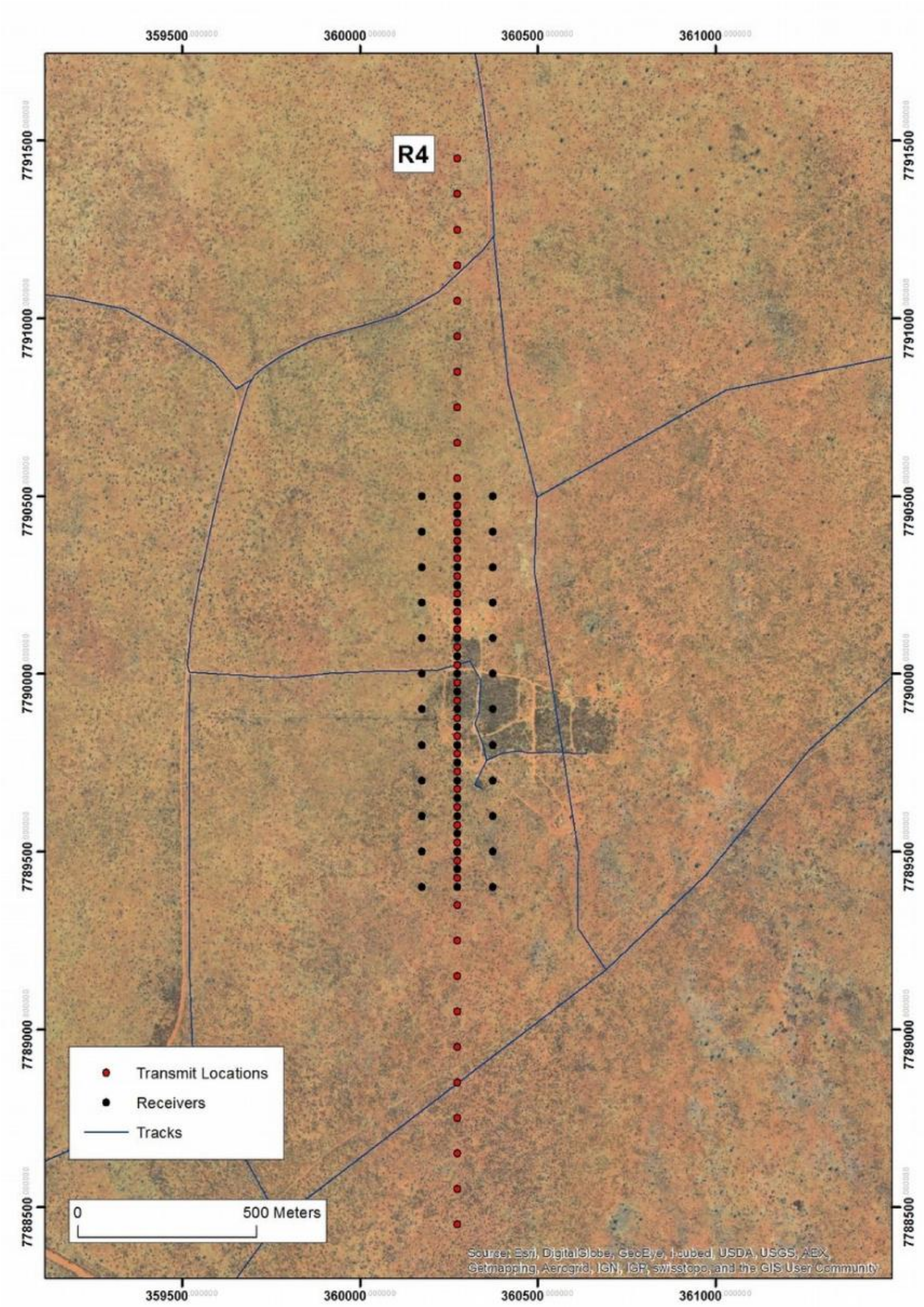

Figure 10: Rover Project R4 3D MIMM survey.

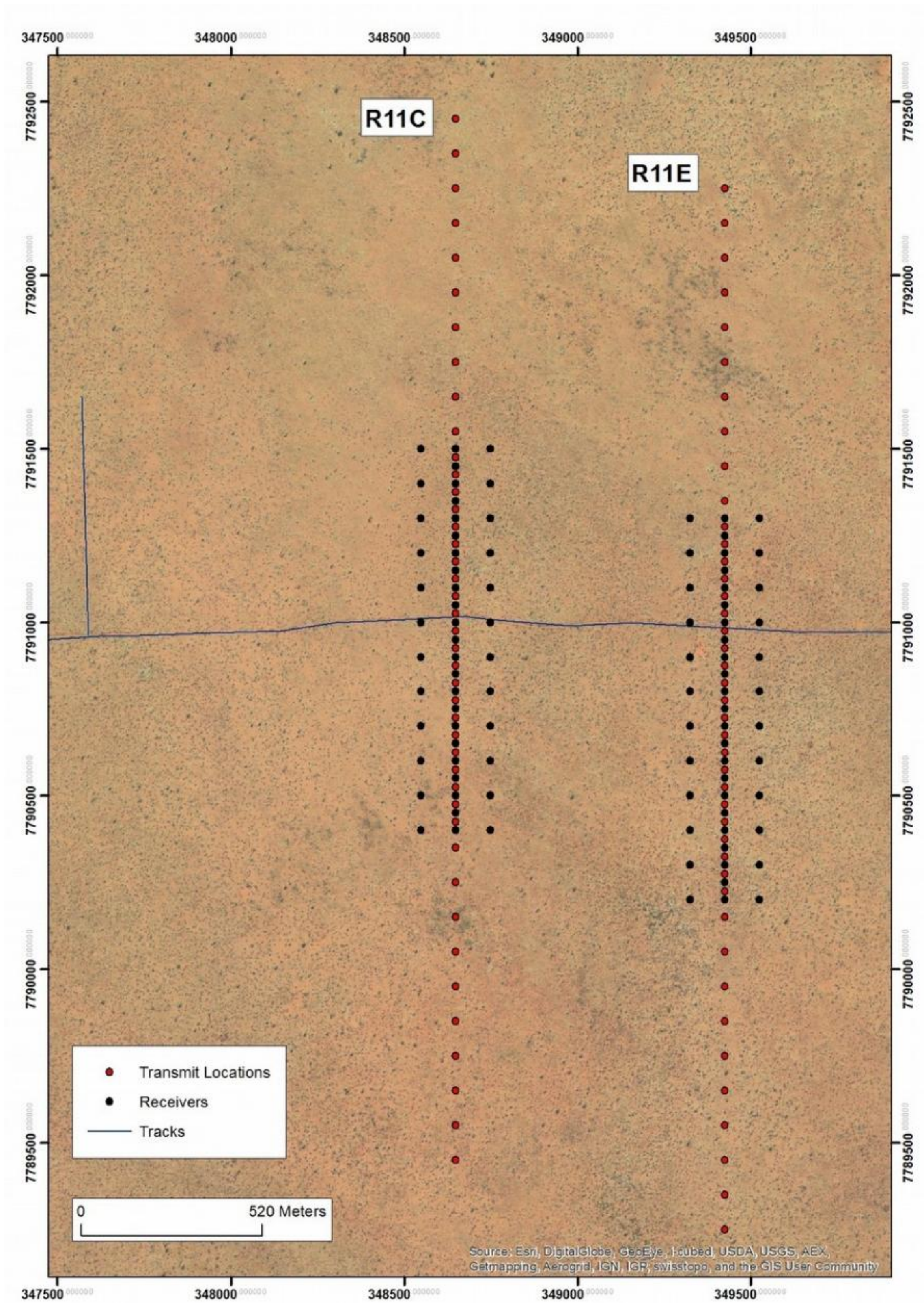

Figure 10: Rover Project R11C & R11E 3D MIMM survey.

I.P. Specifications	
Receiver (Rx)	M.I.M. Distributed Acquisition System
Configuration	Pole-Dipole
Transmitter (Tx)	Zonge GGT-10
A-spacing	50 – 100m
Tx Frequency	25/256 Hz
Rx Sampling	400 samples per second
IP Decay Window	1.5 – 2.5 seconds

Table 3: IP Survey Specs

As is standard operating procedure for MIMDAS surveys, all potential dipoles were laid out and active for all transmitter sites along the line, resulting in readings taken synchronously on both sides of the transmitter site.

For efficiency transmitter electrodes were placed midway between receiver dipoles resulting in non-integer 'n' values e.g. 0.5, 1.5, 2.5 etc. The remote or 'back-current' electrode was placed at 357001E 7791047N for R4 and 352429E, 7791052N for both R11C and R11E. The remote electrode location is approximately a maximum line length from the closest line.

Magnetotellurics (M.T.)

The MT data were acquired over the same potential dipole array as that used for the IP, with the addition into the distributed acquisition network of two pairs of orthogonal magnetometers. This style of MT acquisition is commonly referred to as 'EMAP' mode and is described in Torres-Verdin and Bostik (1992). One set of magnetometers were used as a cross-reference to attenuate non-spatially coherent noise. Table 4, below summarises the acquisition specifications.

MT Specifications	
Receiver	M.I.M. Distributed Acquisition System
Sampling Frequencies	100 & 1600 samples per second
Useable MT Frequency Range	0.5859 – 150 Hz
Dipole-length	50 - 100m
Array	MT E-Map

Table 4: M.T. Survey Specs

The data was processed using the GRS proprietary 'Dirt-Burglar' software (note: a version of which is provided as a product of the survey with which to view or re-process the supplied time-series data).

Results from the Survey

The MIMDAS trial was completed over selected target areas to assess the potential of the technique to define targets below significant basin and Ooradidgee cover sequences. The survey at Rover 4 was considered the test case as it represented the area with the shallowest cover (approx.200m) and the best drilling control.

The results for the R4 area were disappointing with the main chargeability response occurring immediately above the copper and gold mineralisation. It appears the chargeability response is associated with the clay alteration above the deposit.

The resistivity data in both the MIMDAS and the MT survey has successfully mapped the base of the Ooradidgee sediments but there is no indication of the sulphide mineralization in the inverted resistivity sections.

This result was repeated to some degree at Rover 11E where the broad chargeability response appears to map alteration rather than ironstone hosted sulphide mineralisation.

It is concluded that the technique will not generate targets with a high enough probability of success to warrant additional work.

7.0 REHABILITATION

Rehabilitation has been required for two activities;

3D MIM Survey – this rehabilitation has been completed.

Drillholes – 11 drillholes were requested to be left open by Andromeda for potential future use by Emmerson. These are no longer required and will be rehabilitated as required. This rehabilitation is scheduled late October with completion by end of October 2017.

All rehabilitation was and will be completed and performed as detailed in the Rover Mining Management Plan – Authorisation 0945-01.

8.0 CONCLUSIONS

As stated above the execution of the 3D MIMDAS Survey was aimed at generating targets for drill testing, but as these results didn't deliver any targets that warranted drill testing, Emmerson decided to withdraw from the HOA and this withdrawal was executed on 29 September 2017.

14. Appendix II. 3D MIMDAS Survey Rover Prospect, Australia; Acquisition and Modelling Report

Minotaur **A.C.N. 108 483 601**

Minotaur Exploration Ltd
8 Beulah Rd, Norwood 5067, South Australia
Tel: +61 8 8132 3400 Fax: +61 8132 3499
Email: admin@minotaurexploration.com.au

GEOPHYSICAL REPORT GPY2018/01

ROVER GROUND EM INTERPRETATION REPORT

ROVER PROJECT
NORTHERN TERRITORY

A Thompson

May 2018

DISTRIBUTION Minotaur Exploration
Andromeda Metals

ABSTRACT

This report captures the interpretation of the trial ground EM survey conducted at the Rover Project located approximately 85 km SW of Tennant Creek in central Northern Territory. The Rover Project is currently being considered for a farm in by Minotaur with Andromeda. The ground EM survey was conducted over two prospects Rover 1 and Rover 4 to determine whether the known mineralization could be resolved using the most advanced ground EM surveys.

There was no response over the Western Lode at Rover 1 or from any of the Rover 4 lodes and this was thought to be due to the small size of the lodes, the depth of the mineralization, particularly at Rover 1 and the poor conductance of the targets.

It is recommended that no further ground EM be conducted at this project.

TABLE OF CONTENTS

Page

LIST OF FIGURES

LIST OF TABLES

1 INTRODUCTION

From the 24th of April to the 3rd of May, 2018, a ground EM survey was conducted by GEM Geophysics at the Rover Project. The Rover Project is located approximately 85 km southwest of Tennant Creek in central NT (Figure 1).

A total of 3.7 line km of moving loop ground EM were surveyed along 4 north-south lines using an in-loop and slingram configuration (figure 2).

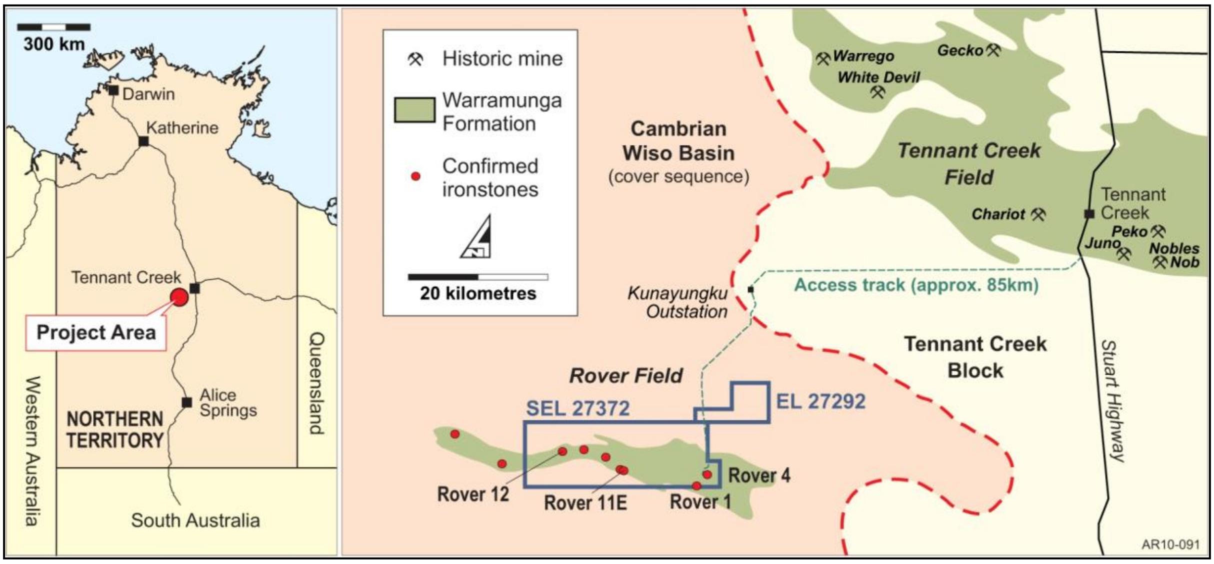

Figure 1: Plan map showing location of Rover Project.

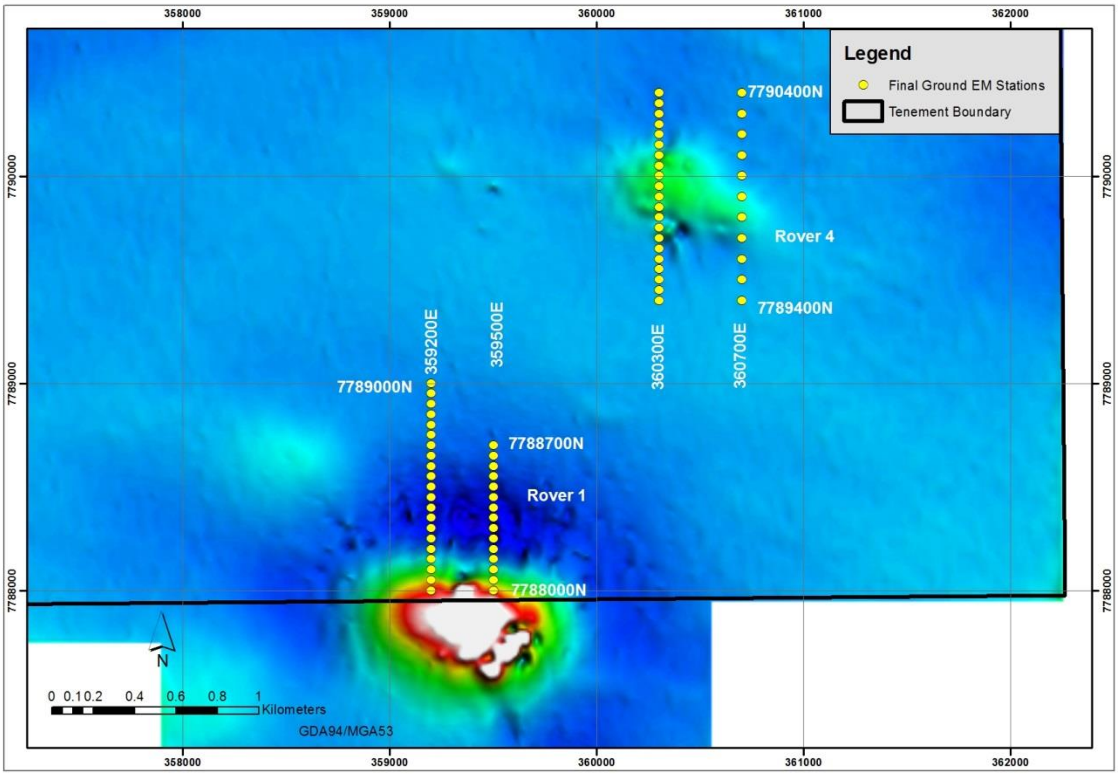

Figure 2: Plan map of the Rover Ground EM Survey over RTP1VD Magnetic image

2 LOGISTICS

Table 1 lists the survey specifications and table 2 list the line locations for the EM.

Table 1. Survey Specifications

Transmitter	Zonge ZT-30 or Equivalent
Receiver and Probe	3 Component Jessy Deep SQUID
Loop Size	200m
Tx Frequency	1 Hz
Station Spacing	50m
Survey Setup	In-Loop and Slingram

Table 2. Line locations.

		Start		Finish				
Prospect	Line	East	North	East	North	Stn Spacing	Line Length	No Stations
Rover 1	359200E	359200	7788000	359200	7789000	50	1000	21
Rover 1	359500E	359500	7780000	359500	7788700	50	700	15
Rover 4	360300E	360300	7789400	360300	7790400	50	1000	21
Rover 4	360700E	360700	7789400	360700	7790400	100	1000	11
Total number of line km							3.7	
Total number of stations								68

3 DATA QUALITY AND SURVEY ISSUES

Data quality was generally good. Production rates were generally slow due to long daily commute and thick scrub. The in-loop data on all lines was heavily affected by IP effects due to the composition of the overburden.

4 RESULTS

Rover 1

Two lines were surveyed over the Rover 1 Prospect (figure 3). Due to the location of the mineralization on the tenement boundary, the lines were not able to be surveyed over the top of the mineralization. Forward modelling of the Rover 1 mineralisation however suggested that there should be a long wavelength response observed in the Z Component data leading up to the mineralization given its significant depth.

Line 359200E was surveyed up to the edge of the tenement over the Western Lode however no response was observed in the vicinity of the mineralized position in either the in-loop (figure 4) or slingram data Z Component data (figure 5). The in-loop data was heavily affected by IP effects at late time which may have impacted the effectiveness of the survey however the slingram data is not affected by IP responses and there was no response in this dataset either.

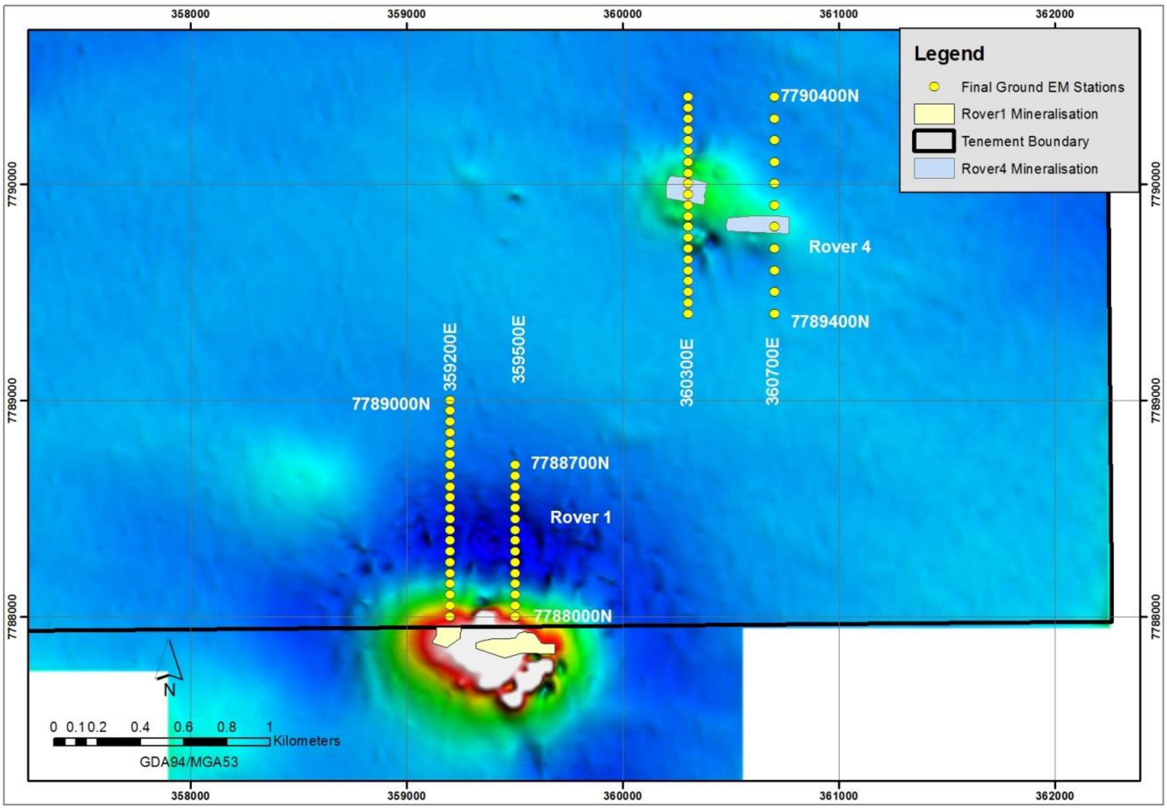

Figure 3. Plan map showing Ground EM plates over DHEM model.

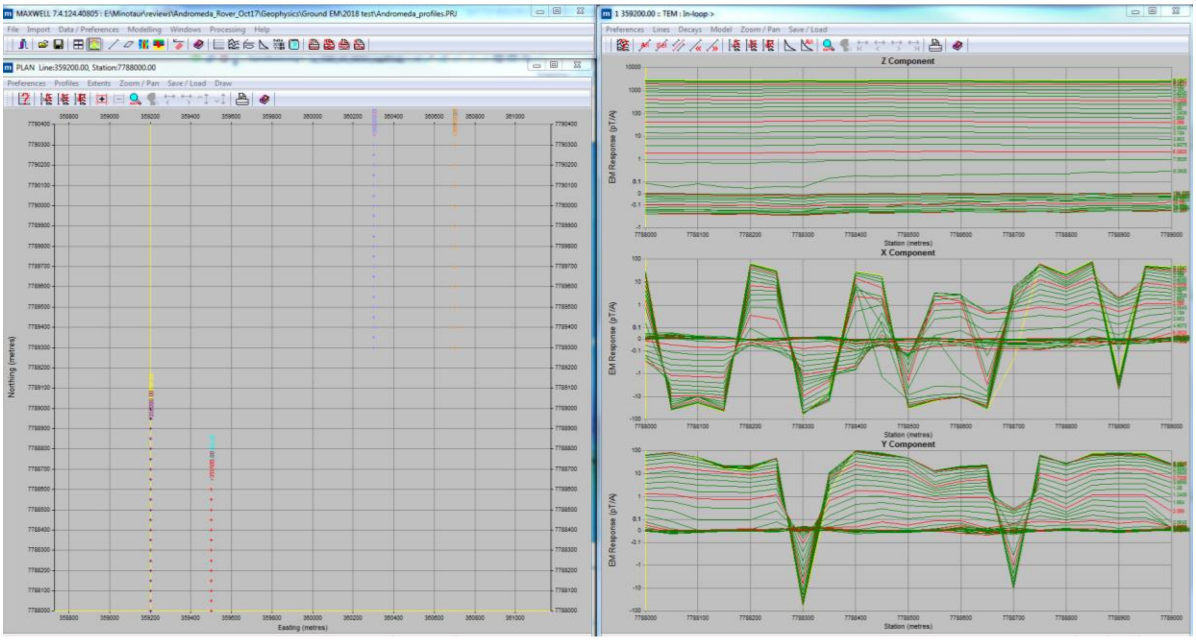

Figure 4. Line 359200E In-Loop Ground EM three Component B Field Profiles

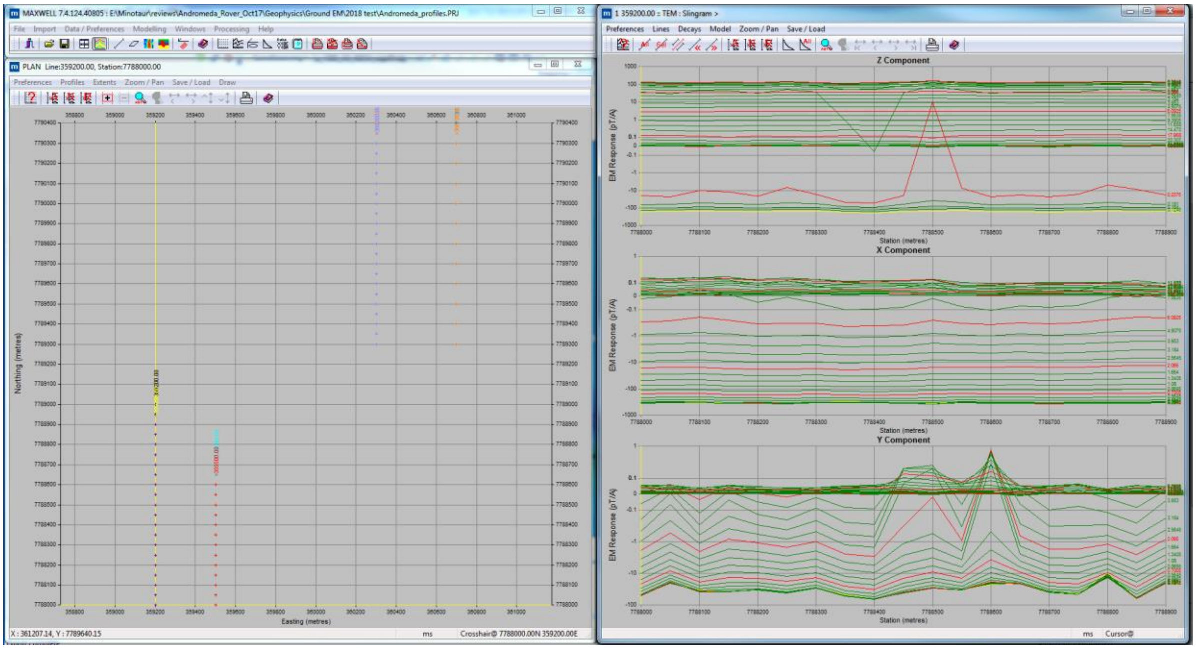

Figure 5: Line 359200E Slingram Ground EM three Component B Field Profiles

Line 359500E was surveyed up to the edge of the Andromeda tenement approaching the Jupiter lode which is the larger of the 2 known mineralized bodies at Rover 1. Again no response was observed in either the in-loop (figure 6) or slingram Z Component data (figure 7). A weak response can be observed developing at the southern end of the line in the mid-time, X Component data which may indicate there may be some response associated with the mineralization to the south of the line in this component (figure 8).

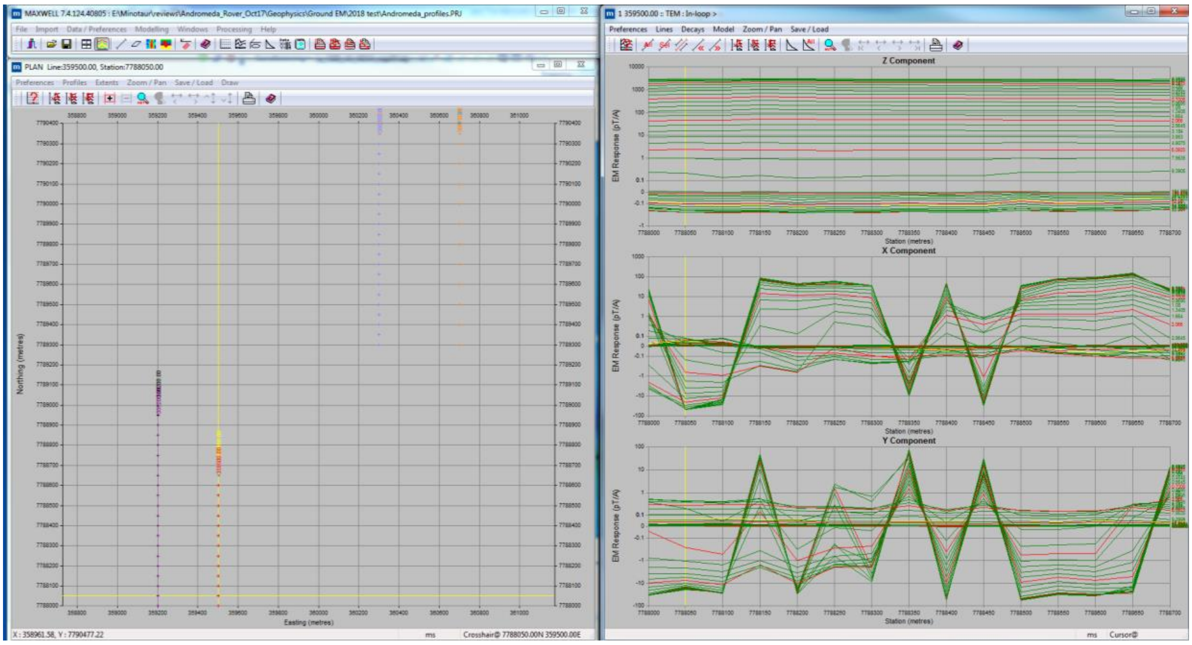

Figure 6. Line 359500E, In-loop, Ground EM, 3 Component, B Field, profiles

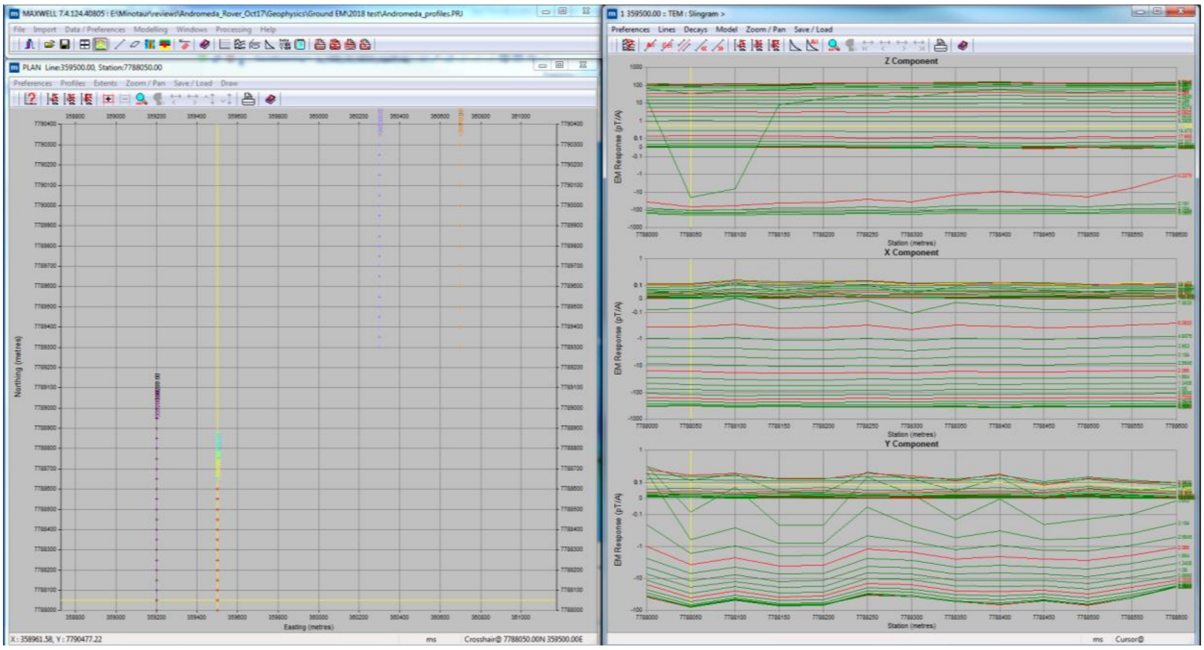

Figure 7. Line 359500E, Slingram, Ground EM, 3 Component, B Field, profiles

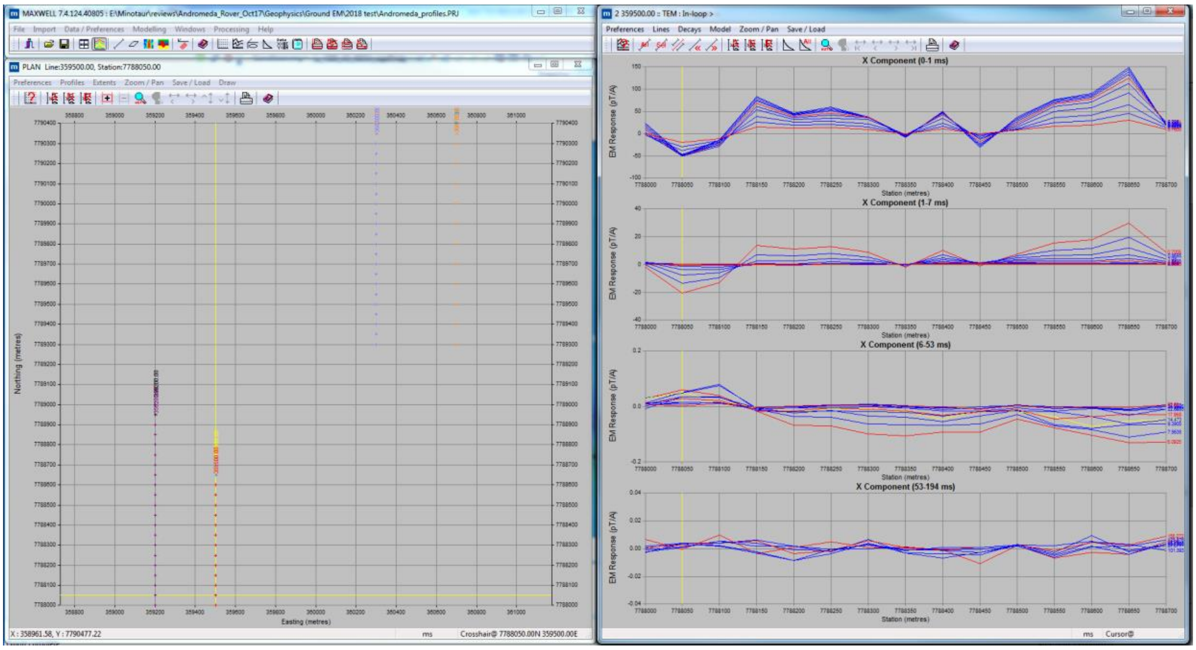

Figure 8. Rover 1, Line 359500E, in-loop, X Component, B Field, profiles

Rover 4

The known mineralization at Rover 4 consists of 2 separate lodes (figure 9). Two lines were surveyed at this Prospect. Lines 360300E and 360700E were surveyed to determine whether ground EM could detect this mineralisation (figure 10).

No responses were observed in either the moving loop or slingram data over either of the mineralized bodies (figures 11-14). A broad, weak response was however observed in the in-loop X Component data of line 360700E at the northern end of the line. Modelling of this response indicated a 400m by 400m body at a depth of 165 meters and dipping at 58 degrees to the south. The body has a modelled conductivity-thickness product of 100 S (figure 15). This body is associated with a subtle east-west oriented magnetic and gravity feature (figures 16-17).

Table 3. Summary of Rover 4 modelling results

Location	Model	East	North	Depth	Dip	Az	Depth Ext	Strike Ext	Cond
Rover 4	360700E	360730	7790635	165	58	180	400	400	100

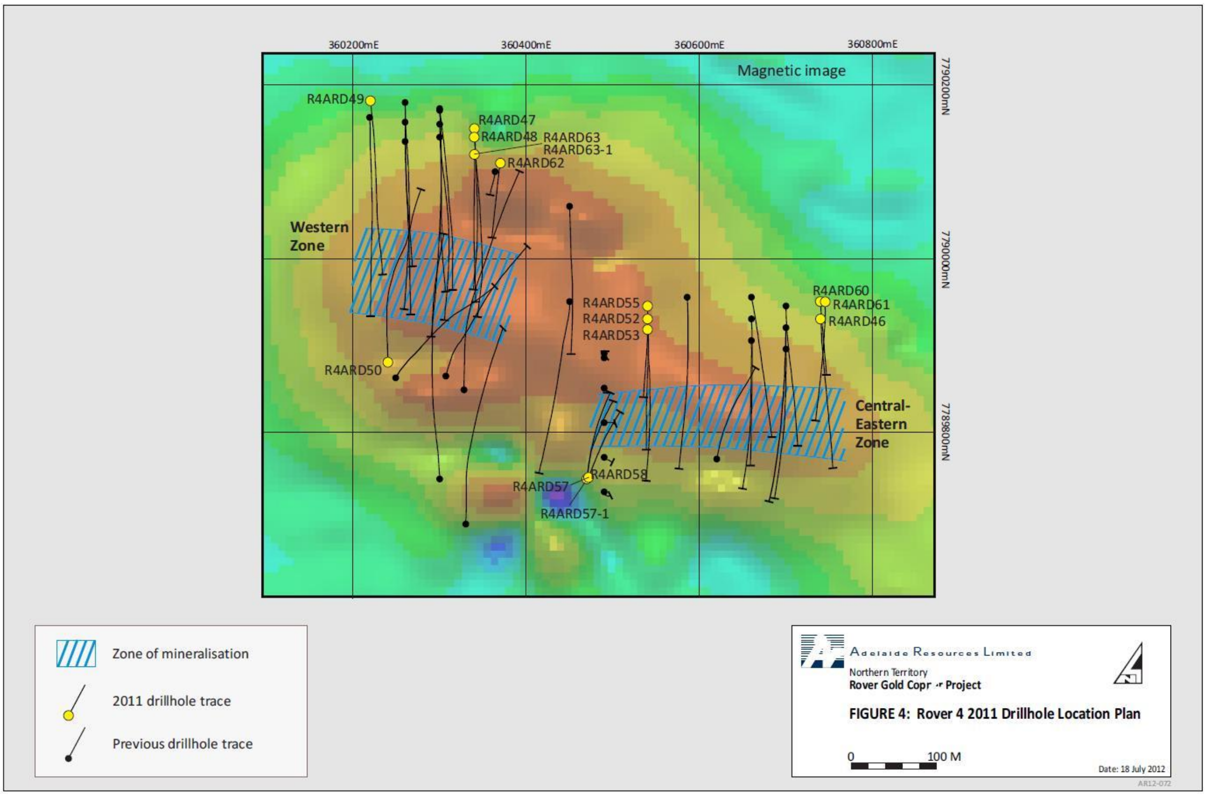

Figure 9. Plan map showing location of drilling and mineralization at Rover 4.

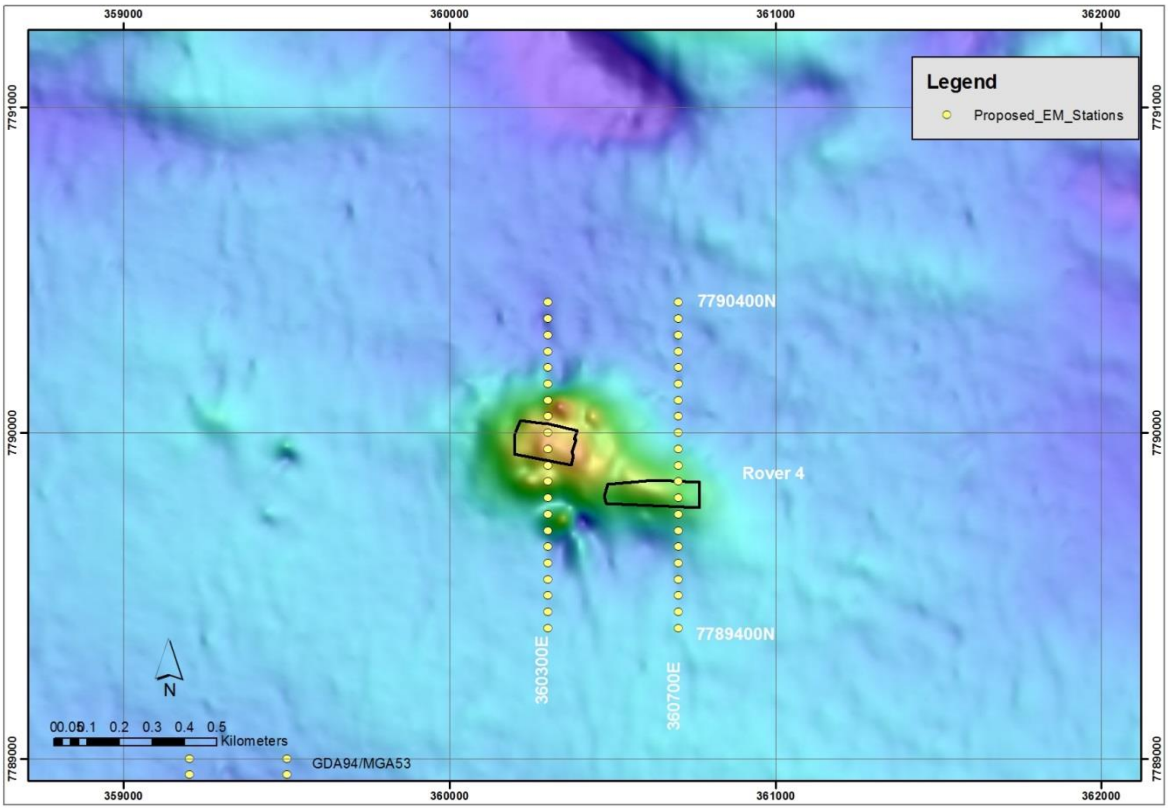

Figure 10. Plan map showing ground EM lines over RTP1VD magnetic image and outline of Rover 4 known mineralized lodes

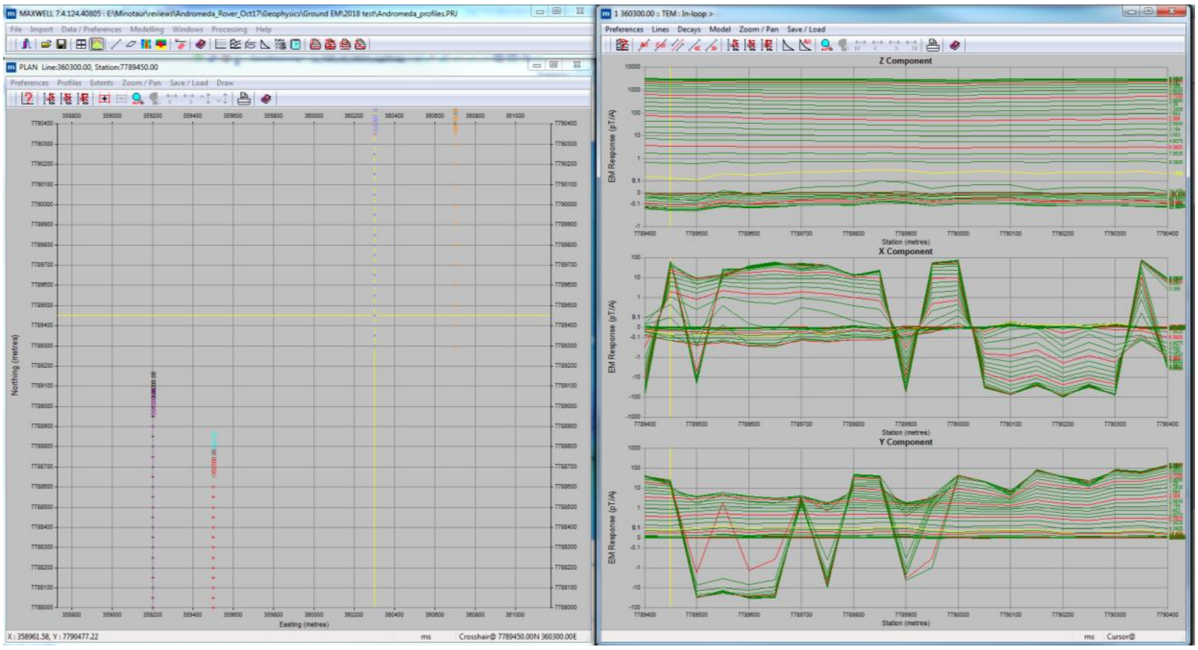

Figure 11. Rover 4, Line 360300E, In Loop, 3 Component, B Field, EM Profiles

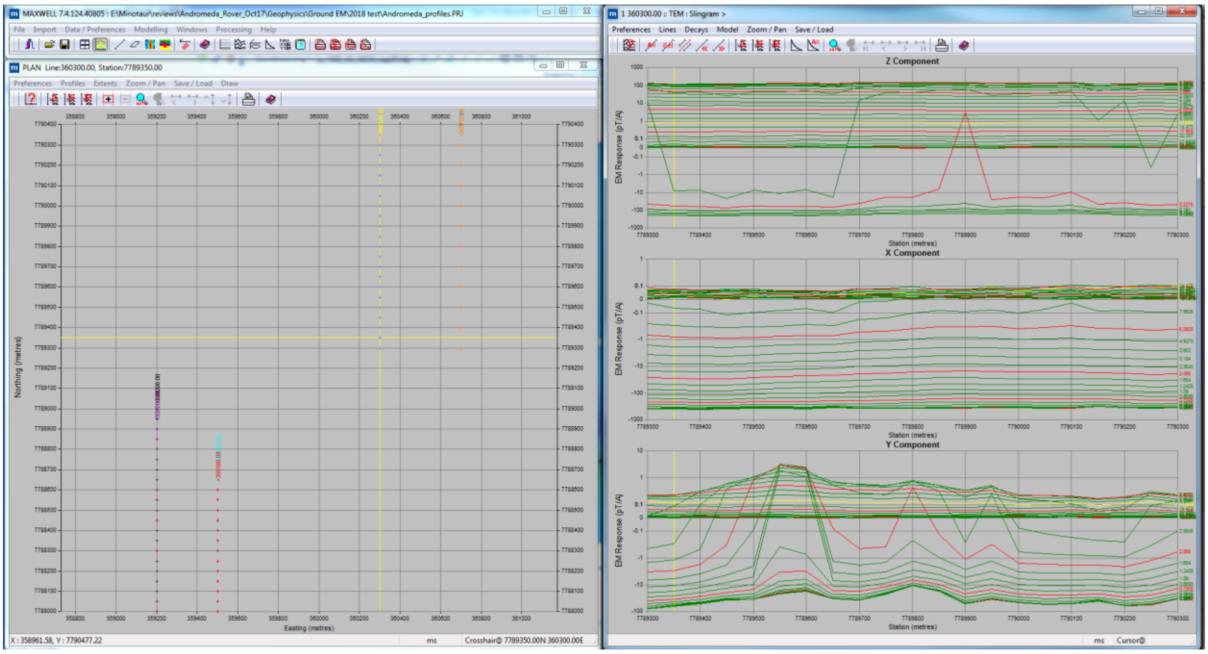

Figure 12. Rover 4, Line 360300E, Slingram, 3 Component, B Field, EM Profiles

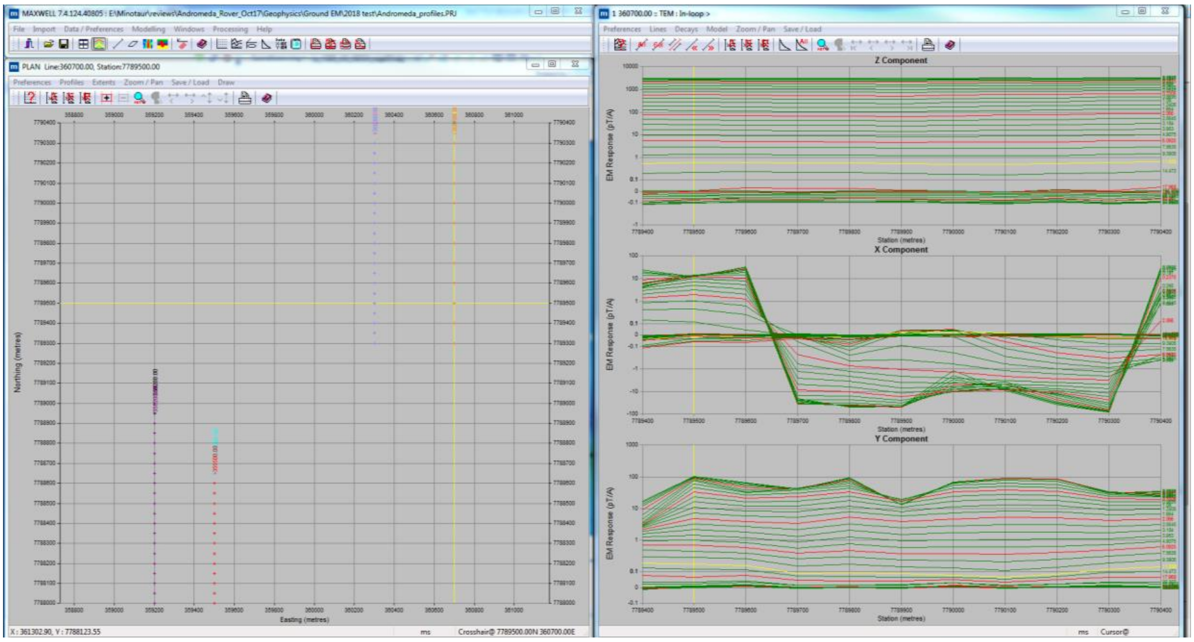

Figure 13. Rover 4, Line 360700E, In-Loop, 3 Component, B Field, EM Profiles

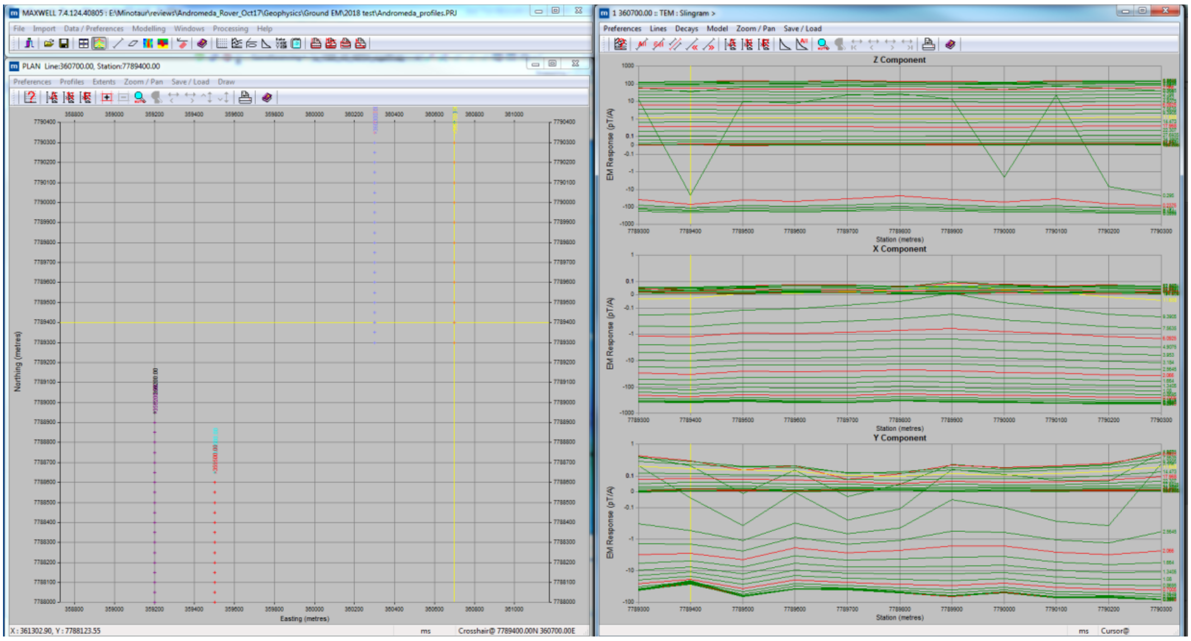

Figure 14. Rover 4, Line 360700E, Slingram, 3 Component, B Field, EM Profiles

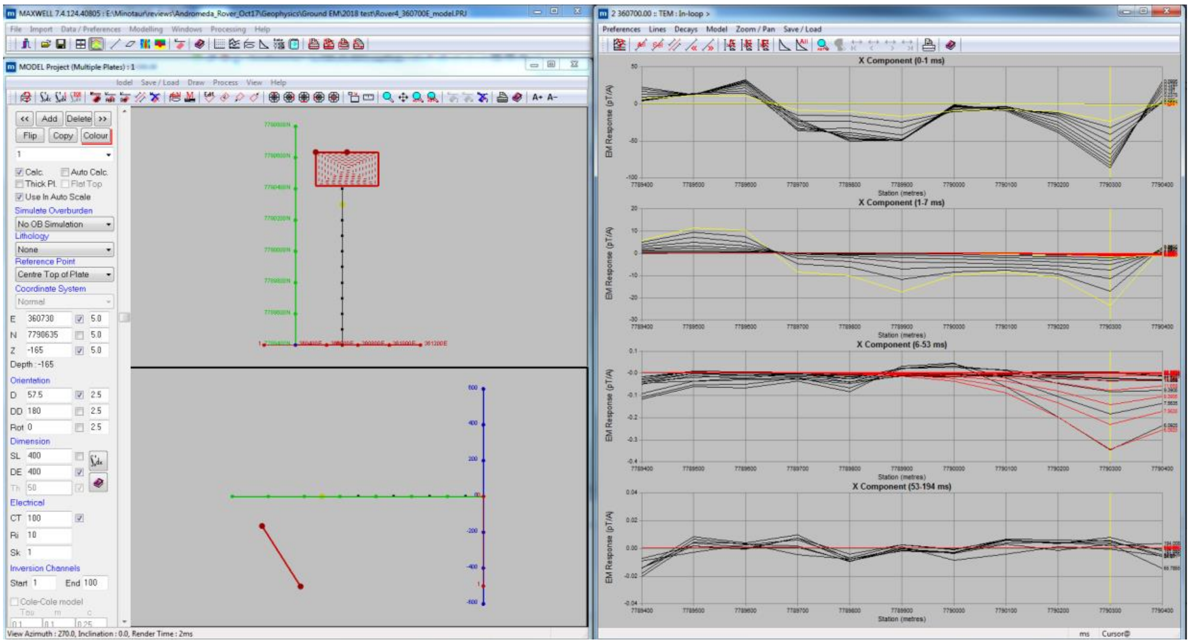

Figure 15. Line 360700E plan (top left) and section view (bottom left) of X Component in-loop ground EM models with observed (black) and model (red) early, mid and late time X Component surface B Field in-loop EM profiles (right)

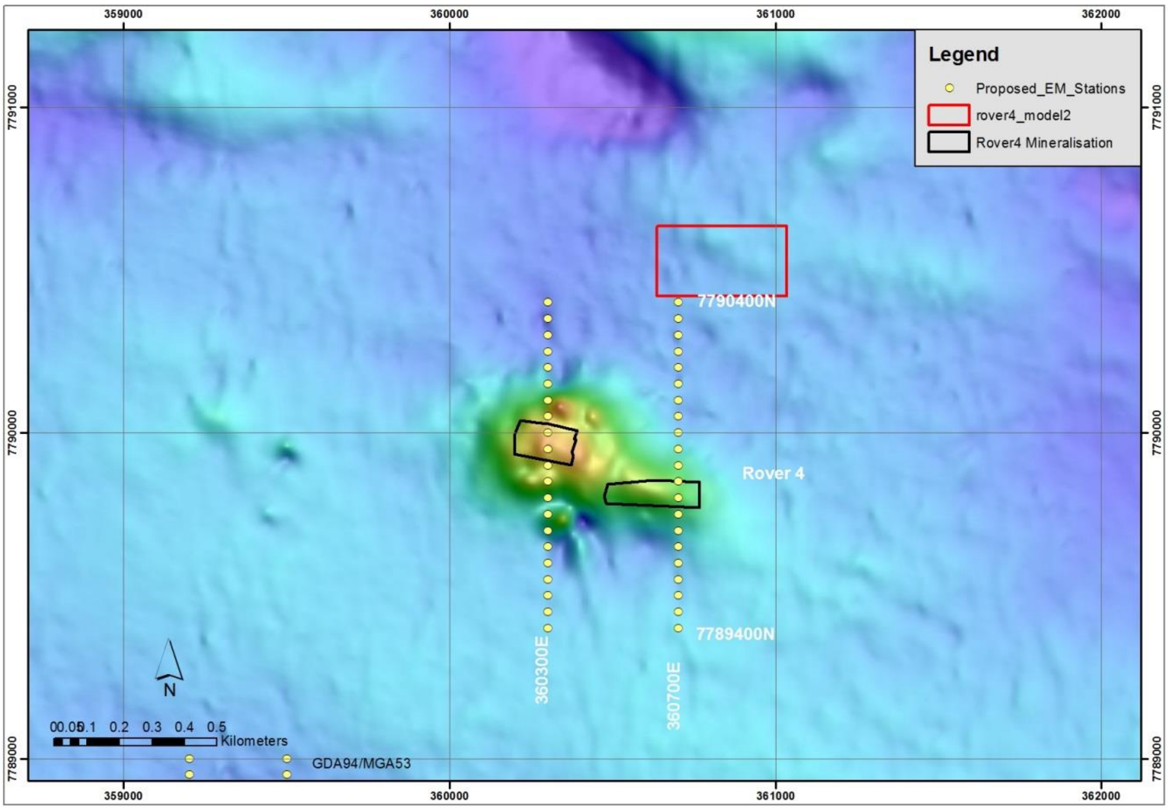

Figure 16. Rover 4 ground EM modelling results over 1VDRTP Magnetic image

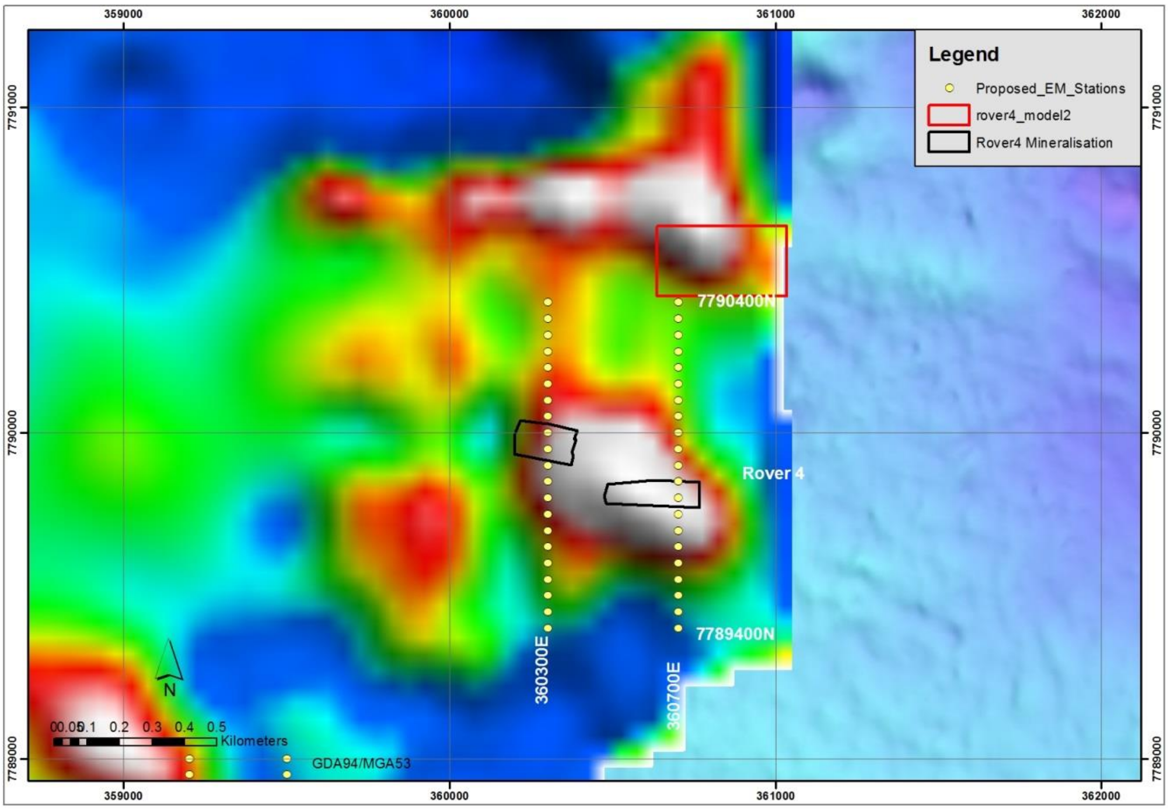

Figure 17. Plan map of Rover 4 ground EM modelling results over 1VD ground gravity image

5 CONCLUSIONS

Surface moving loop EM was conducted over the Rover 1 and Rover 4 mineralised bodies to determine whether these bodies could be detected using ground EM techniques. The survey was conducted in both in-loop and slingram configuration. A total of 3.7 line km of data was collected along 4 north-south lines.

No response was observed in the moving loop data over the Western Lode at Rover 1 and only a weak response in the X Component data at the southern end of the line approaching the Jupiter Load at Rover 1. It should be noted that access over the main Jupiter load at Rover 1 was restricted due to the location of the mineralisation to the south of the tenement boundary.

At Rover 4, no responses were observed over the known mineralised bodies. A weak response was observed in the in-loop X Component data on the northern margin of line 360700E. Modelling of this response gives a low conductance body which correlates with a subtle east-west magnetic and gravity feature to the north of the survey line. A summary of the modelling results is given in table 5.

Table 4. Summary of DHEM modelling results

Location	Model	East	North	Depth	Dip	Az	Depth Ext	Strike Ext	Cond
Rover 4	360700E	360730	7790635	165	58	180	400	400	100

The lack of success of the ground EM to effectively resolve the mineralization at Rover is thought to be due to a combination of the following:

- significant depth of the targets,
- the small size of the targets and
- the poor conductivity of the mineralisation.

In particular the lack of any pyrrhotite in the mineralization significantly reduces the conductivity of the mineralization. On top of this, the survey was quite expensive due to the long commute time and the thick scrub that the crew had to survey through.

It is recommended that ground EM not be used to detect Rover style mineralization although it could be used to explore for other mineralization types in the area that contain pyrrhotite. IP surveys may be a better option to resolve the low conductance mineralization.

15. Appendix III. Geophysical Report GPY2018/01 Rover Ground EM Interpretation Report.

Geophysical
Resources &
Services Pty Ltd
A.B.N. 68 107 279 327

**1/80 Ebbern St, Darra
Queensland, 4076
Australia**

3D MIMDAS Survey
Rover Prospect, Australia
Acquisition & Modelling Report

July, 2017

Prepared by
Peter Rowston

FAMR 2017 186 Emmerson Rover 3D DC/IP MT

DISCLAIMER

This report has been prepared in good faith with all due care and attention – It is based on the data acquired and information supplied by Emmerson Resources Ltd. Geophysical Resources and Services Pty Ltd accepts no responsibility for the conclusions drawn and any consequences arising from the conclusions in this report. Any use of this report or any reliance upon this report by any person, other than the use of the whole of this report by the client is outside of its intended purpose.

TABLE OF CONTENTS

Table of Contents

INTRODUCTION

Geophysical Resources and Services Pty Ltd (GRS) were commissioned by Emmerson Resources Ltd to run a survey of 3D M.I.M. Distributed Acquisition System (MIMDAS) Induced Polarisation (IP) and Magnetotellurics (MT) at the Rover Field near Tennant Creek in the Northern Territory. The survey consisted of three blocks over separate prospects known as R4, R11C and R11E located approximately 75km south-west of Tennant Creek. All coordinates mentioned are GDA94 UTM Zone 53.

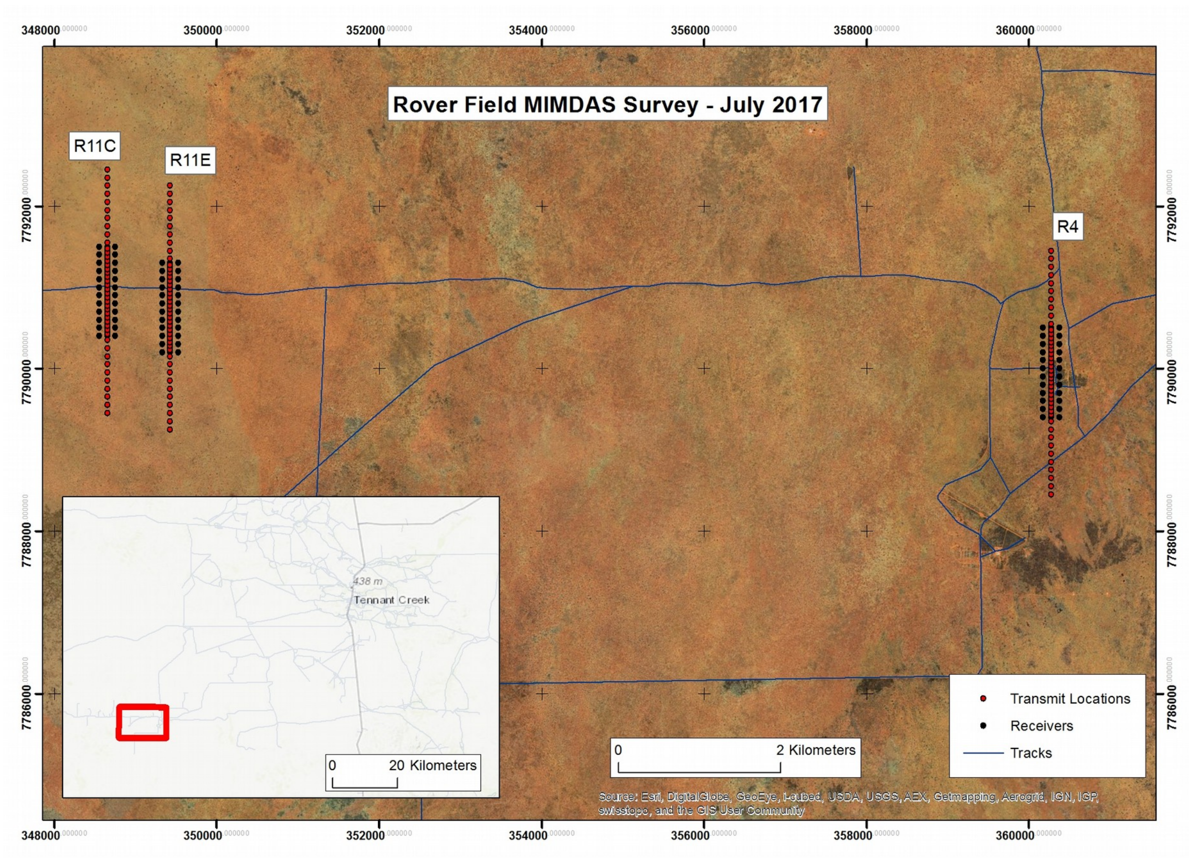

Figure 1: Location Map, Rover Field, Australia. (Aerial photo courtesy of Esri)

The following sections document the survey specifications and data processing employed and provides a discussion of the modelling undertaken. The attached appendices contain the Production Report, Array Layouts and Receiver Locations. A description of the MT Processing Scheme and the Chargeability Standard used is also provided. Modelled Sections, Pseudosection Plots and Inversion Fits accompany this document along with the Digital Data.

SURVEY SPECIFICATIONS

Resistivity and Induced Polarisation (I.P.)

The three blocks all had the same geometry consisting of three, 100m spaced 1100m lines with transmitters extending out of the single middle transmit line by 950m. Receiver spacing was 100m on the outside and 50m on the centre line while transmit locations were 50m inside and 100m outside the grid as show in Figure 2. A summary of the survey specifications are provided in Table 1 below.

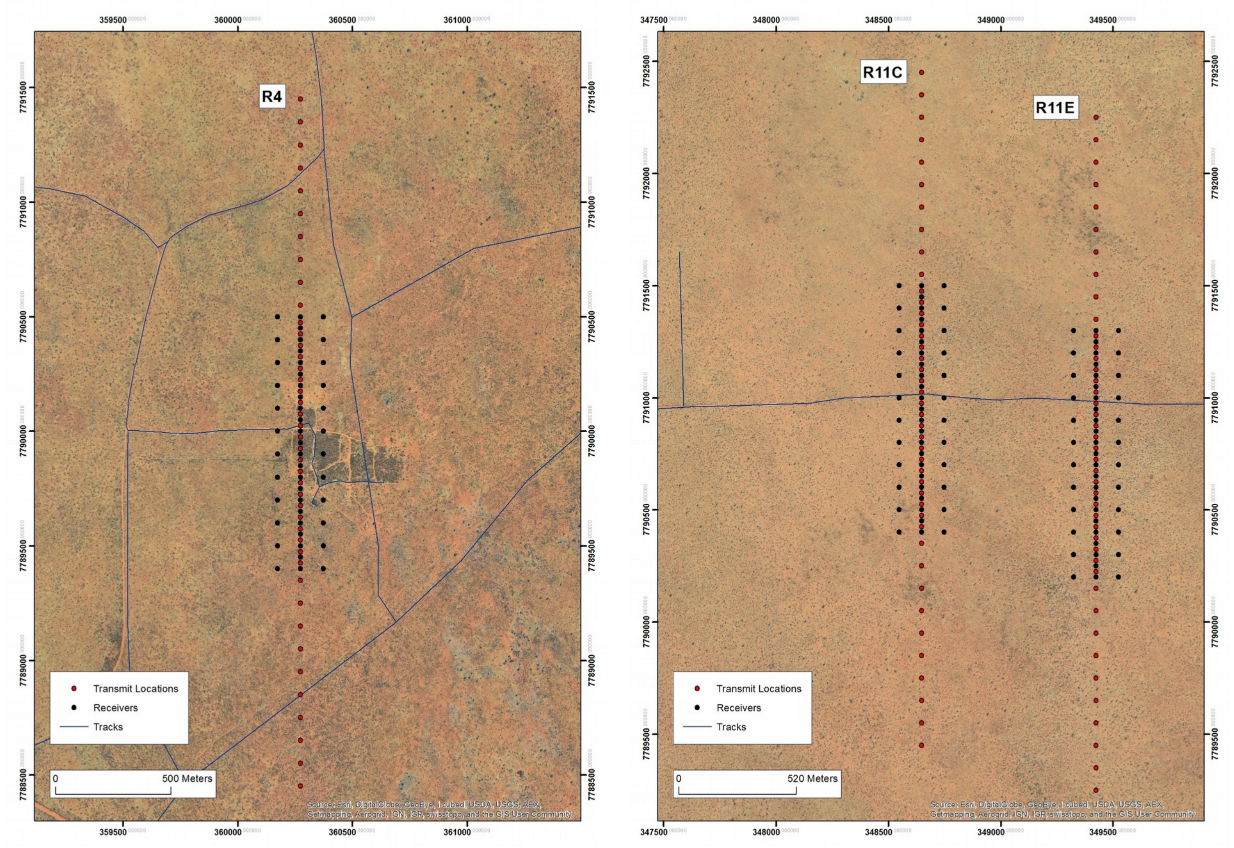

Figure 2: Rover Surveys Block Layout. (Aerial photo courtesy of Esri)

I.P. Specifications	
Receiver (Rx)	M.I.M. Distributed Acquisition System
Configuration	Pole-Dipole
Transmitter (Tx)	Zonge GGT-10
A-spacing	50 – 100m
Tx Frequency	25/256 Hz
Rx Sampling	400 samples per second
IP decay window	1.5 – 2.5 seconds

Table 1: IP survey specifications.

As is standard operating procedure for MIMDAS surveys, all potential dipoles were laid out and active for all transmitter sites along the line, resulting in readings taken synchronously on both sides of the transmitter site.[1]

For efficiency transmitter electrodes were placed midway between receiver dipoles resulting in non integer ‘n’ values e.g. 0.5, 1.5, 2.5 etc. The remote or ‘back-current’ electrode was placed at 357001E 7791047N for R4 and 352429E, 7791052N for both R11C and R11E. The remote electrode location is approximately a maximum line length from the closest line.

Magnetotellurics (M.T.)

The MT data were acquired over the same potential dipole array as that used for the IP, with the addition into the distributed acquisition network of two pairs of orthogonal magnetometers. This style of MT acquisition is commonly referred to as ‘EMAP’ mode and is described in Torres-Verdin and Bostik (1992). One set of magnetometers were used as a cross-reference to attenuate non-spatially coherent noise. Table 2 (below) summarises the acquisition specifications.

Appendix 3 lists the MT and IP Array Layouts and the coordinates of the electrodes.

MT Specifications	
Receiver	M.I.M. Distributed Acquisition System
Sampling Frequencies	100 & 1600 samples per second
Useable MT Frequency Range	0.5859 – 150 Hz
Dipole-length	50 - 100m
Array	MT E-Map

Table 2: M.T. survey specifications.

[1] For the purposes of displaying the raw data as pseudo-sections, data collected on the western side of each transmitter site are usually displayed separately from the data acquired on the eastern side. The two data sets are referred to as the ‘dipole-pole’ and ‘pole-dipole’ data respectively

DATA PROCESSING & TREATMENT

The data was processed using the GRS proprietary 'Dirt-Burglar' software (note: a version of which is provided as a product of the survey with which to view or re-process the supplied time-series data). Brief descriptions of the various processing streams are provided below.

Magnetotellurics (MT)

A detailed description of the MT processing stream is provided in Appendix 7. In summary, the processing used is similar in most respects to classical MT processing algorithms with the exception that it uses generally longer FFT lengths coupled with Finite Impulse Response (FIR) filtering of the spectral ensembles. This approach combines the advantages of using both long and short FFT lengths into a single FFT length.

As described in the previous sections, two magnetometer sites along the line were deployed and one was used as a cross-reference. This process improves the amplitude information at high frequencies and in the dead band by reducing spatially non-coherent noise.

Resistivity and Induced Polarisation (IP)

For the IP method, the MIMDAS system measures full waveform 'time-series' data for both the input excitation (current waveform) and received signal (voltage waveform). All 'raw' time-series data are recorded and then processed using the user controlled MIMDAS operating software 'Dirt-Burglar'. The IP processing stream applied is summarised in point form below.

Time-Series Processing and Stacking

- Collect time series of both the transmitted current waveform and the received voltage waveforms for all receiver sites in the array at the operator defined sampling rate and transmission frequency
  - Note: In the case of the Rover surveys the current waveform was a 100% duty cycle square wave with a frequency of 25/256 Hz, sampled at 400 samples per second
- Convert raw time series A/D counts into real units (i.e. Volts & Amps) via calibrations for sensors and individual receiver units (DAU's)
- Stack transmitted and received time series with a modified Halverson 'Linear Drift Removal' stacking algorithm. This algorithm removes DC and any linear drift.

Fourier Domain Operations

- FFT the individual stacked data
- Calculate the frequency domain system response (i.e. received signal/transmitted signal) for individual stacks
- Selectively reject outliers
- Average the estimates, weighted by their observational errors
- Average any repeat readings, weighted by their observational errors
- Multiply the averaged system response with unit 50% duty cycle frequency response at fundamental period

Parameter Estimation

- Convert back to time domain, and
- Estimate the time domain normalised M.I.M. Chargeability estimation based upon a selected off-time window. (e.g. 1.5 – 2.5 seconds)

A more detailed description of the M.I.M. Chargeability Standard is provided in Appendix 6.

DATA QUALITY

Magnetotellurics (MT)

The MT data in general are characterised by clean impedance estimates between 1.17 and 200 Hz (see Figure 3). Low natural signal below this nominated bandwidth resulted in these impedances to be less well constrained. Cross-referencing the MT data recorded on the line with that from the remote magnetometer site – also on the line - resulted in an improvement in data quality within the bandwidth (see Figure 4).

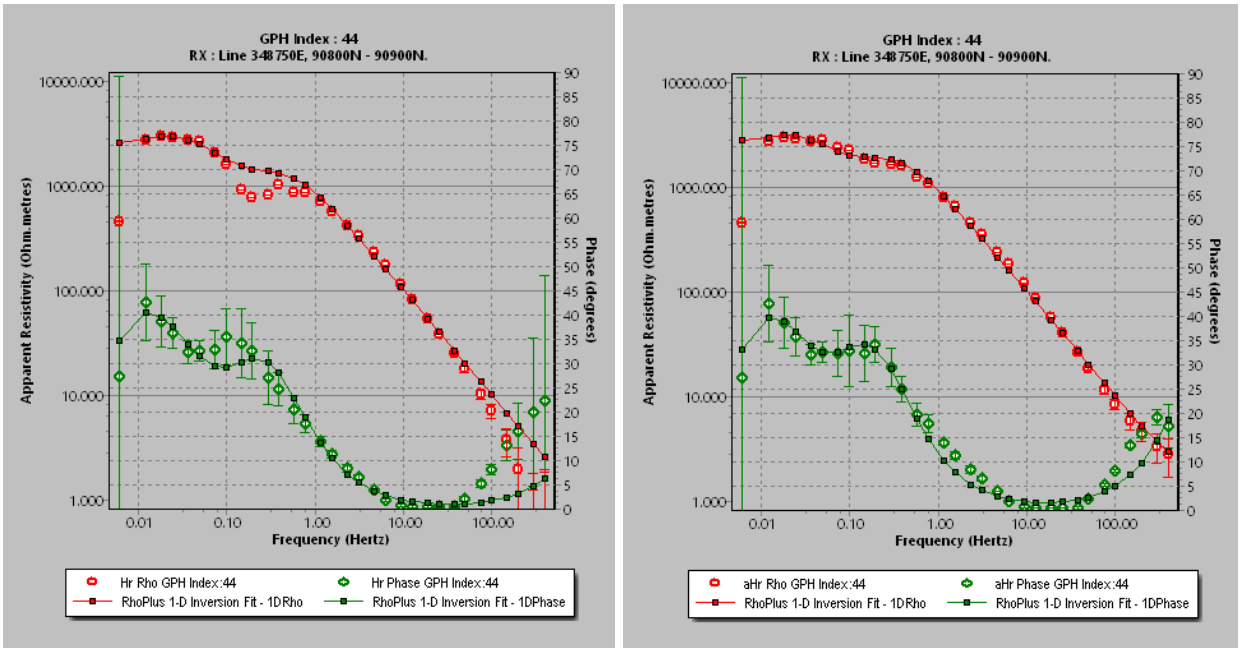

Figure 3: M.T. Impedance Curves, without cross-reference on the left and with cross-reference on the right.

Note that in Figure 3 the high quality data results in very low error estimates, i.e. they are not visible over the symbol used at each data point. This is particularly evident at higher frequencies where MT signal is typically higher. The error estimates become more clearly visible as data quality decreases at lower frequencies.

Processed MT data are provided along with this report.

Resistivity / IP

The IP data quality remained good throughout, although with a drop in signal at R11C, with currents ranging from 0.9 – 3.8A. Examination of the receiver time series data shows little effect from external sources. An example of a typical receivedsignal is shown in Figure 4 and typical repeatability in Figure 5.

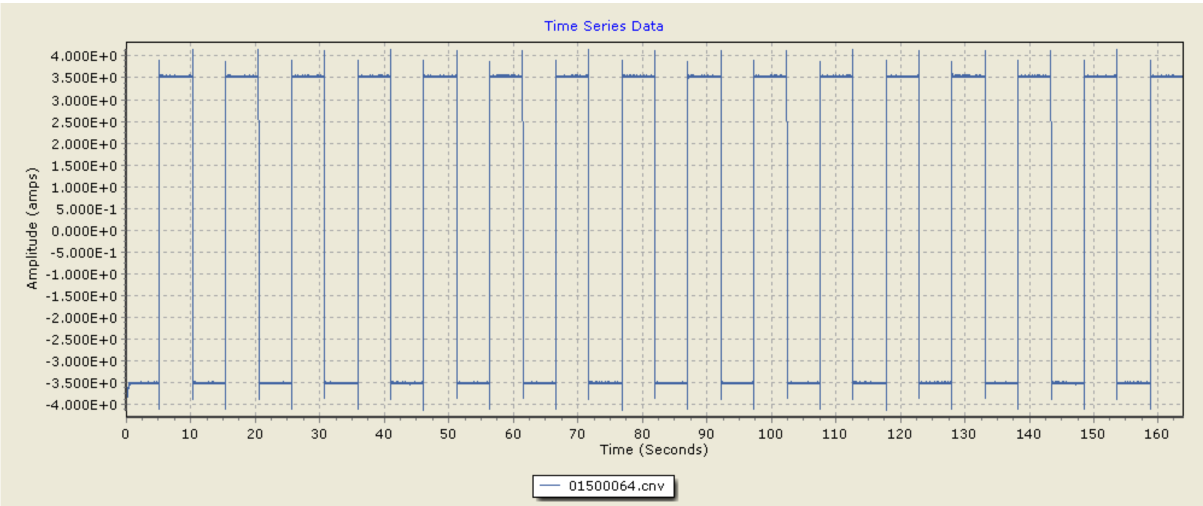

Figure 4: Example of time series data at R11E.

The 2D data are included along with this report. The 2D data are in the standard UBC2D and geosoft IP format, a description of which is in Appendix 2.
The unprocessed 'time-series' data are also provided. These data can be viewed and re-processed with the 'DirtBurglar-Lite' program. Assistance in these operations can be requested from GRS.

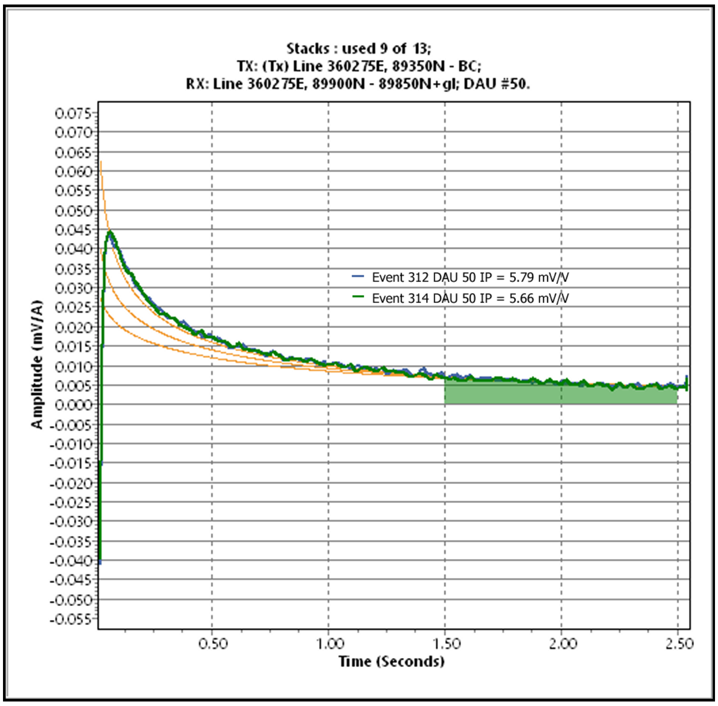

Figure 5: Example of Typical IP Repeatability. N=10.5, TX 89350N on block R4.

MODELLING

Smooth Model Inversion Models

MT Inversions

2D MT data were modelled using Kerry Key's MARE2DEM software. (Key, K., and Ovall, 2011).

As true "observational errors" in geophysical data are largely unrealisable, particularly in natural field data, an error floor was added to the MT data prior to inversion to avoid "over-fitting" the data. This floor was 3.5% of the apparent resistivity and 1 degree of phase and this was added to the standard deviation between the stacked ensemble results. The program MARE2DEM was left to converge to the best level of fit within a maximum of 99 iterations. For all lines the inversion converged to a chi factor of between 1.0

2D Resistivity/IP Inversions

The final three co-linear (transmitter and receivers on the same line) resistivity and IP lines have been modelled using the 'UBC' 2D smooth model inversion algorithm – the details of which are provided in Oldenburg and Li (1999 and 1994). Useful and less rigorous descriptions of the algorithm can also be found at the UBC 'Geophysical Inversion Facility' website at www.geop.ubc.ca/ubcgif/.

In brief the UBC algorithm defines the inversion using a typical 'smooth model' approach. That is the inversion scheme aims to produce a model minimising the misfit between the calculated and measured data whilst also minimising a second function (namely the model objective function) which contains terms describing the model structure and complexity (complexity being the opposite of smoothness). These terms can be set by the user and allows the inversion to favour an earth structure which approximates the user's knowledge of the geology. These constraints can bias horizontal or vertical structure i.e. layer cake stratigraphy or steeply dipping regimes and also can allow the user to specify a non homogeneous seed model.

The 2D inversions for the co-linear Rover lines were run using mostly default options, except a chi factor of between 0.15 to 0.4 was used for IP convergence and a weighting favouring vertical structure was used. The final inverted sections generally fit the measured data to a level better than 1% of observed Primary Voltage (DC) and better than 0.25 mV/V on observed Chargeability. That is, all 2D models converged with an extremely close data fit, a closeness that would not normally have been sought in routine investigation. The 2D modelling output files are provided on the disks in Appendix 1.

3D Resistivity/IP Inversions

The final Resistivity and I.P. data have been modelled using the 'UBC' 3D smooth model inversion codes. Details of the modelling algorithms are provided in Oldenburg and Li (1994 and 1999). The overall methodology is similar to the 2D inversion briefly described above although the solution of the system is achieved via a different numerical approach.

Data considered to be of poor quality (largely determined by repeatability and inspections of the time series) was edited from the data set. This was carried out such that the inversion could would not be influenced by noisy data. Given the level of data redundancy afforded by the 3D acquisition mode and collection of both pole-dipole and dipole-pole data, the reduction in data volume has little to no bearing on the model result. Mostly all default parameters were employed for the UBC3D models provided, with the exception of a weighting file that was employed to favour horizontal structure in the overburden and vertical structure beneath it, and instead of the best fitting halfspace as a reference model a 2 layer model was used. This model was constructed from the 2D Inversions and reasonably fitted the Resistivity Data. The weighting file increased the smoothing requirement in the X & Y directions (east and north) for the first 9 cells, the approximate thickness of the overburden.

The final inverted volumes generally fit the measured data to a level better than 2% of observed Primary Voltage (DC) and better than 0.25 mV/V on observed Chargeability. That is, all 3D models converged with an extremely close data fit, As with the 2D this is a closeness that would not normally have been sought in routine investigation. The 3D modelling output files are provided on the disk in Appendix 1.

REFERENCES

Key, K., and Ovall, J. (2011). ‘A parallel goal-oriented adaptive finite element method for 2.5-D electromagnetic modelling’, *Geophysical Journal International*, ***186***(1), 137–154.

Oldenburg, D. W. and Li, Y., 1994, ‘Inversion of induced polarization data’, *Geophysics*, **59**, 1327-1341.

Li, Y. and Oldenburg, D. W., 1999, ‘3-D Inversion of induced polarization data’, *Geophysics*, **65**, 1931-1945.

Torres-Verdin C., and Bostick Jr. F.X., 1992, ‘Principles of spatial surface electric field filtering in magnetotellurics: Electromagnetic array profiling (EMAP)', *Geophysics*, **57**, 603-622.

APPENDIX 1 – Digital Data

Disk Number	USB Contents Description	GRS Reference Code
1	Final Report; IP/Resistivity and MT Processed Data; Model Files; Time Series Data & Software.	FAMD186a

APPENDIX 2 – Production Report

Date	Day	Area	Line/ Block	Activity	Comment	Prod	Mob/ Standby /RDO	Down
16/07/ 2017	Sunday			Crew arrives Alice Springs			1	
17/07/ 2017	Monday			Pick up supplies, drive TC			1	
18/07/ 2017	Tuesday	Rover	Rover4	Inductions, get food, head to camp			1	
19/07/ 2017	Wednesday	Rover	Rover4	Layout block		1		
20/07/ 2017	Thursday	Rover	Rover4	Read IP	8Tx	1		
21/07/ 2017	Friday	Rover	Rover4	Read IP	21Tx	1		
22/07/ 2017	Saturday	Rover	Rover4	Read IP + MT	11Tx	1		
23/07/ 2017	Sunday	Rover	Rover 11C	Move Blocks		1		
24/07/ 2017	Monday	Rover	Rover 11C	Set up	Re-supply in town	1		
25/07/ 2017	Tuesday	Rover	Rover 11C	Read IP	13Tx	1		
26/07/ 2017	Wednesday	Rover	Rover 11C	Read IP	20Tx	1		
27/07/ 2017	Thursday	Rover	Rover 11C	Read IP + MT	7Tx	1		
28/07/ 2017	Friday	Rover	Rover 11E	Move Blocks		1		
29/07/ 2017	Saturday	Rover	Rover 11E	Read IP	27Tx	1		
30/07/ 2017	Sunday	Rover	Rover 11E	Read IP + MT	13Tx	1		
31/07/ 2017	Monday	Rover		Pack up and head to Tennant Creek		1		
01/08/ 2017	Tuesday			Mob TC - Cloncurry			1	
02/08/ 2017	Wednesday			Mob Cloncurry - Tambo			1	
03/08/ 2017	Thursday			Mob Tambo - Darra			1	

APPENDIX 3 – Data / Models / Model Fits Plots

MARE2DEM MT Resistivity Model

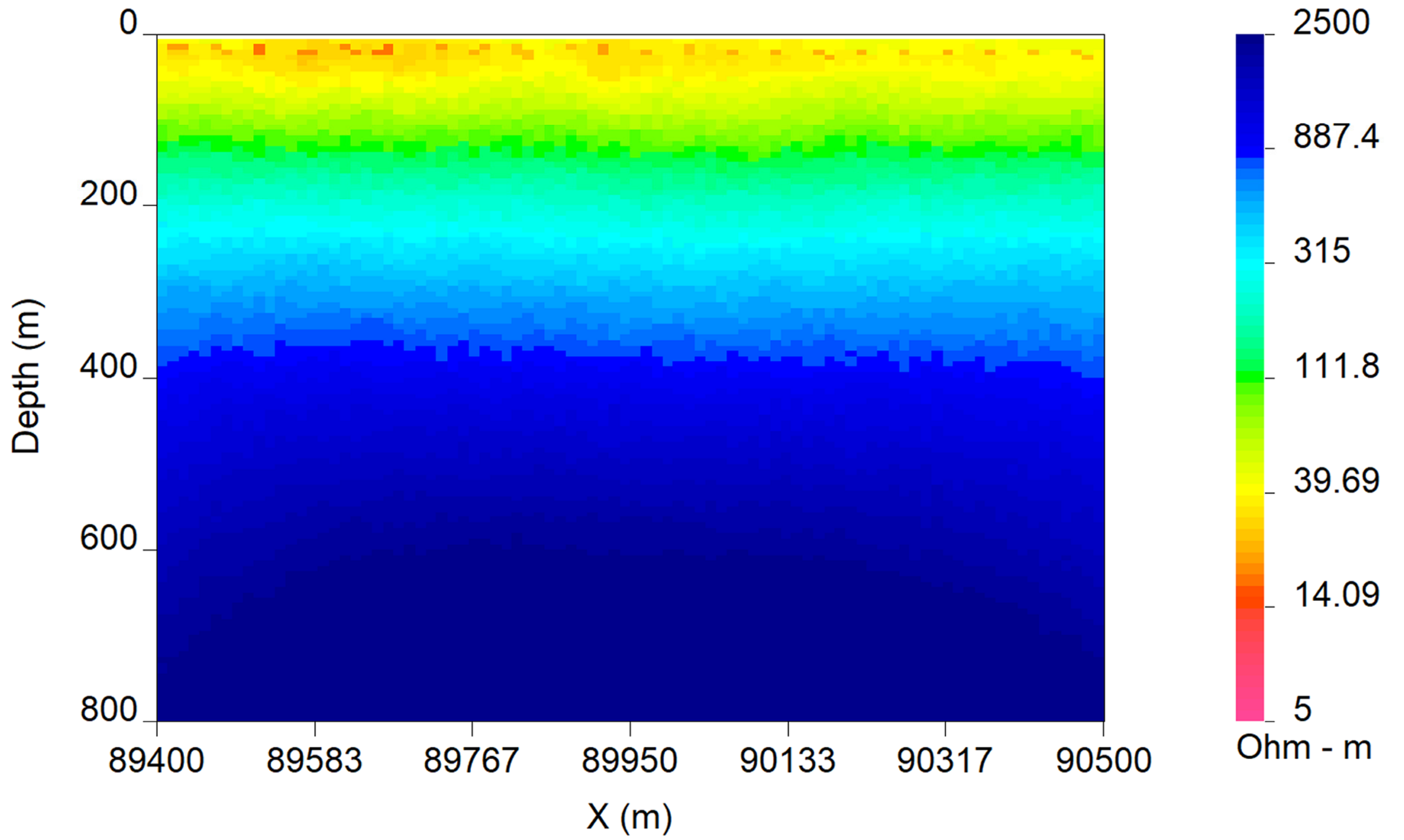

UBC2D Resistivity Model

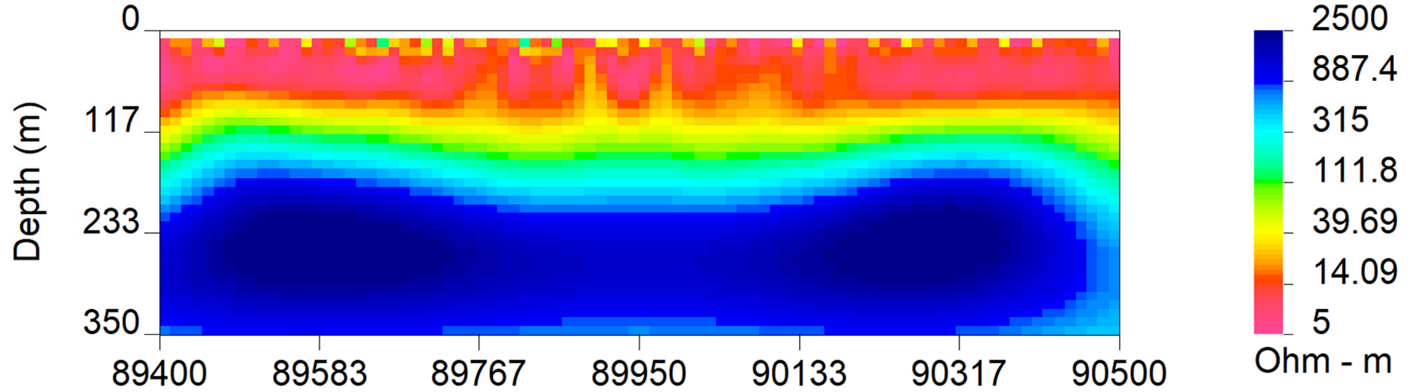

UBC2D Chargeability Model

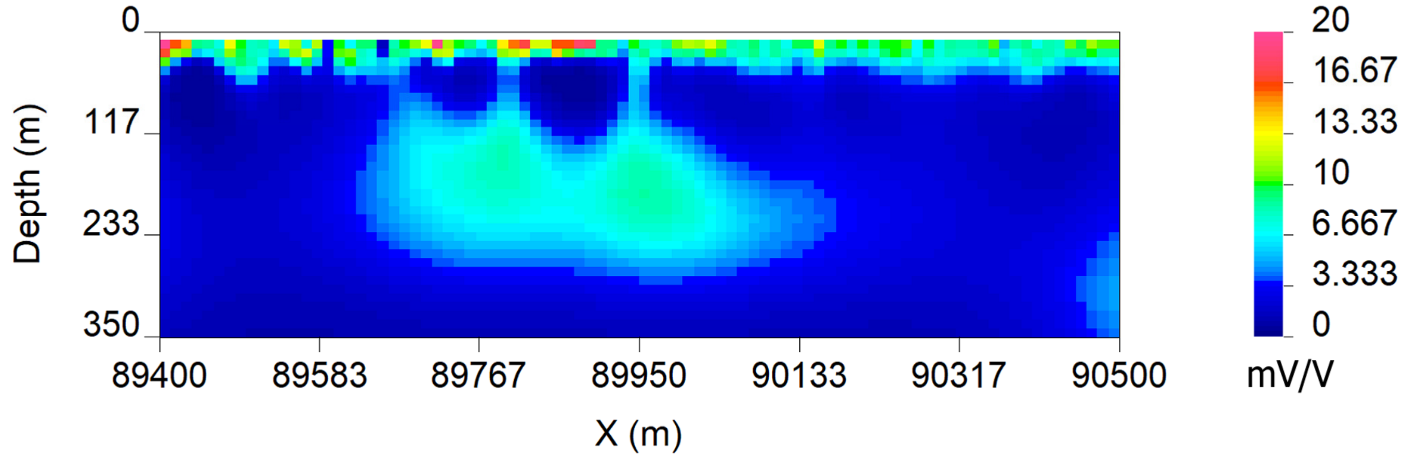

Geophysical Resources & Services
MARE2DEM/UBC2D Models Line 360275E
Prospect : Rover 4 08/2017

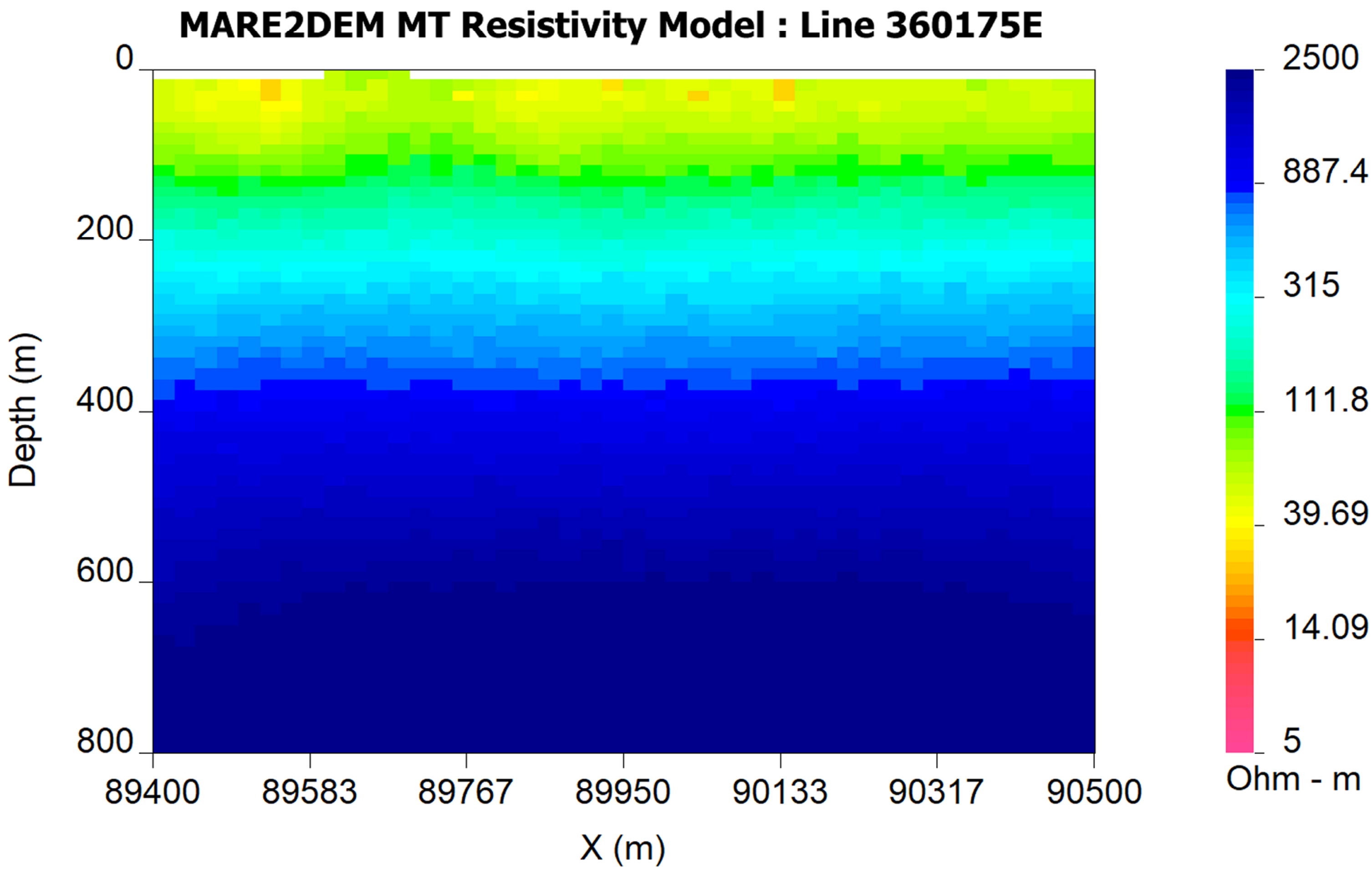

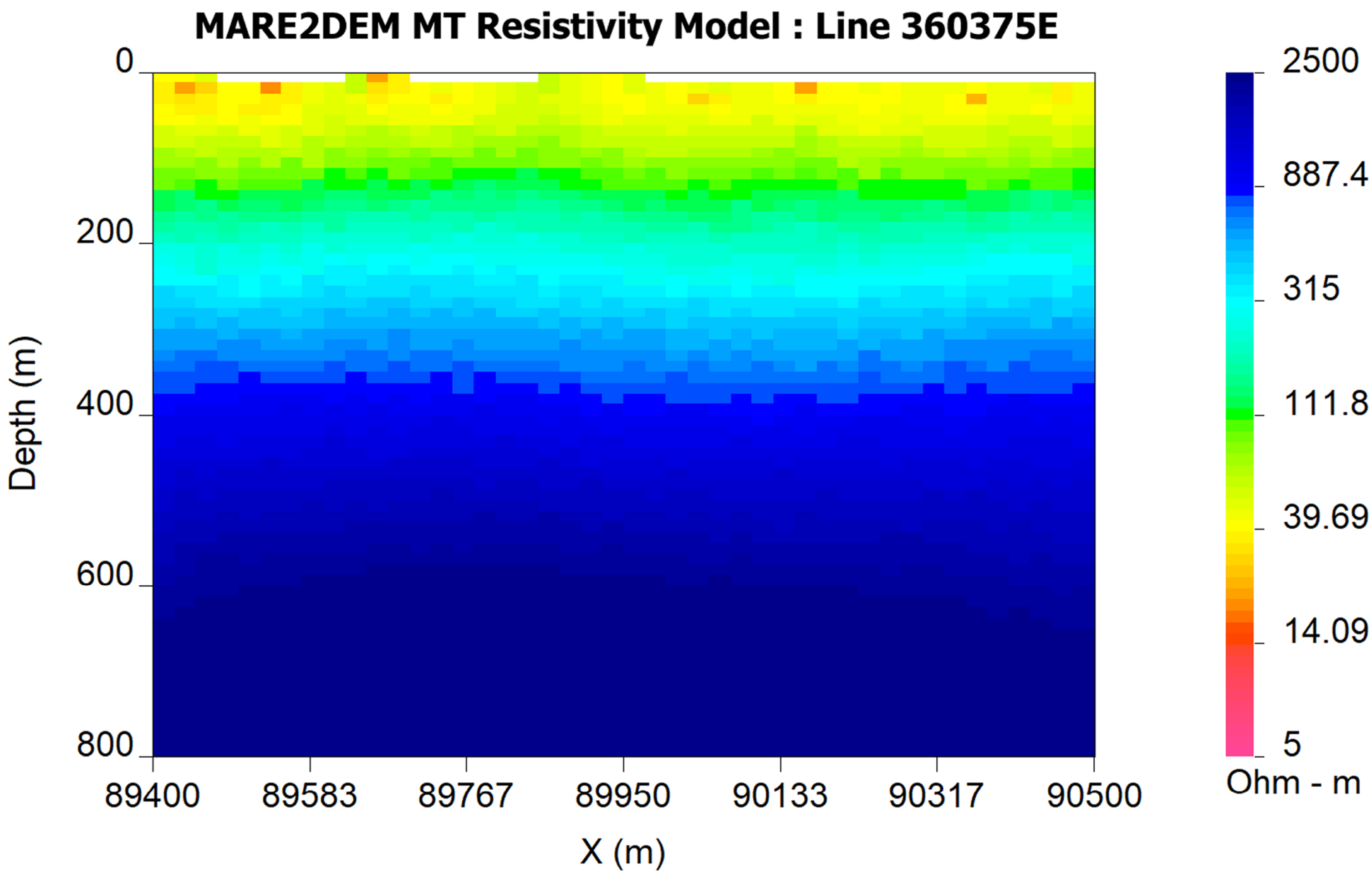

Geophysical Resources & Services
MARE2DEM Models Lines 360175E & 360375E
Prospect : Rover 4 09/2017

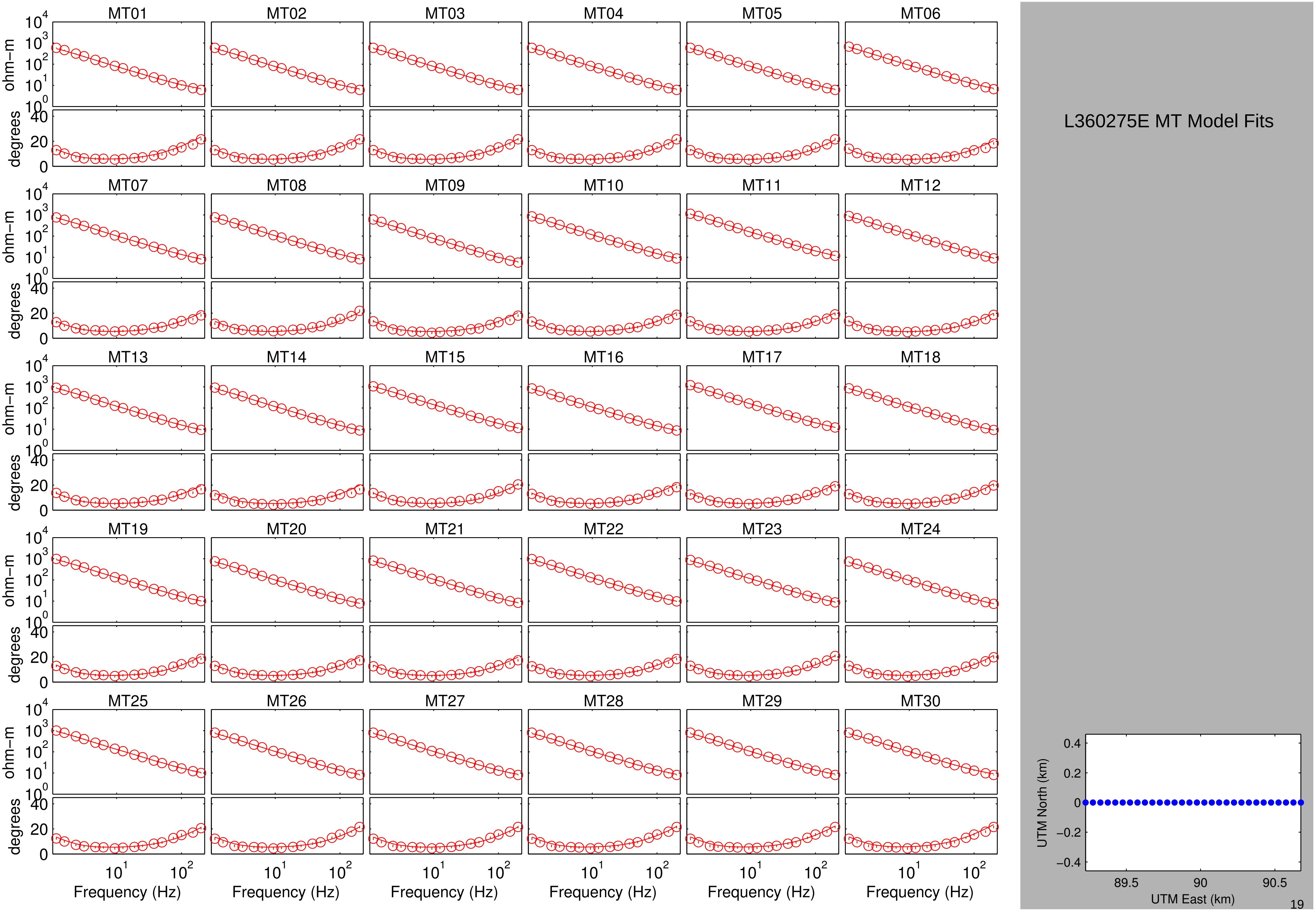
L360275E MT Model Fits
MT01
MT02
MT03
MT04
MT05
MT06
MT07
MT08
MT09
MT10
MT11
MT12
MT13
MT14
MT15
MT16
MT17
MT18
MT19
MT20
MT21
MT22
MT23
MT24
MT25
MT26
MT27
MT28
MT29
MT30
ohm−m
degrees
Frequency (Hz)
UTM North (km)
UTM East (km)

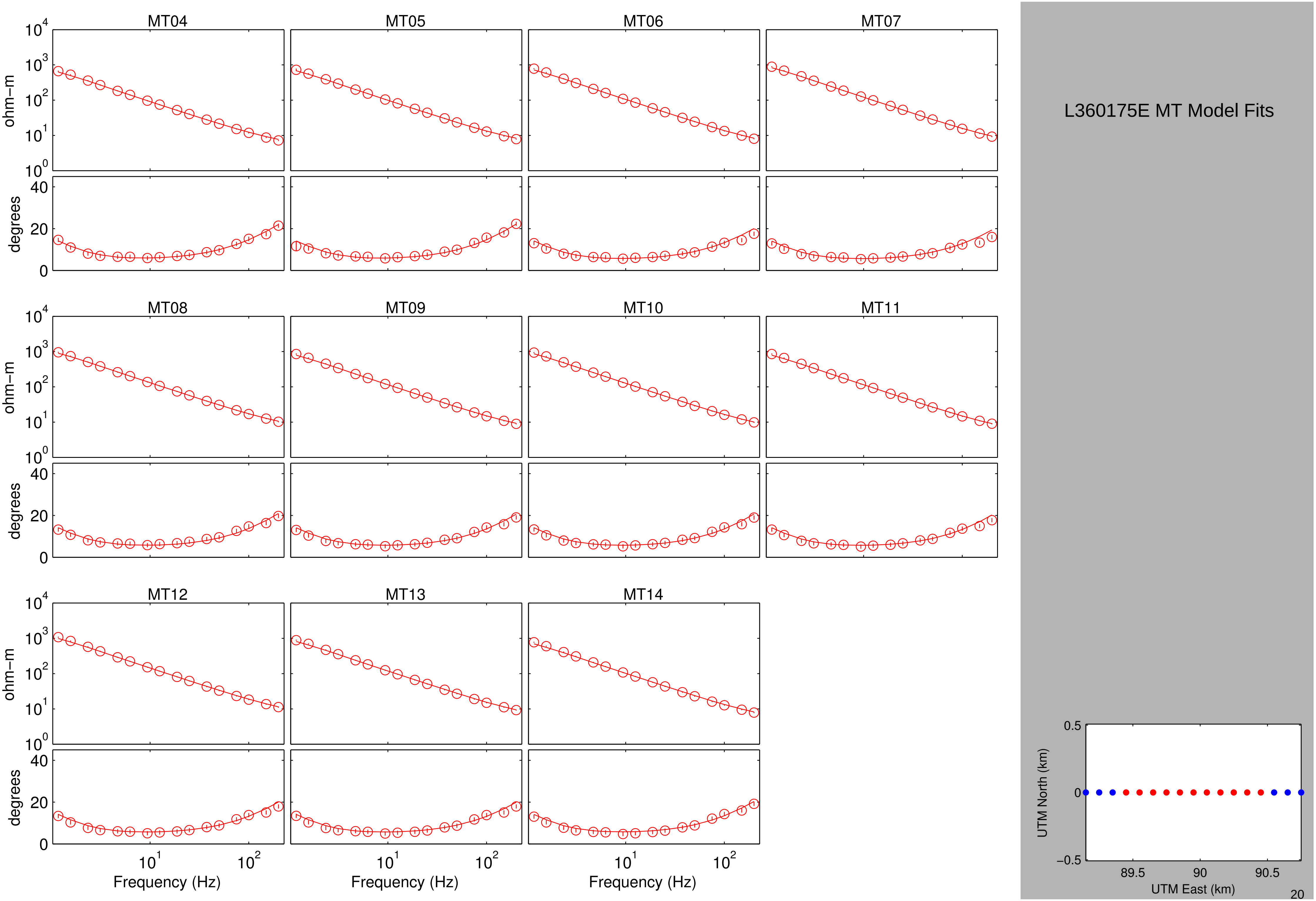

L360175E MT Model Fits
MT04
MT05
MT06
MT07
MT08
MT09
MT10
MT11
MT12
MT13
MT14
ohm−m
degrees
Frequency (Hz)
UTM North (km)
UTM East (km)

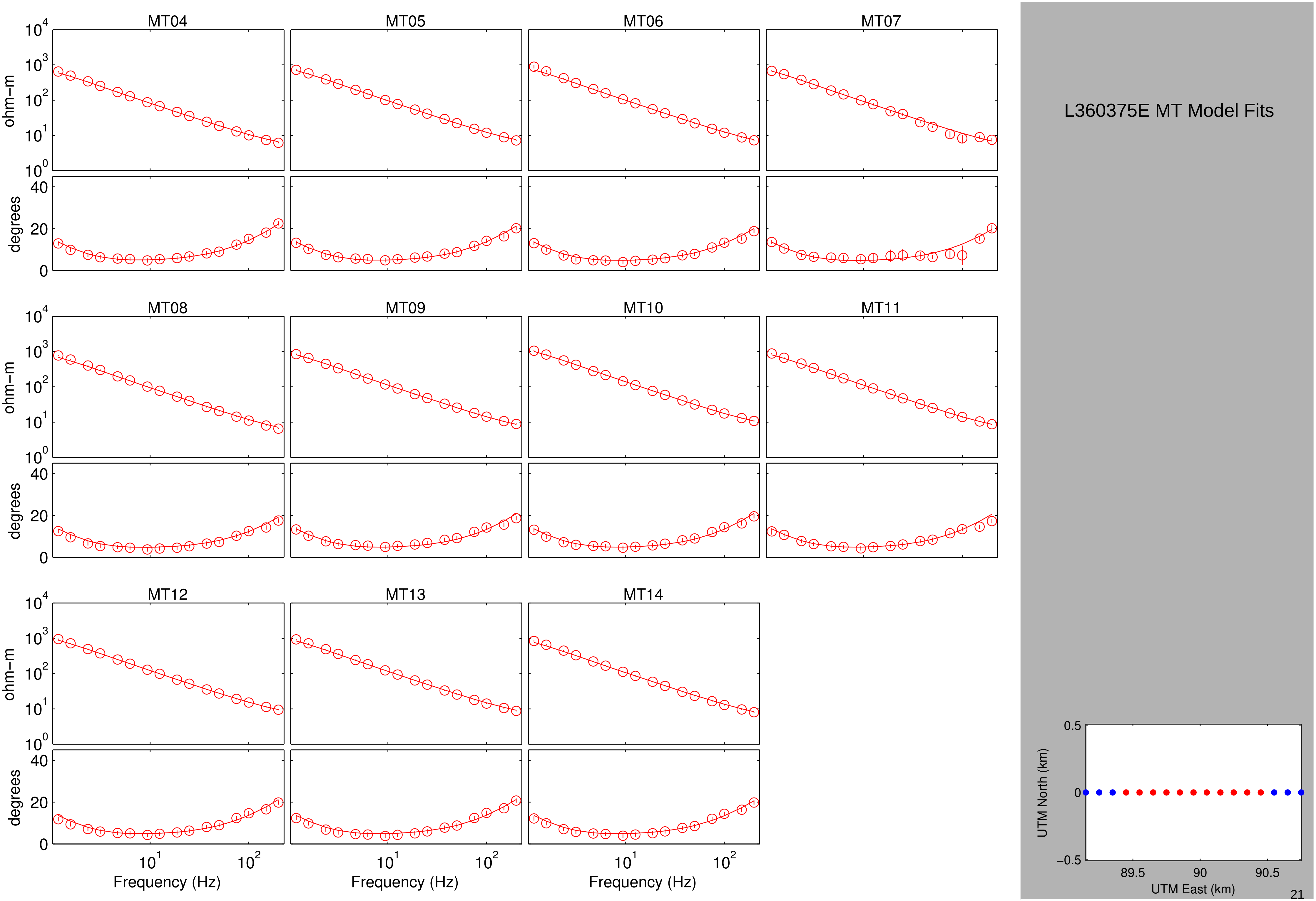
MT04
MT05
MT06
MT07
MT08
MT09
MT10
MT11
MT12
MT13
MT14
ohm−m
degrees
Frequency (Hz)
L360375E MT Model Fits
UTM North (km)
UTM East (km)
89.5
90
90.5
0.5
0
−0.5

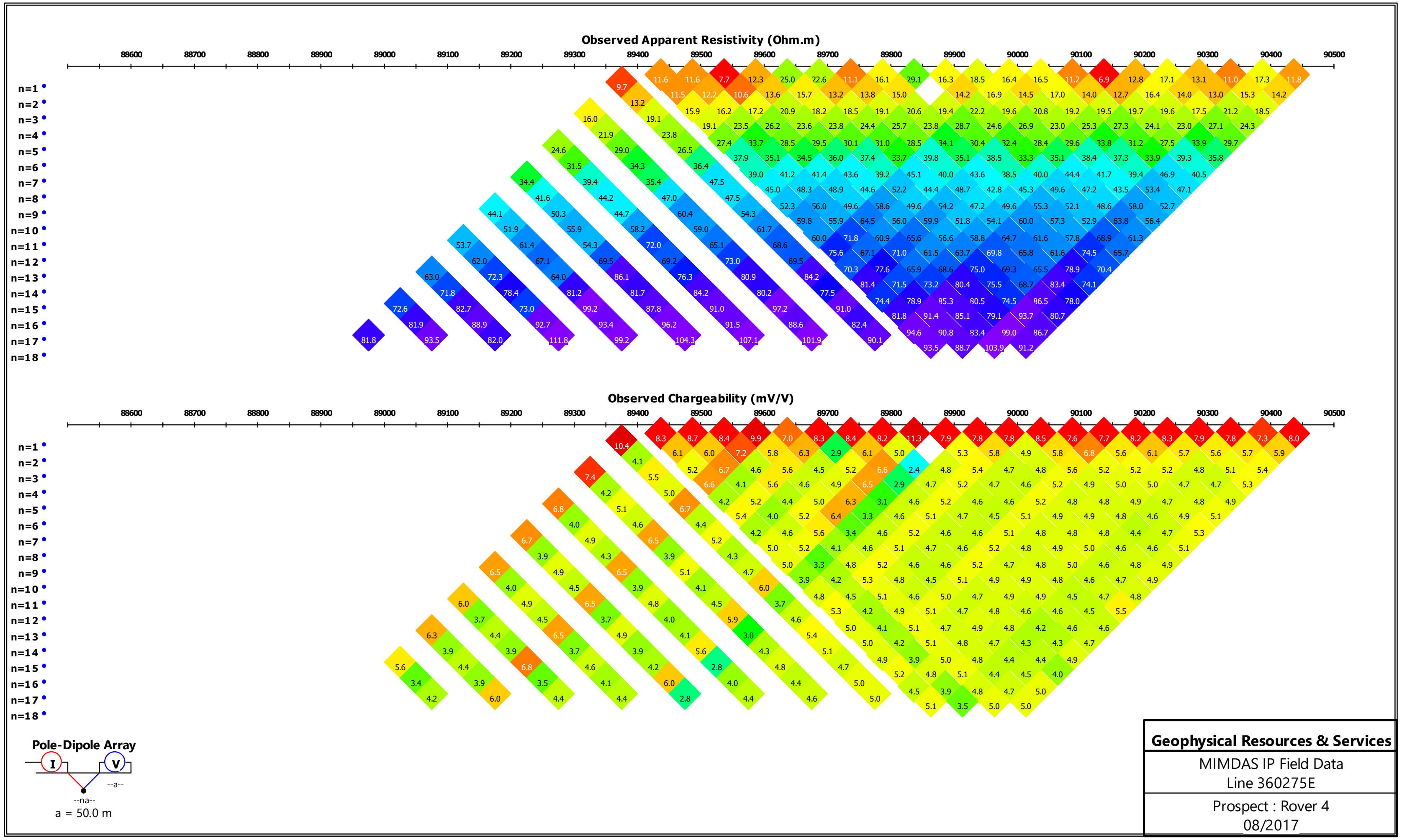

Observed Apparent Resistivity (Ohm.m)
88600 88700 88800 88900 89000 89100 89200 89300 89400 89500 89600 89700 89800 89900 90000 90100 90200 90300 90400 90500
n=1 n=2 n=3 n=4 n=5 n=6 n=7 n=8 n=9 n=10 n=11 n=12 n=13 n=14 n=15 n=16 n=17 n=18
Observed Chargeability (mV/V)
88600 88700 88800 88900 89000 89100 89200 89300 89400 89500 89600 89700 89800 89900 90000 90100 90200 90300 90400 90500
n=1 n=2 n=3 n=4 n=5 n=6 n=7 n=8 n=9 n=10 n=11 n=12 n=13 n=14 n=15 n=16 n=17 n=18
Pole-Dipole Array
I
V
--a--
--na--
a = 50.0 m
Geophysical Resources & Services
MIMDAS IP Field Data
Line 360275E
Prospect : Rover 4
08/2017

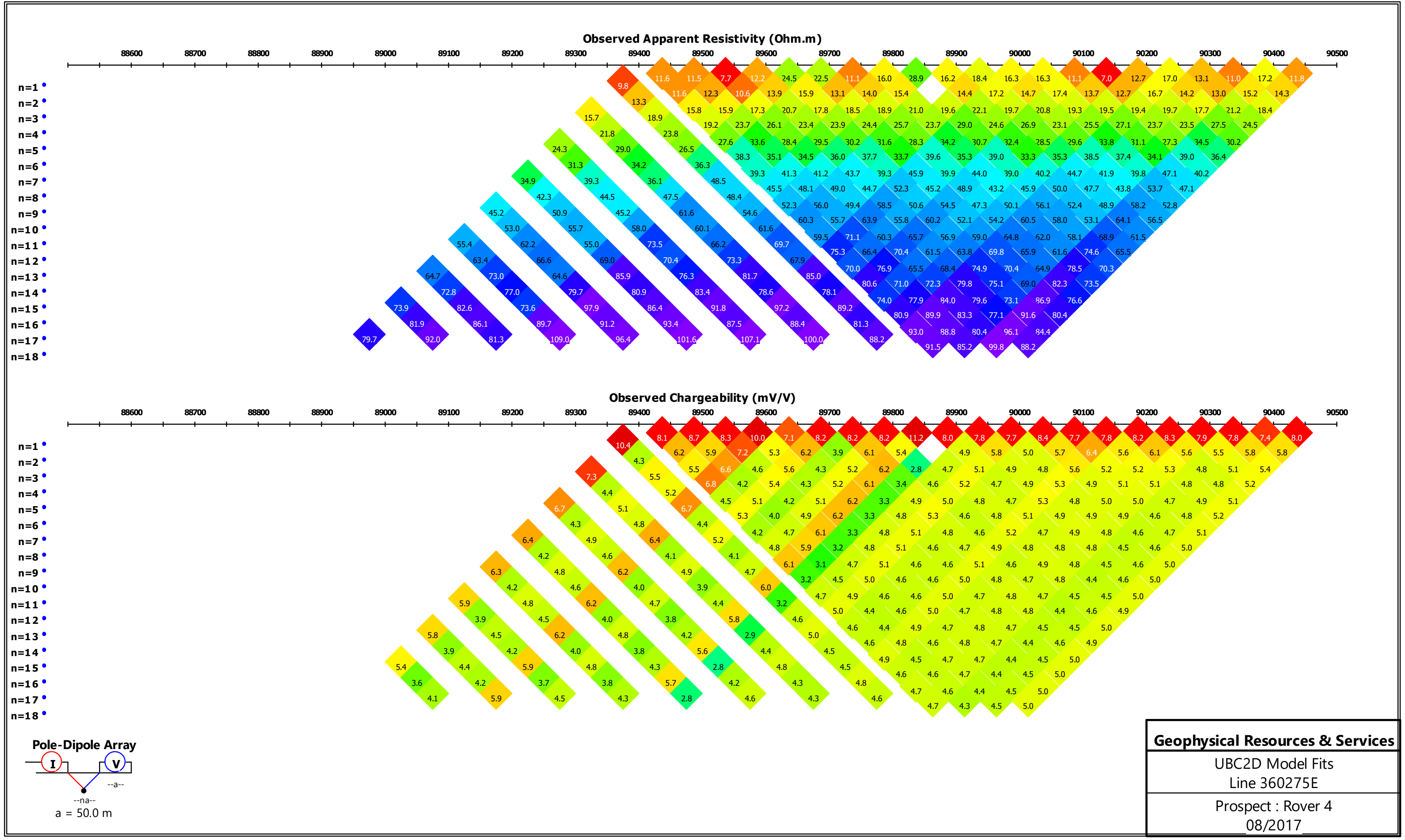
Observed Apparent Resistivity (Ohm.m)
88600 88700 88800 88900 89000 89100 89200 89300 89400 89500 89600 89700 89800 89900 90000 90100 90200 90300 90400 90500
n=1 n=2 n=3 n=4 n=5 n=6 n=7 n=8 n=9 n=10 n=11 n=12 n=13 n=14 n=15 n=16 n=17 n=18
Observed Chargeability (mV/V)
88600 88700 88800 88900 89000 89100 89200 89300 89400 89500 89600 89700 89800 89900 90000 90100 90200 90300 90400 90500
n=1 n=2 n=3 n=4 n=5 n=6 n=7 n=8 n=9 n=10 n=11 n=12 n=13 n=14 n=15 n=16 n=17 n=18
Pole-Dipole Array
I
V
--a--
--na--
a = 50.0 m
Geophysical Resources & Services
UBC2D Model Fits
Line 360275E
Prospect : Rover 4
08/2017

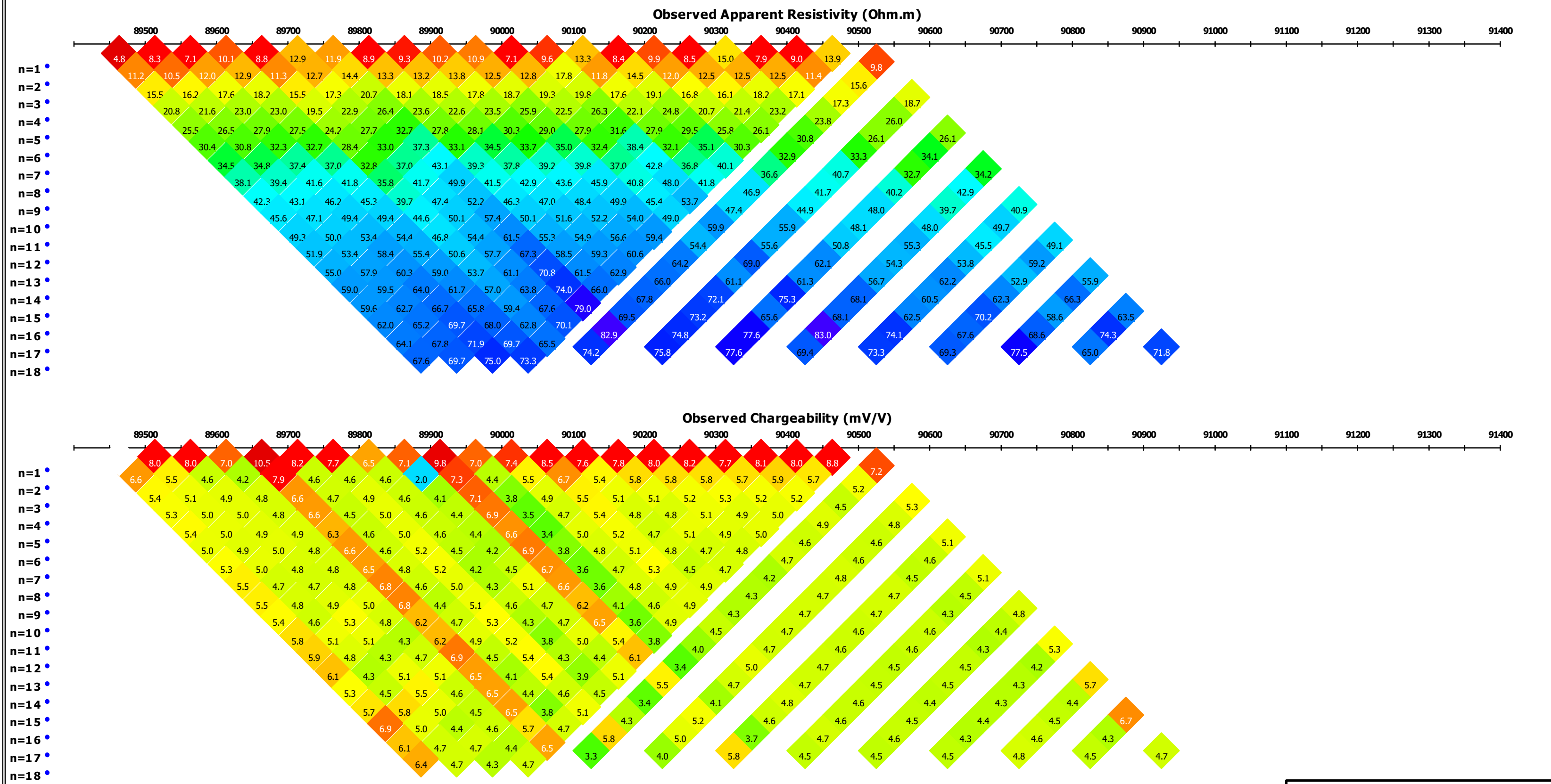

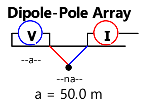

Geophysical Resources & Services

MIMDAS IP Field Data
Line 360275E

Prospect : Rover 4
08/2017

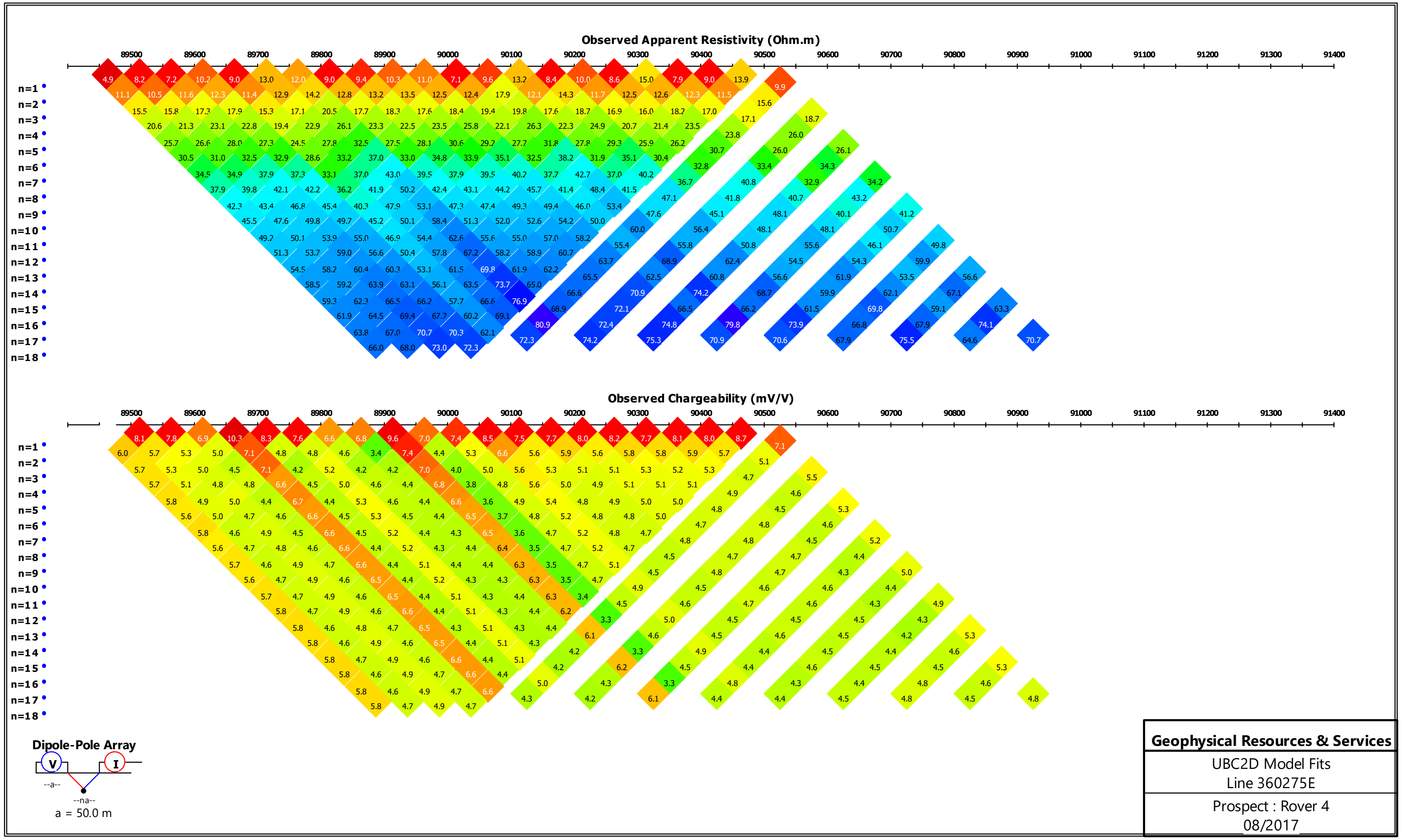

Observed Apparent Resistivity (Ohm.m)
Observed Chargeability (mV/V)
89500
89600
89700
89800
89900
90000
90100
90200
90300
90400
90500
90600
90700
90800
90900
91000
91100
91200
91300
91400
n=1
n=2
n=3
n=4
n=5
n=6
n=7
n=8
n=9
n=10
n=11
n=12
n=13
n=14
n=15
n=16
n=17
n=18
Dipole-Pole Array
V
I
--a--
--na--
a = 50.0 m
Geophysical Resources & Services
UBC2D Model Fits
Line 360275E
Prospect : Rover 4
08/2017

MARE2DEM MT Resistivity Model

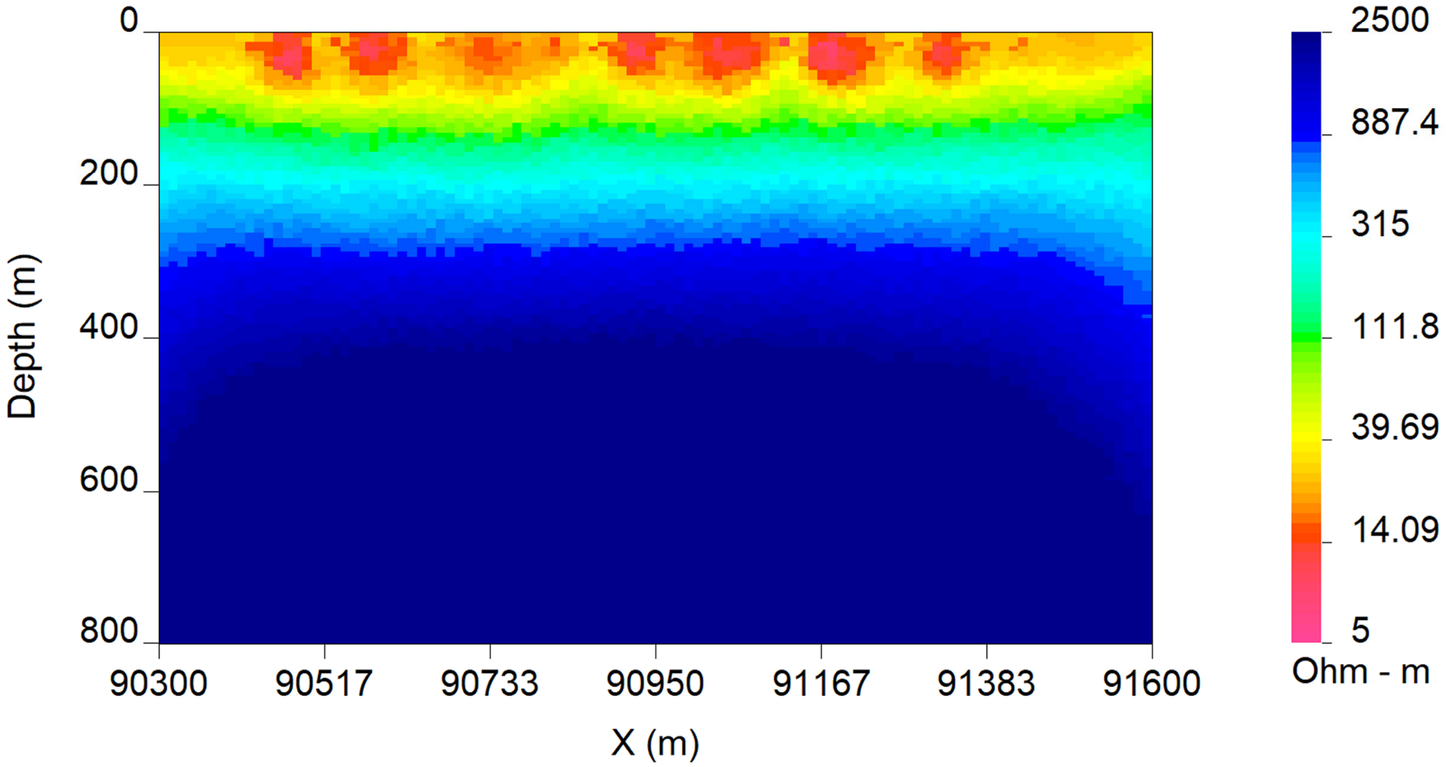

UBC2D Resistivity Model

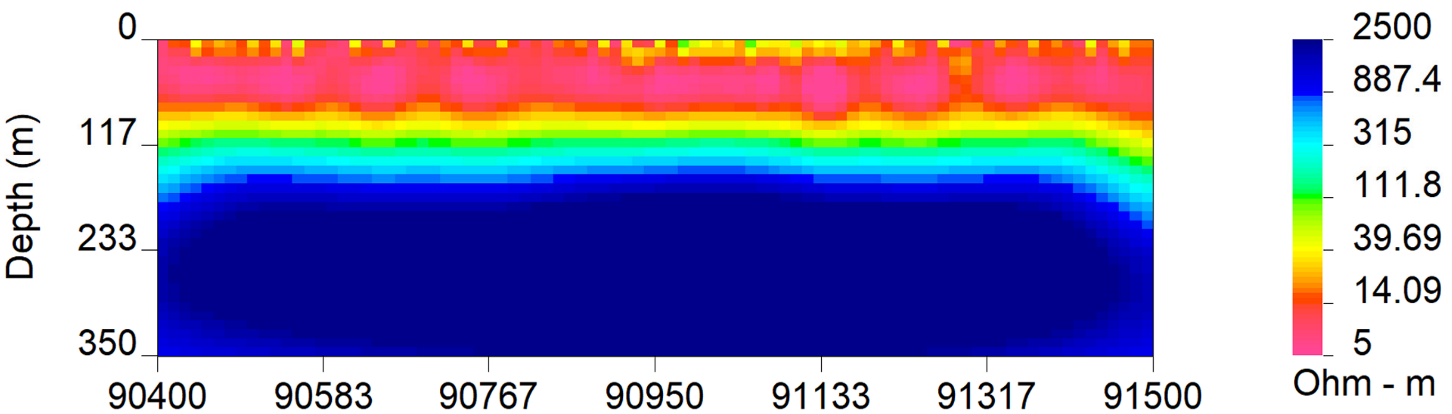

UBC2D Chargeability Model

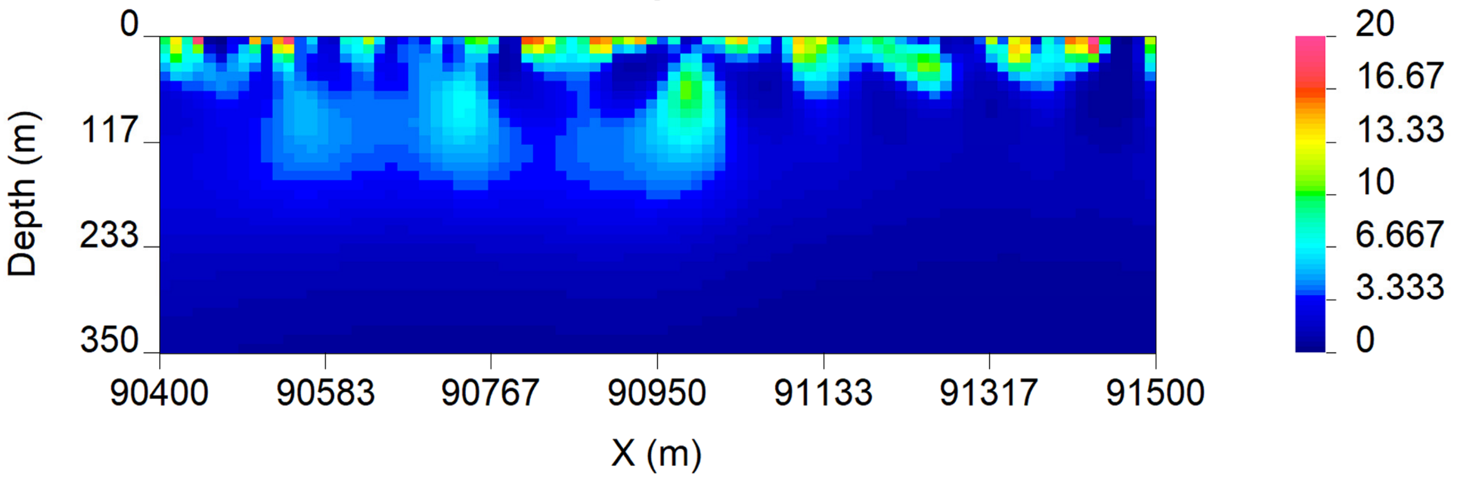

Geophysical Resources & Services
MARE2DEM/UBC2D Models Line 348650E
Prospect : Rover 11C 08/2017

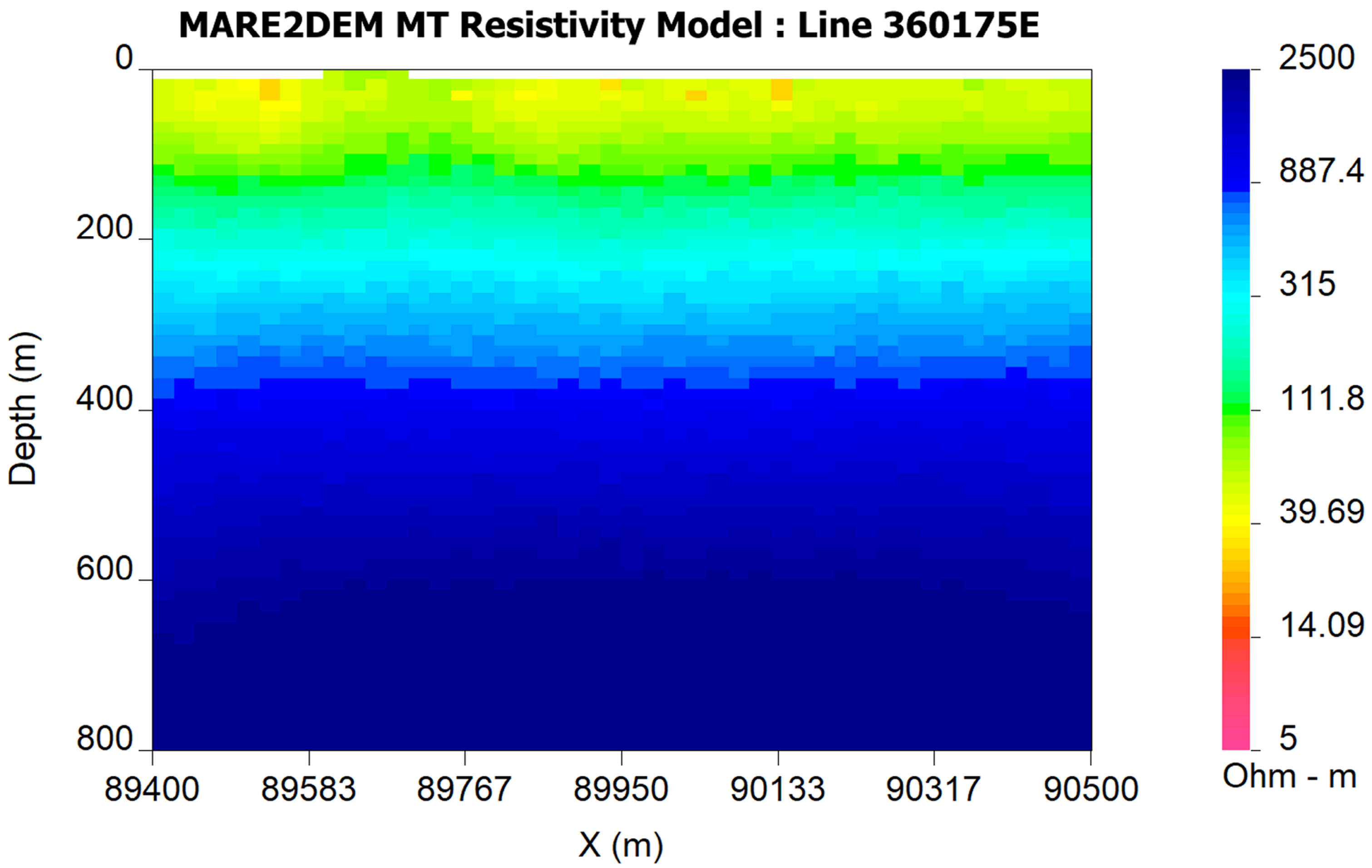

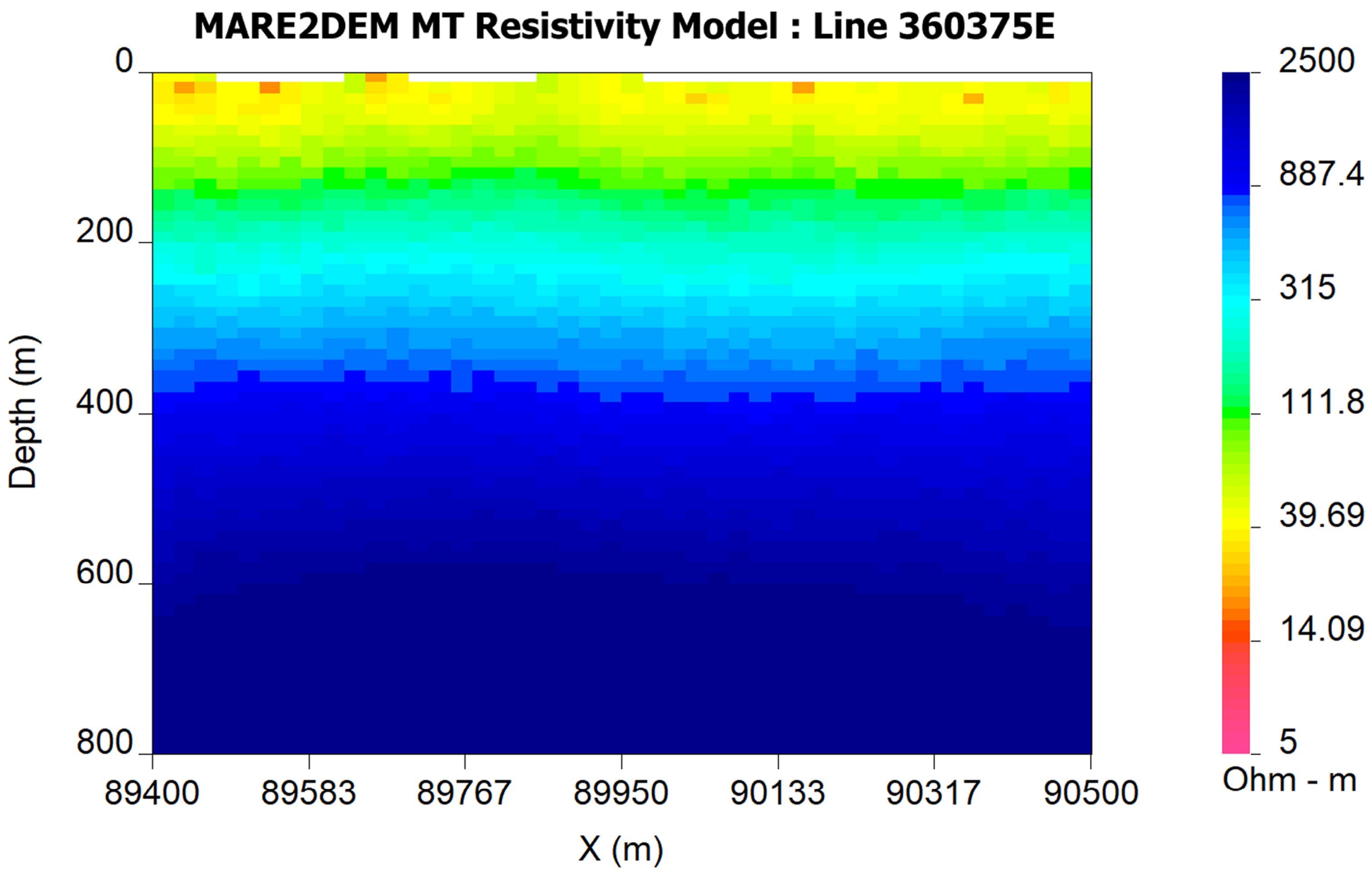

Geophysical Resources & Services

MARE2DEM Models
Lines 360175E & 360375E

Prospect : Rover 4
09/2017

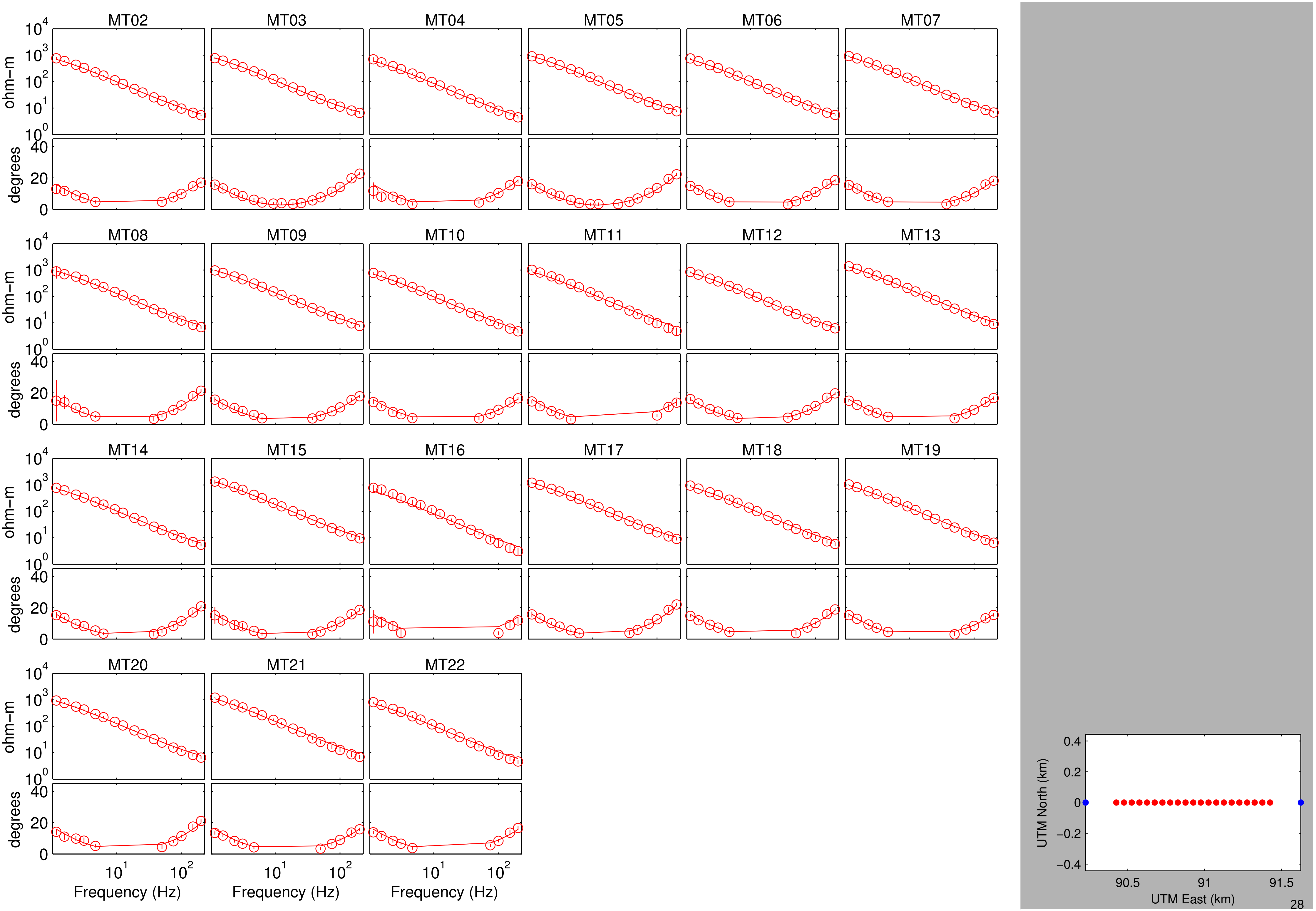
MT02
MT03
MT04
MT05
MT06
MT07
MT08
MT09
MT10
MT11
MT12
MT13
MT14
MT15
MT16
MT17
MT18
MT19
MT20
MT21
MT22
ohm−m
degrees
Frequency (Hz)
UTM North (km)
UTM East (km)

L348550E MT Model Fits

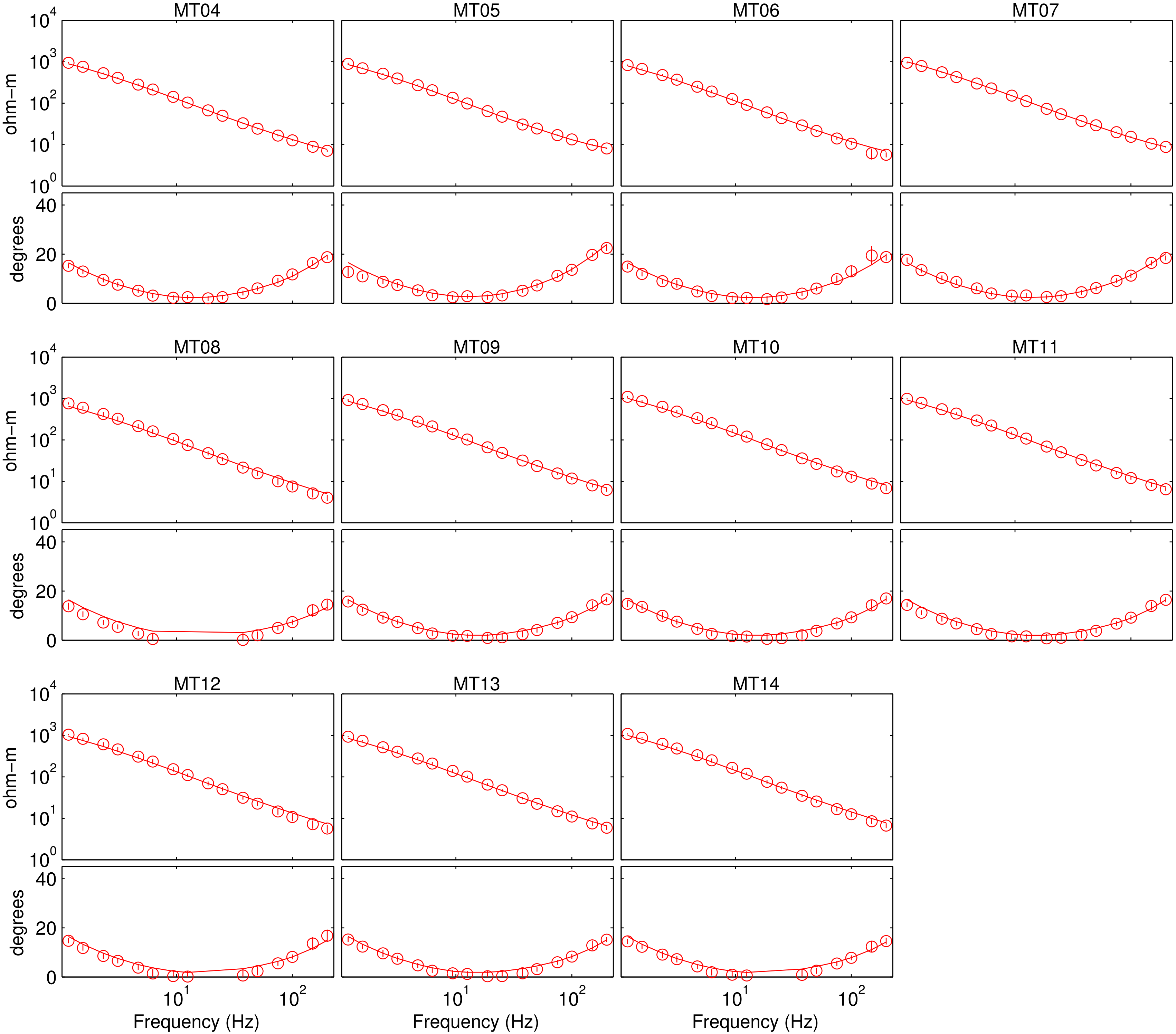

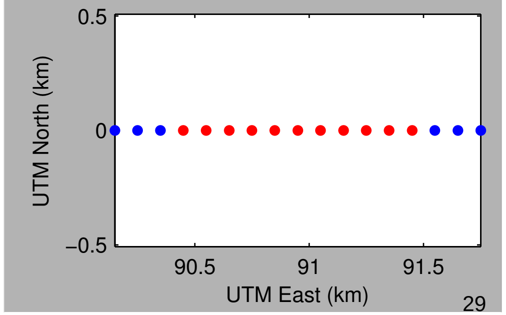

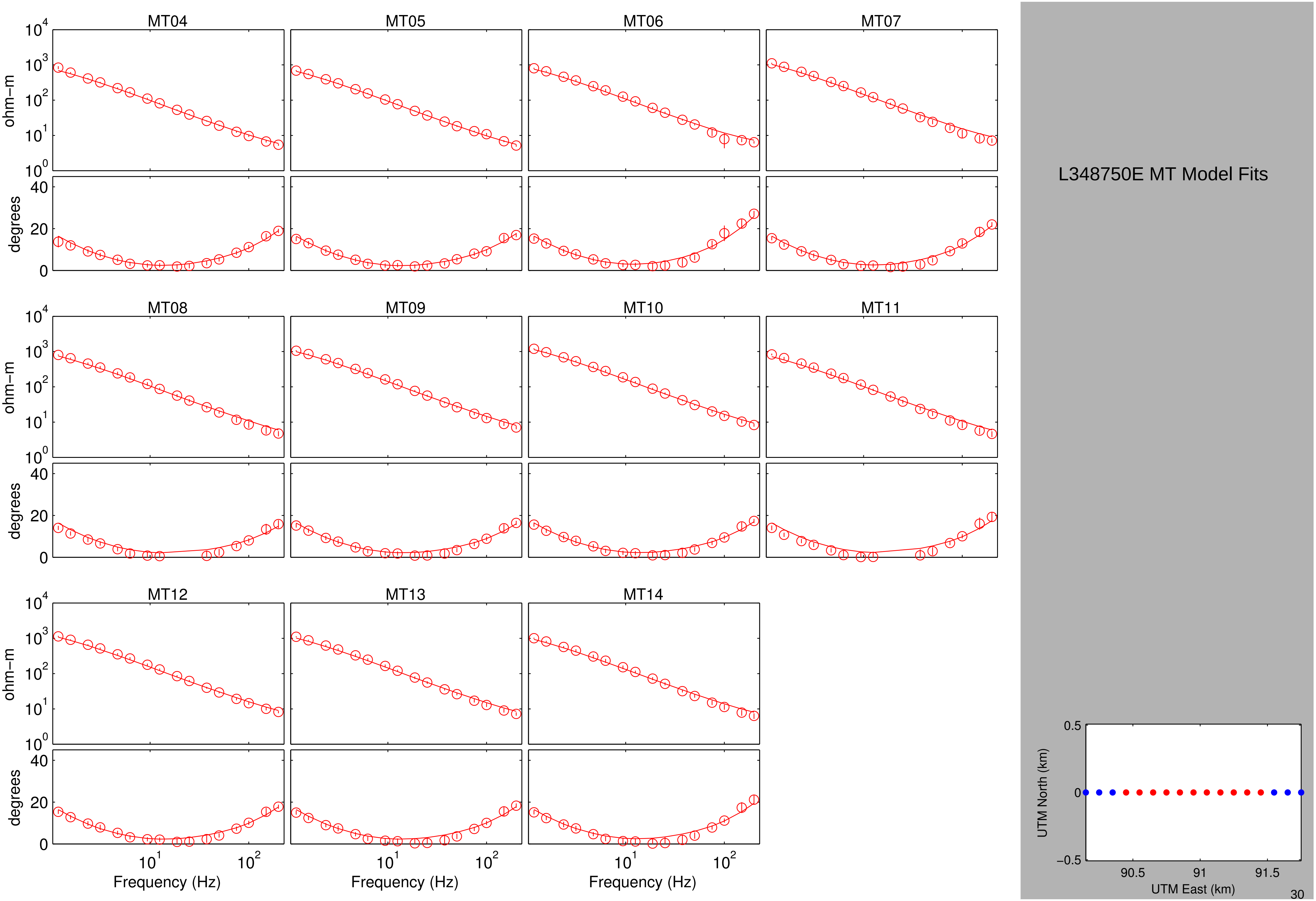
L348750E MT Model Fits
MT04
MT05
MT06
MT07
MT08
MT09
MT10
MT11
MT12
MT13
MT14
ohm−m
degrees
Frequency (Hz)
UTM North (km)
UTM East (km)

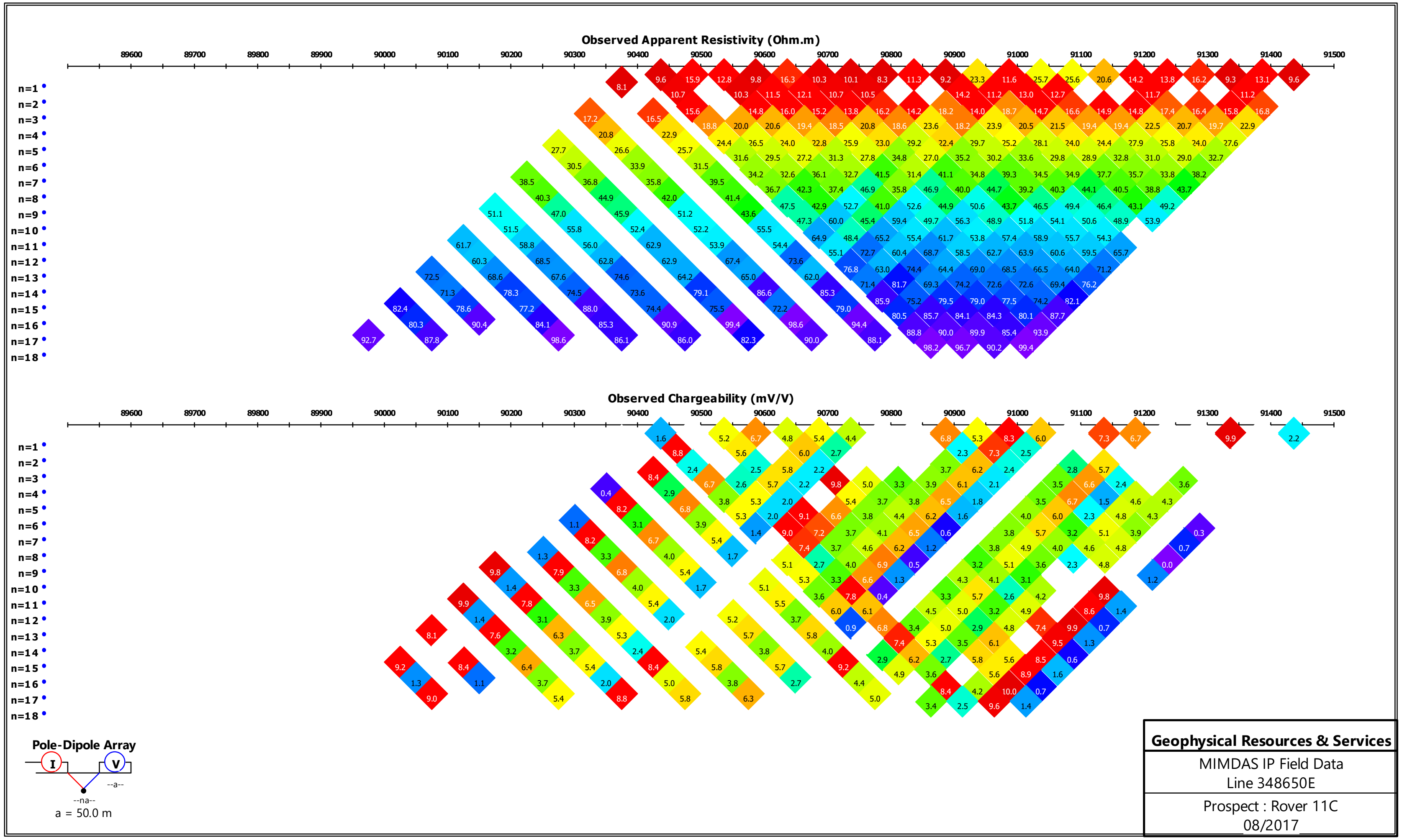
Observed Apparent Resistivity (Ohm.m)
Observed Chargeability (mV/V)
Pole-Dipole Array
a = 50.0 m
Geophysical Resources & Services
MIMDAS IP Field Data
Line 348650E
Prospect : Rover 11C
08/2017

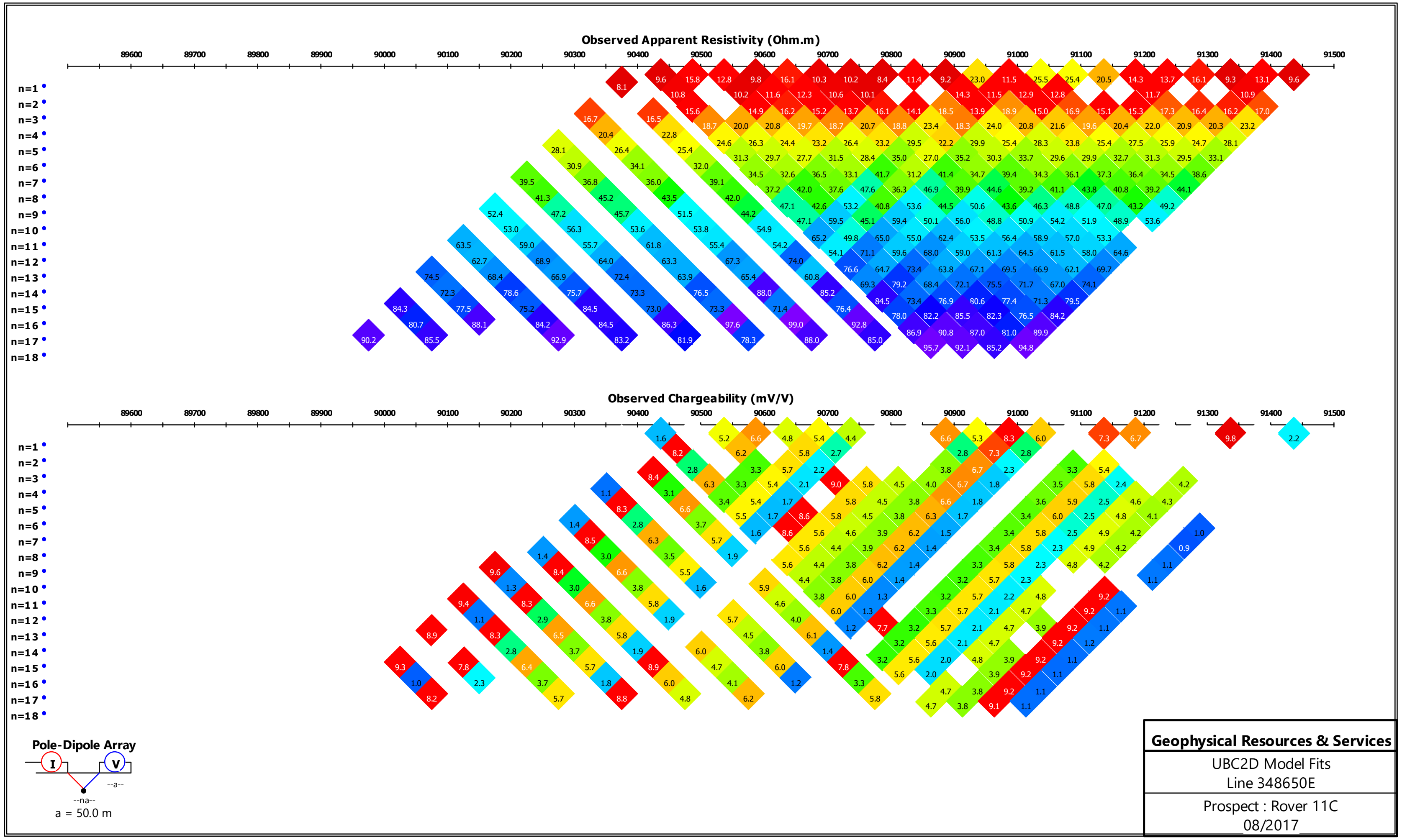
Observed Apparent Resistivity (Ohm.m)
Observed Chargeability (mV/V)
Pole-Dipole Array
a = 50.0 m
Geophysical Resources & Services
UBC2D Model Fits
Line 348650E
Prospect : Rover 11C
08/2017

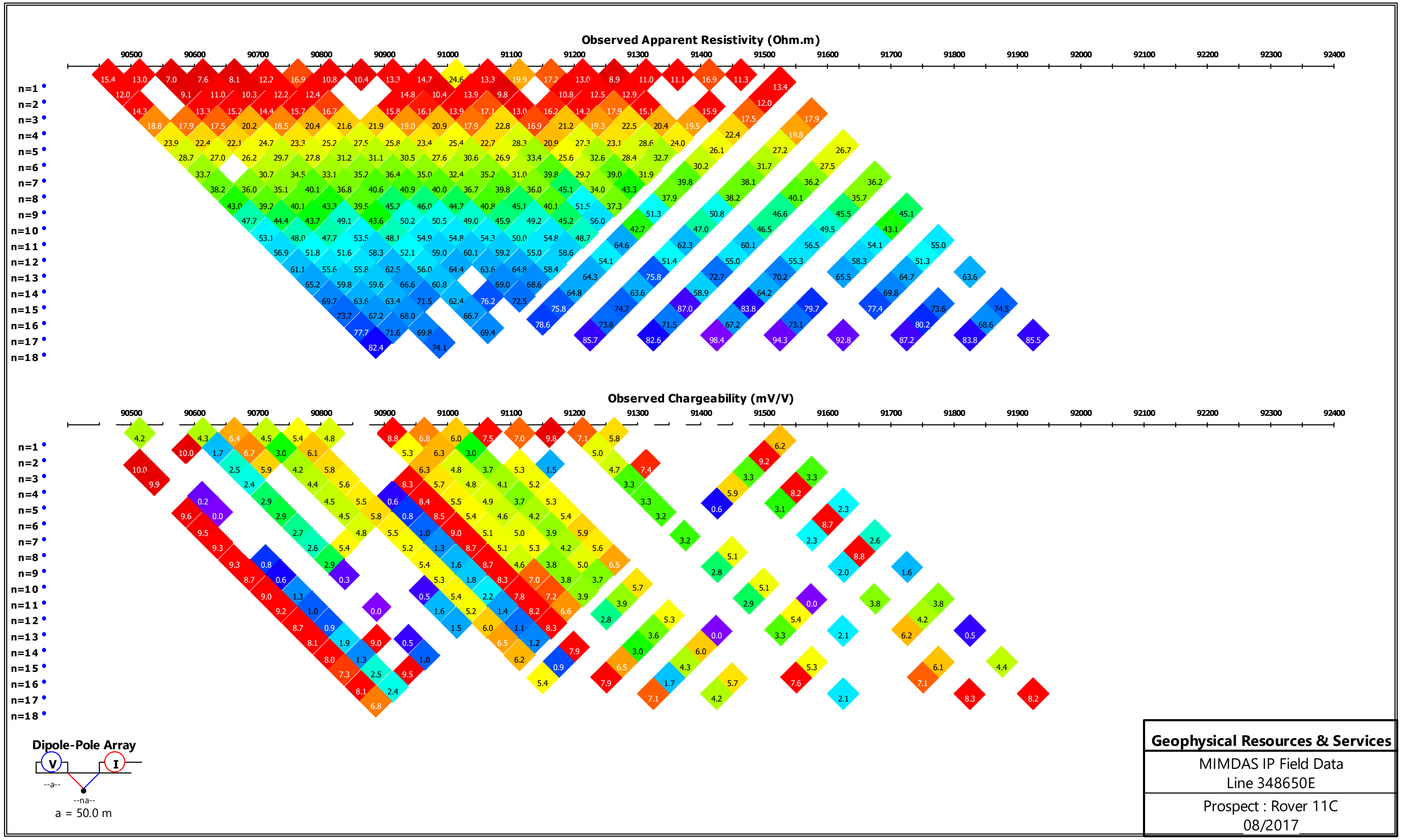

Observed Apparent Resistivity (Ohm.m)
Observed Chargeability (mV/V)
Dipole-Pole Array
a = 50.0 m
Geophysical Resources & Services
MIMDAS IP Field Data
Line 348650E
Prospect : Rover 11C
08/2017

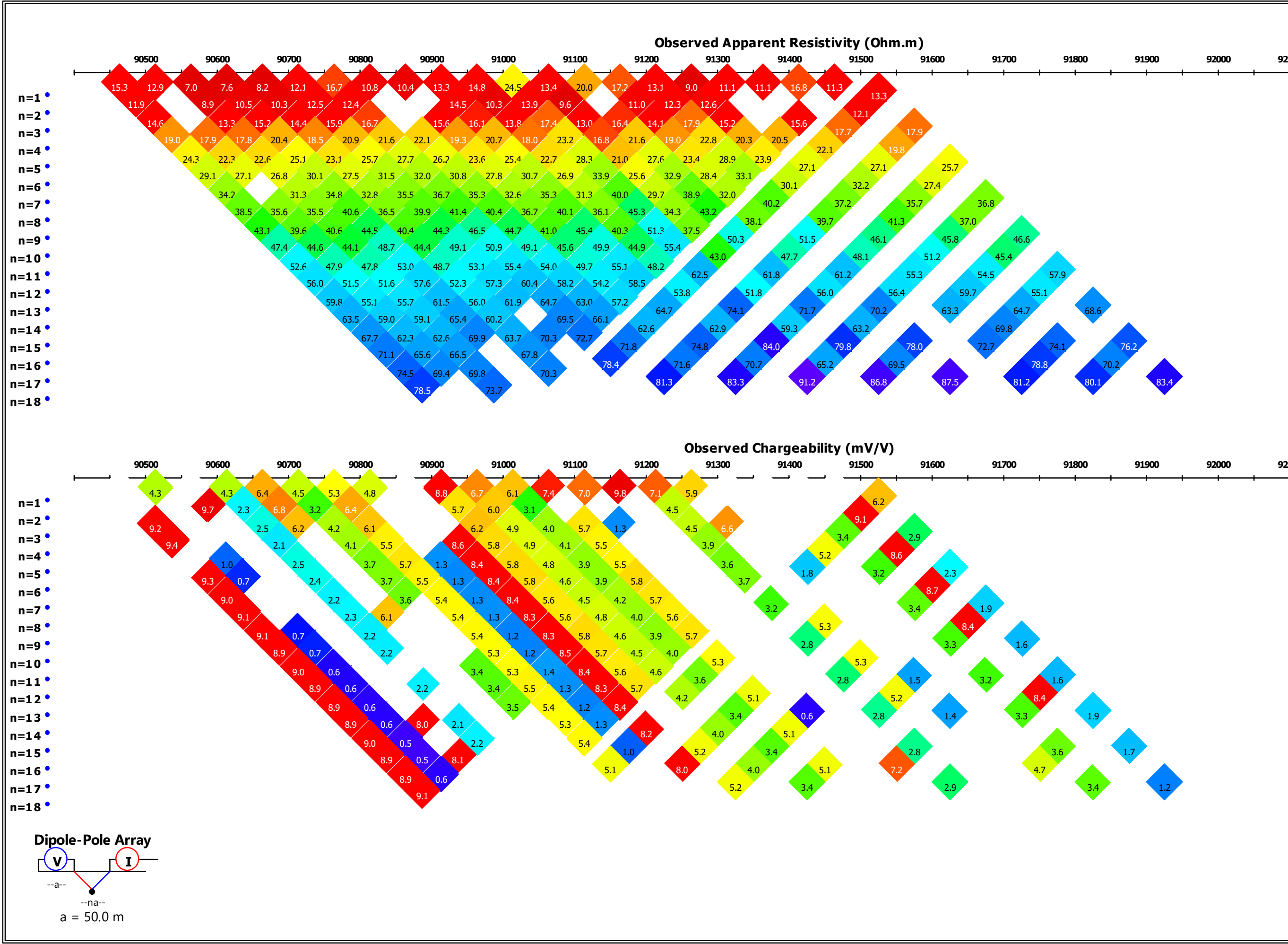

Geophysical Resources & Services

UBC2D Model Fits
Line 348650E

Prospect : Rover 11C
08/2017

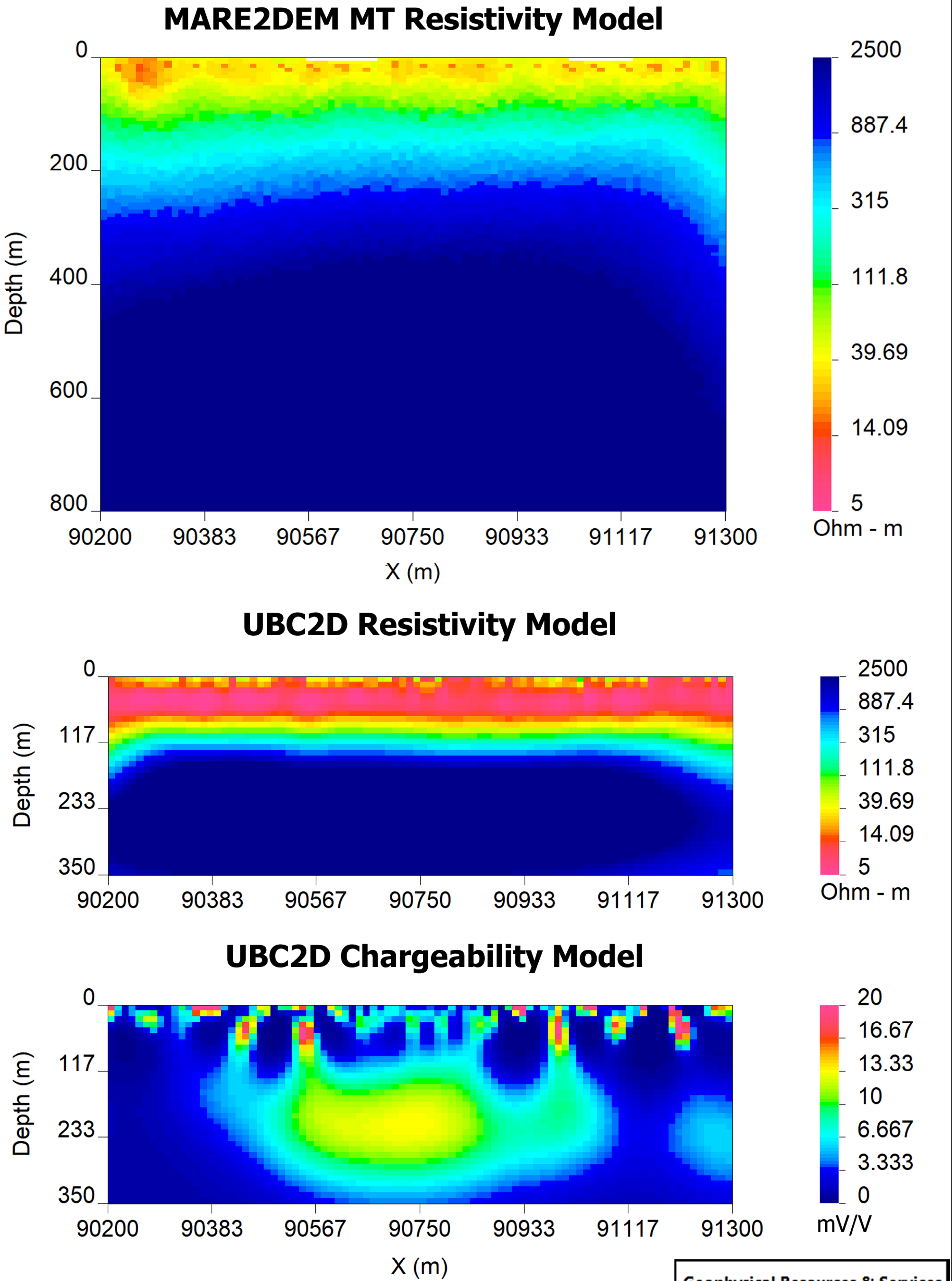

Geophysical Resources & Services

MARE2DEM/UBC2D Models
Line 349425E

Prospect : Rover 11E
08/2017

MARE2DEM MT Resistivity Model : Line 349325E

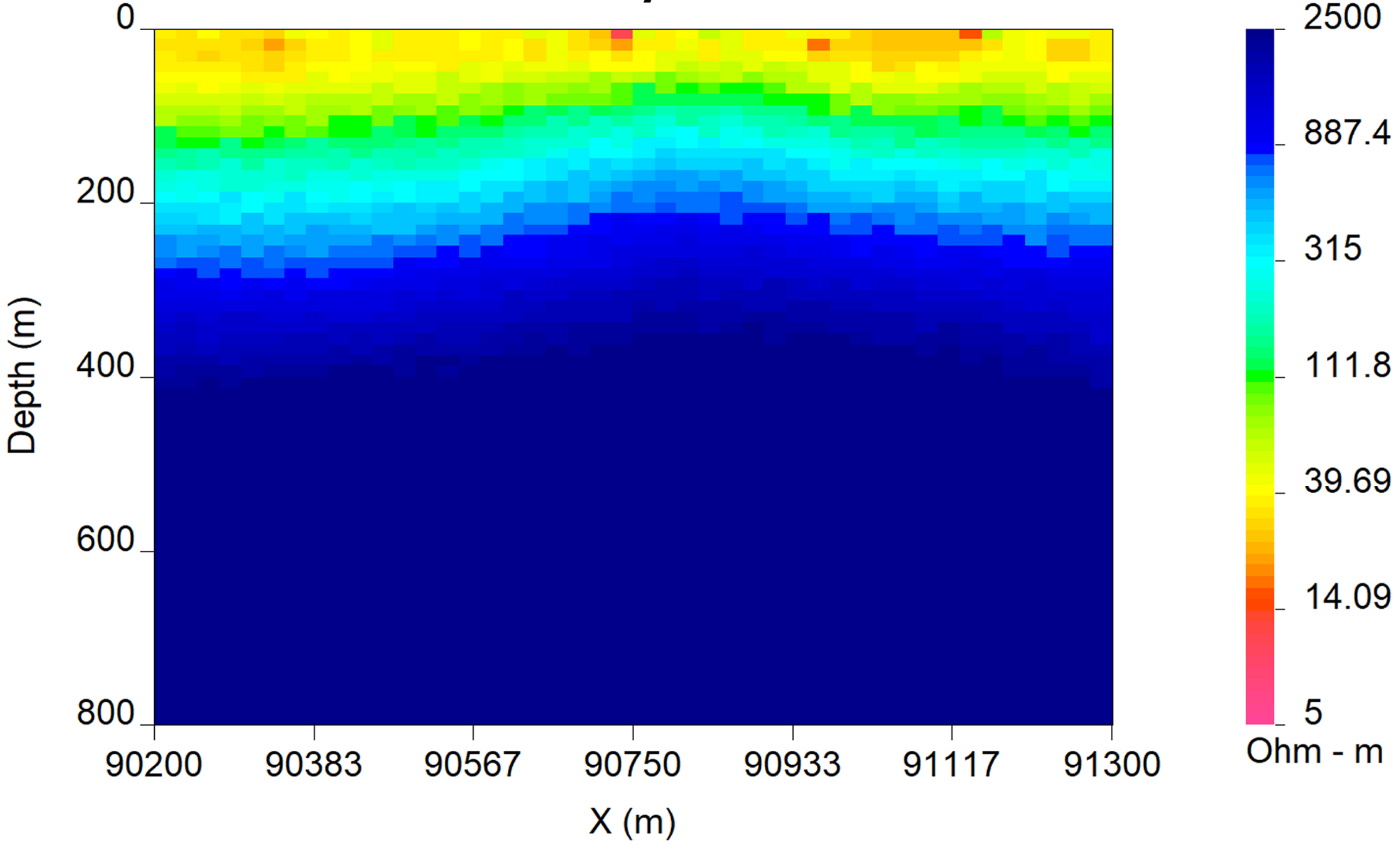

MARE2DEM MT Resistivity Model : Line 349525E

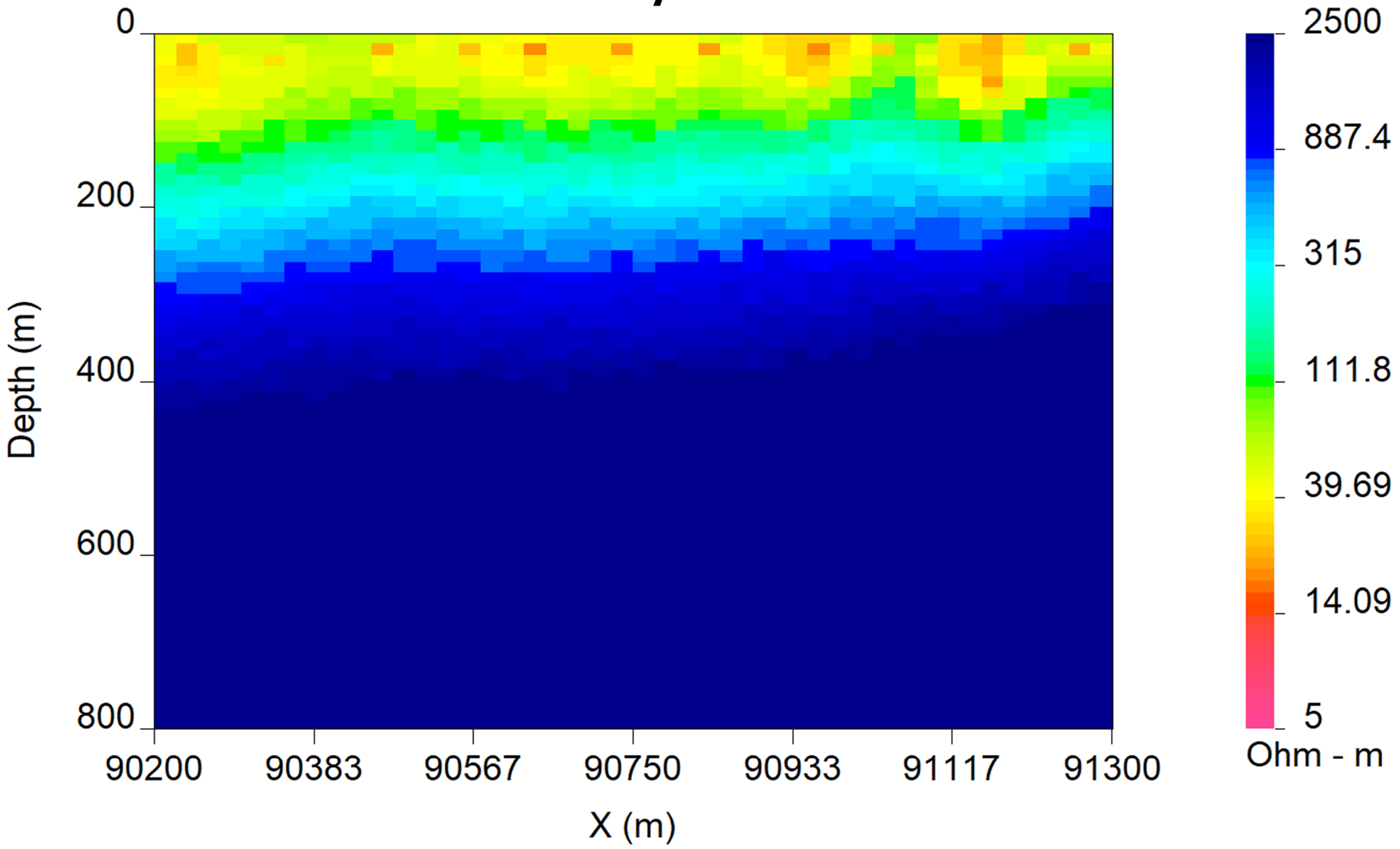

Geophysical Resources & Services
MARE2DEM Models Lines 349325E & 349525E
Prospect : Rover 11E 09/2017

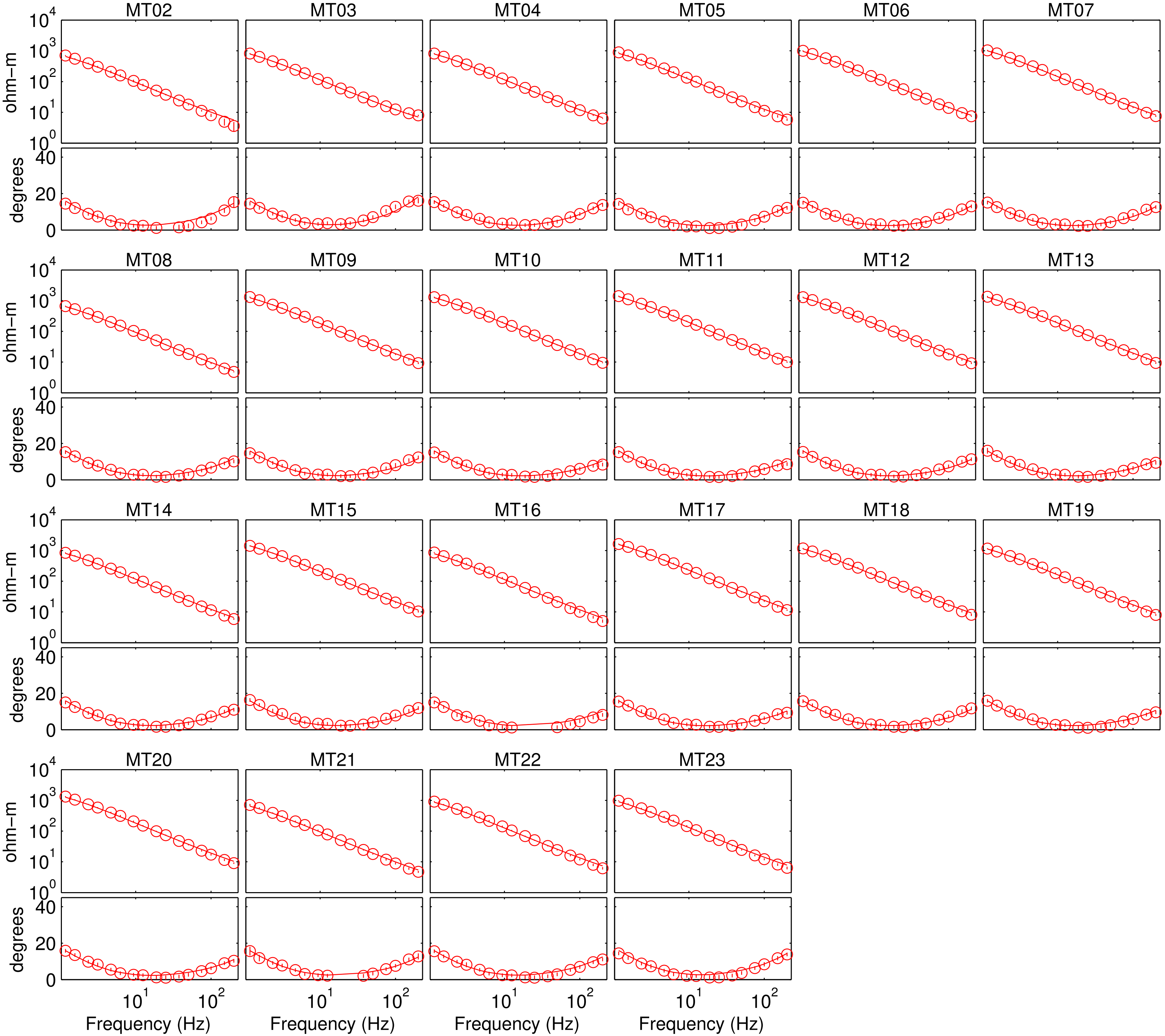
MT02
MT03
MT04
MT05
MT06
MT07
MT08
MT09
MT10
MT11
MT12
MT13
MT14
MT15
MT16
MT17
MT18
MT19
MT20
MT21
MT22
MT23
ohm−m
degrees
Frequency (Hz)

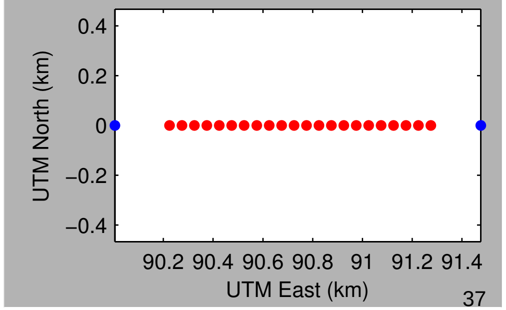
UTM North (km)
UTM East (km)
0.4
0.2
0
−0.2
−0.4
90.2
90.4
90.6
90.8
91
91.2
91.4

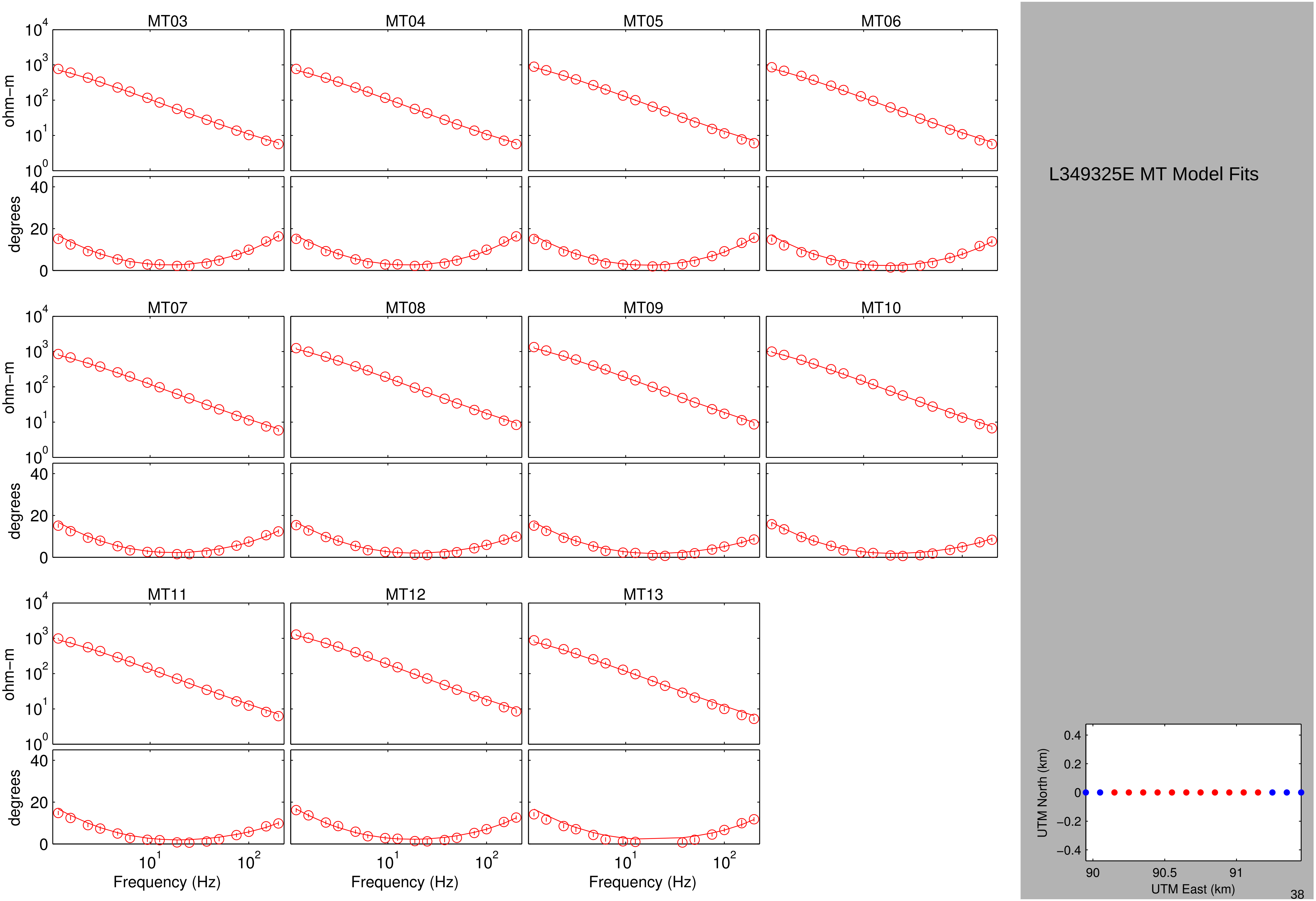
L349325E MT Model Fits
MT03
MT04
MT05
MT06
MT07
MT08
MT09
MT10
MT11
MT12
MT13
ohm−m
degrees
Frequency (Hz)
UTM North (km)
UTM East (km)

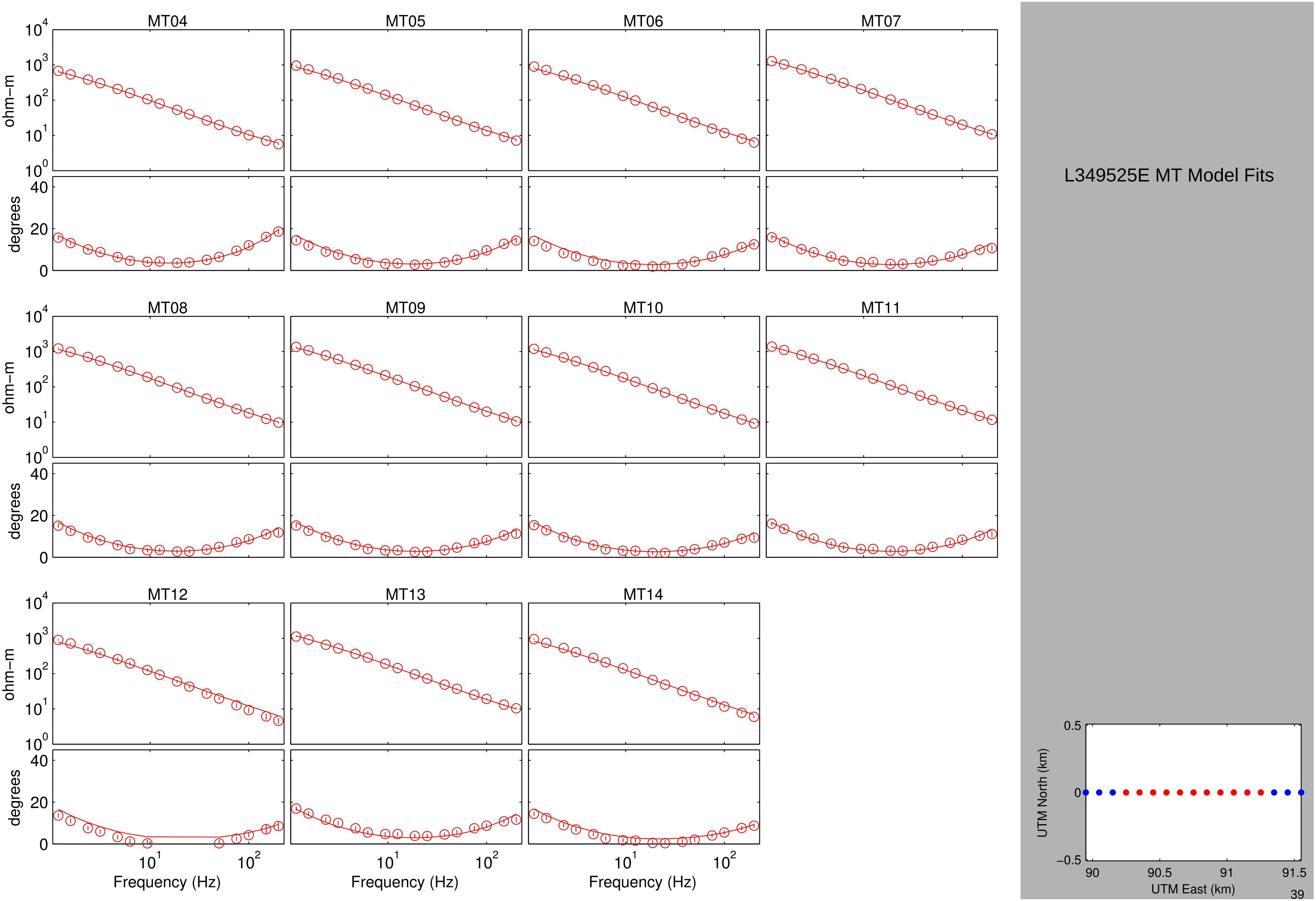
L349525E MT Model Fits
MT04
MT05
MT06
MT07
MT08
MT09
MT10
MT11
MT12
MT13
MT14
ohm−m
degrees
Frequency (Hz)
UTM North (km)
UTM East (km)

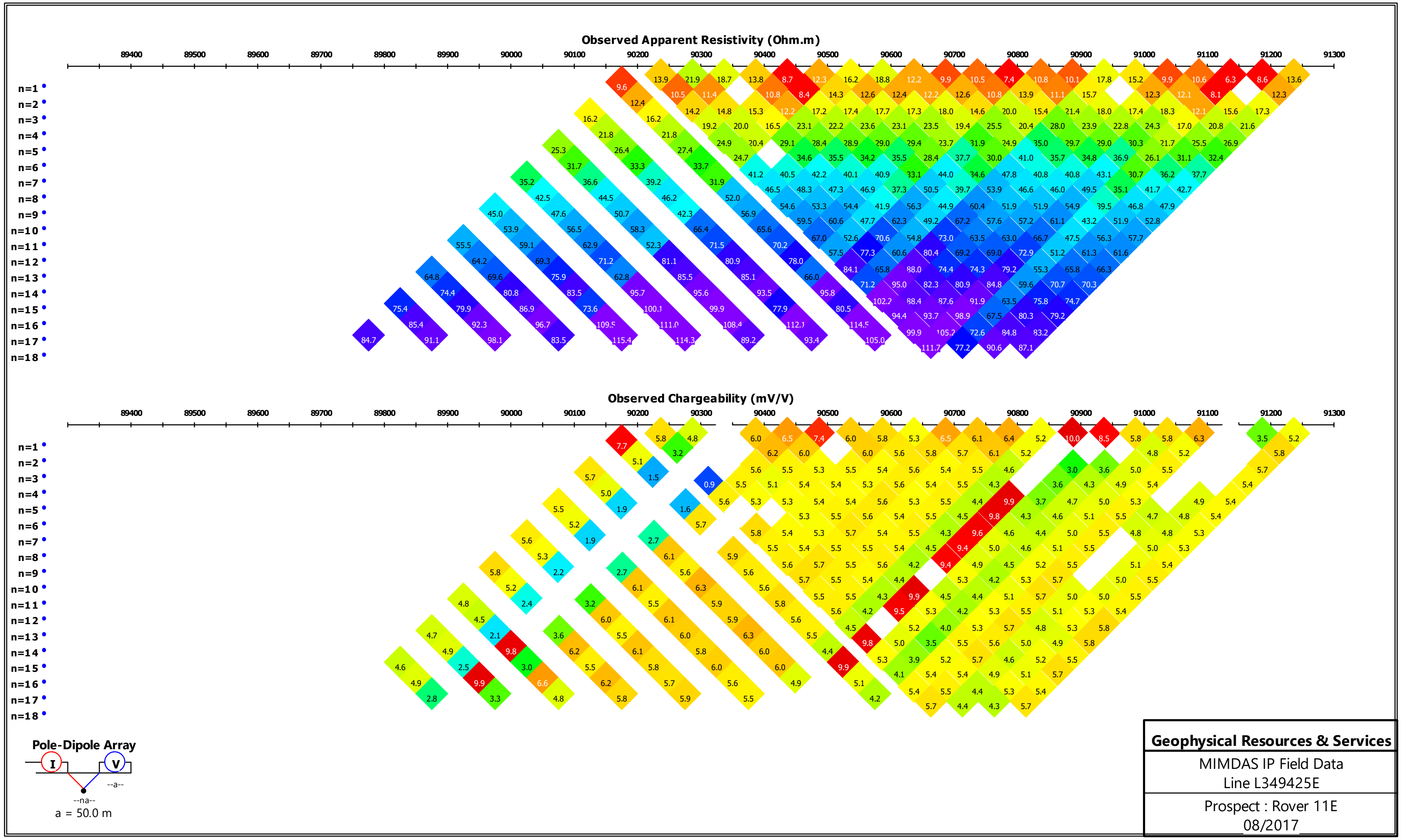

Observed Apparent Resistivity (Ohm.m)
Observed Chargeability (mV/V)
Pole-Dipole Array
a = 50.0 m
Geophysical Resources & Services
MIMDAS IP Field Data
Line L349425E
Prospect : Rover 11E
08/2017

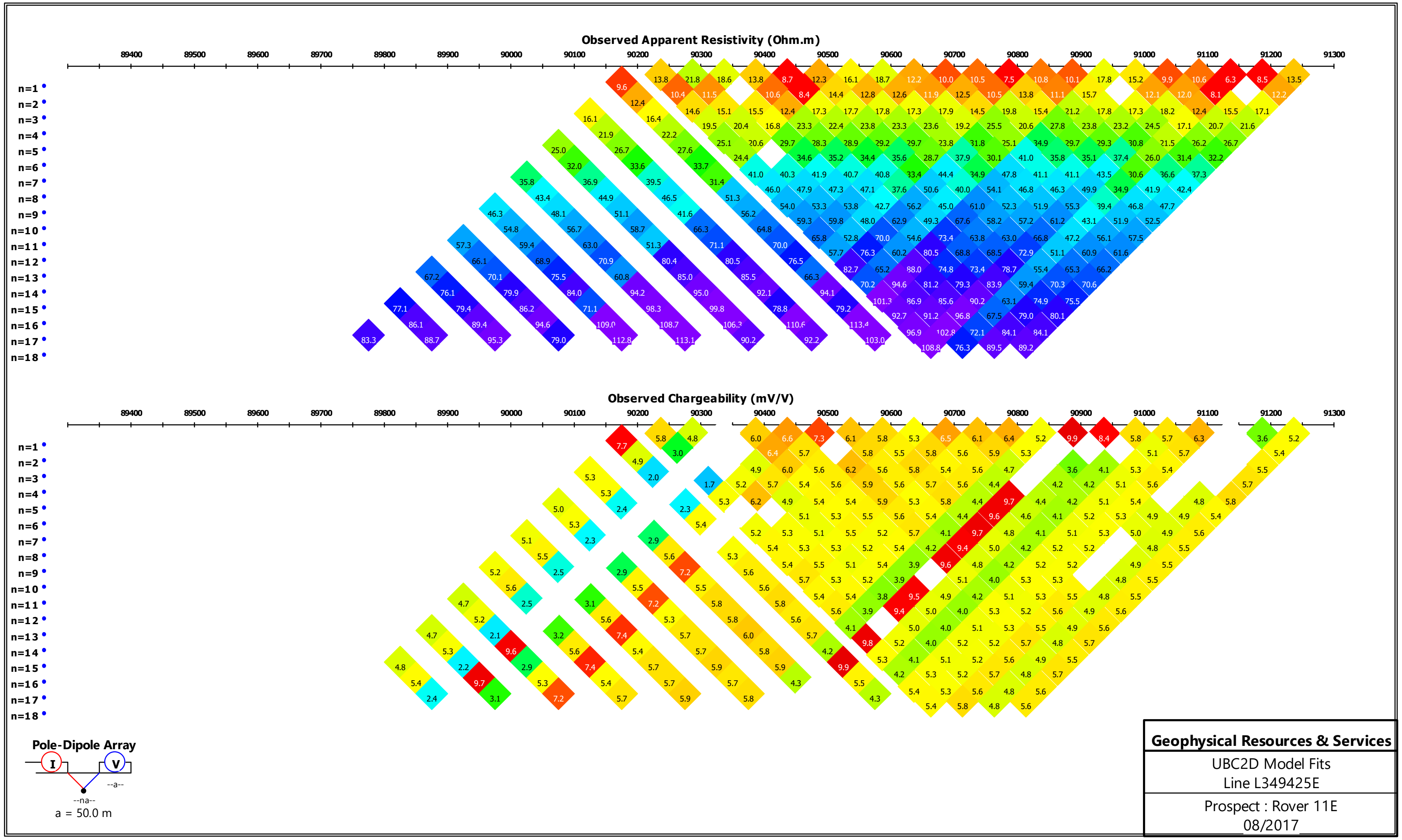
Observed Apparent Resistivity (Ohm.m)
Observed Chargeability (mV/V)
Pole-Dipole Array
a = 50.0 m
Geophysical Resources & Services
UBC2D Model Fits
Line L349425E
Prospect : Rover 11E
08/2017

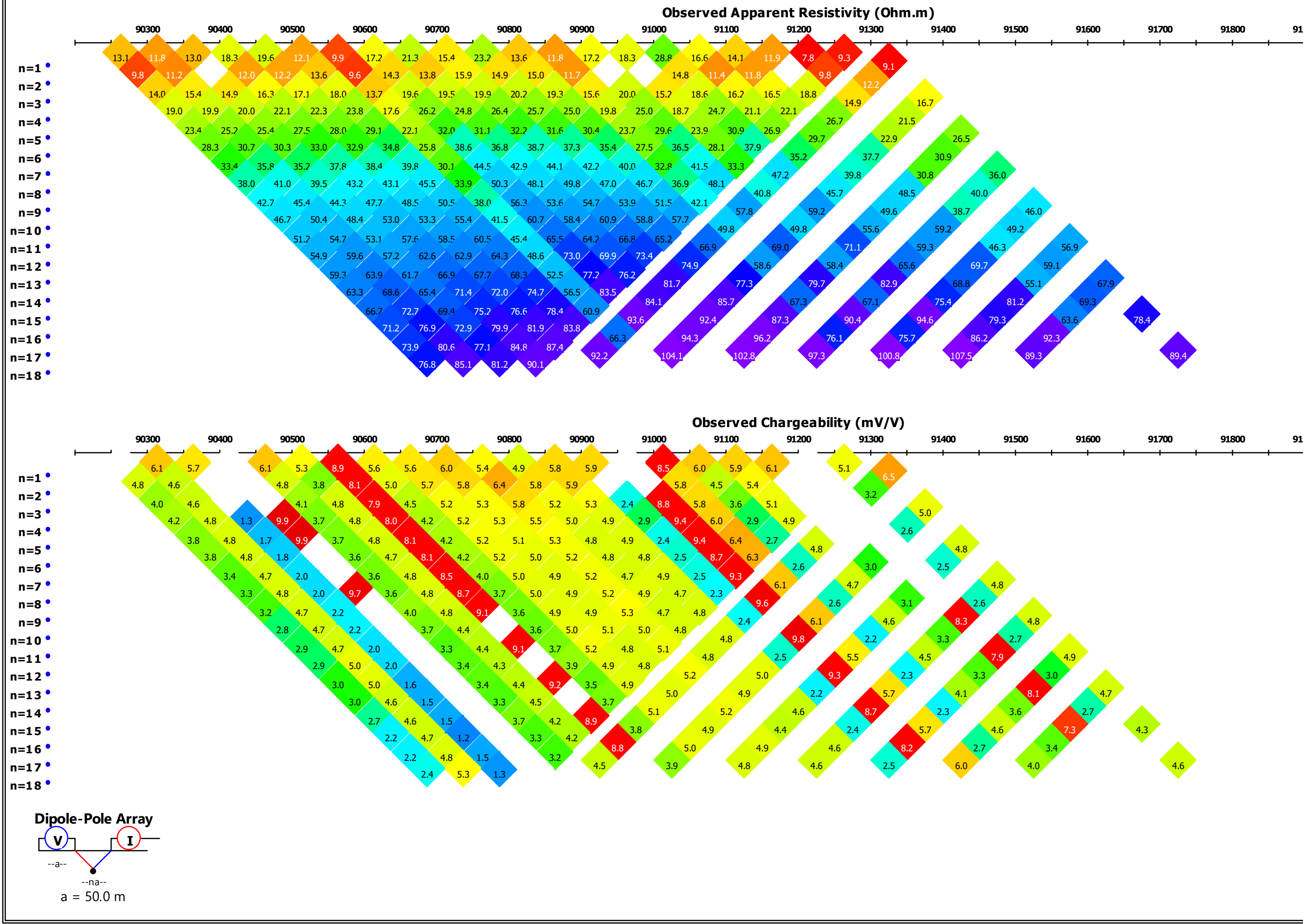

Geophysical Resources & Services

MIMDAS IP Field Data
Line L349425E

Prospect : Rover 11E
08/2017

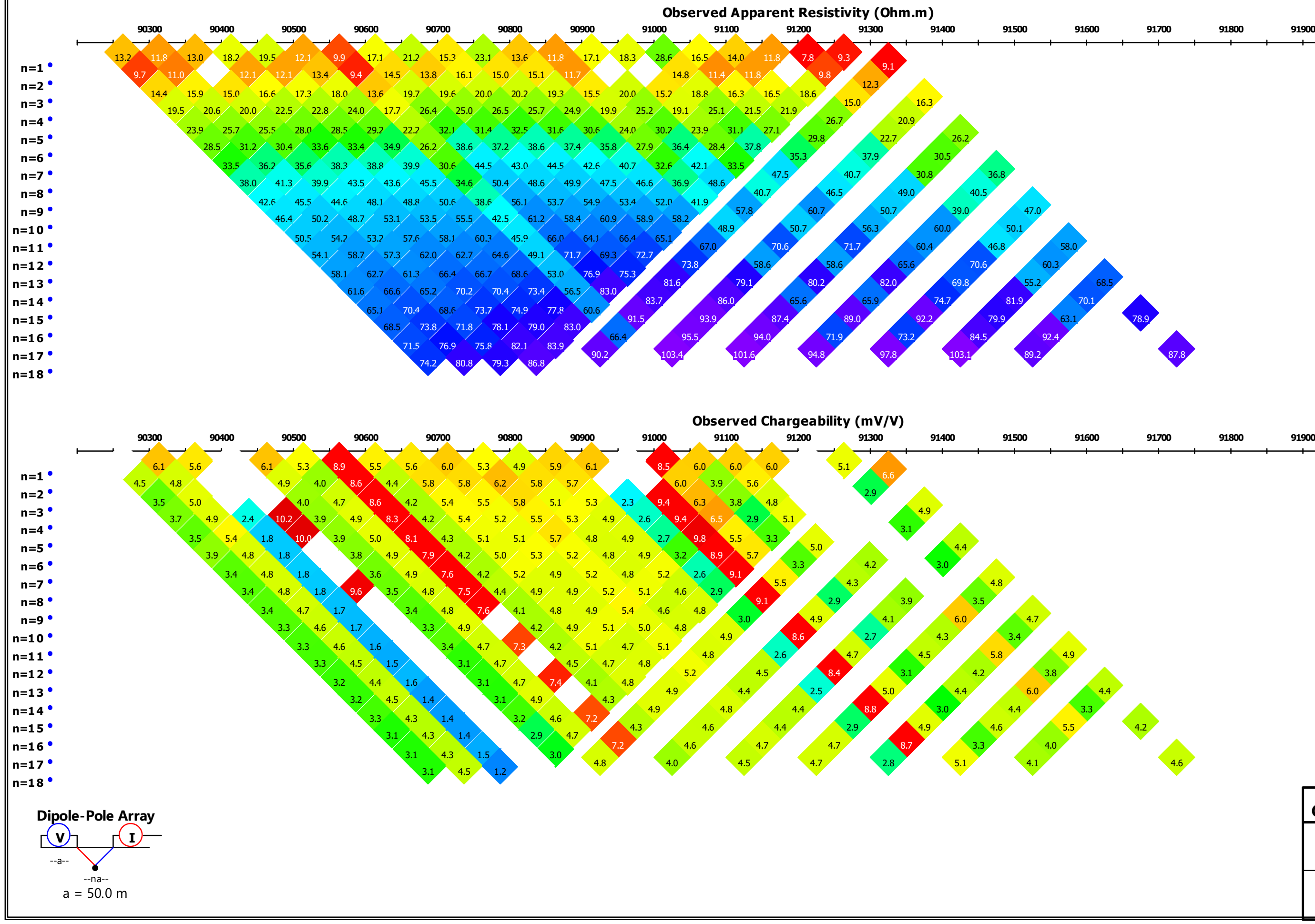

Geophysical Resources & Services

UBC2D Model Fits
Line L349425E

Prospect : Rover 11E
08/2017

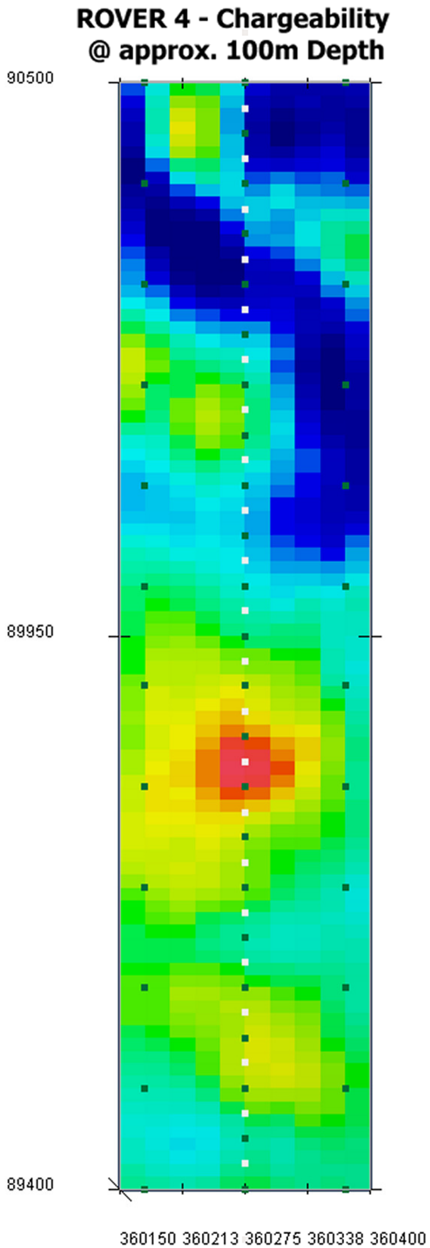

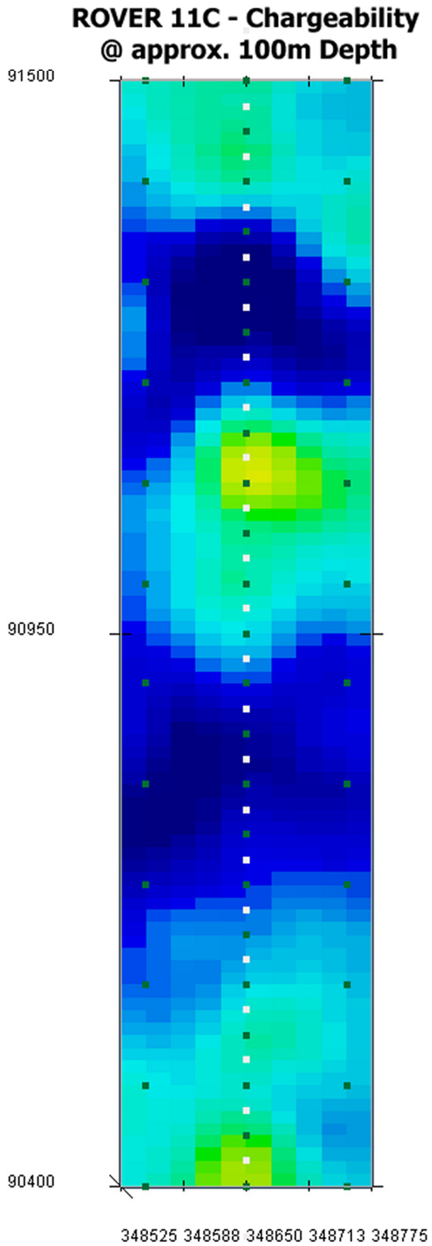

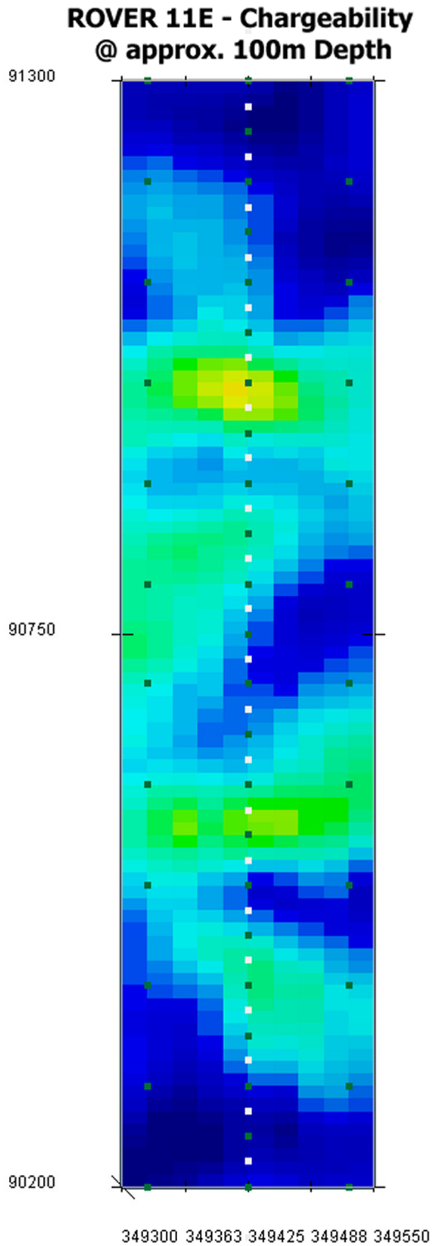

Geophysical Resources & Services

Chargeability Plans @ 100m Depth
3D IP Summary

Prospect : Rover 4,11C,11E
09/2017

APPENDIX 5 – MT and IP Array Layouts

Rover Field

Array Layout – R4

IP

count, rx_site, position, DAU, sensor_id
1 Line 360175E, 89400N - 89500N+gl -22 564 gl
2 Line 360175E, 89500N - 89600N+gl -21 129 gl
3 Line 360175E, 89600N - 89700N+gl -20 141 gl
4 Line 360175E, 89700N - 89800N+gl -19 142 gl
5 Line 360175E, 89800N - 89900N+gl -18 108 gl
6 Line 360175E, 89900N - 90000N+gl -17 605 gl
7 Line 360175E, 90000N - 90100N+gl -16 586 gl
8 Line 360175E, 90100N - 90200N+gl -15 121 gl
9 Line 360175E, 90200N - 90300N+gl -14 36 gl
10 Line 360175E, 90300N - 90400N+gl -13 107 gl
11 Line 360175E, 90400N - 90500N+gl -12 109 gl
12 Line 360175E, 90500N, 360175E - 90500N, 360275E (Ey)+gl -11 294 gl
13 Line 360275E, 90500N - 90450N+gl -10 93 gl
14 Line 360275E, 90450N - 90400N+gl -9 14 gl
15 Line 360275E, 90400N - 90350N+gl -8 550 gl
16 Line 360275E, 90350N - 90300N+gl -7 136 gl
17 Line 360275E, 90300N - 90250N+gl -6 60 gl
18 Line 360275E, 90250N - 90200N+gl -5 281 gl
19 Line 360275E, 90200N - 90150N+gl -4 82 gl
20 Line 360275E, 90150N - 90100N+gl -3 26 gl
21 Line 360275E, 90100N - 90050N+gl -2 553 gl
22 Line 360275E, 90050N - 90000N+gl -1 556 gl
23 (Tx) Line 360275E, 88450N - BC+cm 1 64 CMDF0006
24 Line 360275E, 90000N - 89950N+gl 2 115 gl
25 Line 360275E, 89950N - 89900N+gl 3 124 gl
26 Line 360275E, 89900N - 89850N+gl 4 50 gl
27 Line 360275E, 89850N - 89800N+gl 5 144 gl
28 Line 360275E, 89800N - 89750N+gl 6 524 gl
29 Line 360275E, 89750N - 89700N+gl 7 551 gl
30 Line 360275E, 89700N - 89650N+gl 8 23 gl
31 Line 360275E, 89650N - 89600N+gl 9 97 gl
32 Line 360275E, 89600N - 89550N+gl 10 590 gl
33 Line 360275E, 89550N - 89500N+gl 11 100 gl
34 Line 360275E, 89500N - 89450N+gl 12 151 gl
35 Line 360275E, 89450N - 89400N+gl 13 559 gl
36 Line 360275E, 89400N, 360275E - 89400N, 360375E (Ey)+gl 14 11 gl
37 Line 360375E, 89400N - 89500N+gl 15 563 gl
38 Line 360375E, 89500N - 89600N+gl 16 295 gl
39 Line 360375E, 89600N - 89700N+gl 17 66 gl
40 Line 360375E, 89700N - 89800N+gl 18 577 gl
41 Line 360375E, 89800N - 89900N+gl 19 570 gl
42 Line 360375E, 89900N - 90000N+gl 20 69 gl
43 Line 360375E, 90000N - 90100N+gl 21 552 gl
44 Line 360375E, 90100N - 90200N+gl 22 80 gl
45 Line 360375E, 90200N - 90300N+gl 23 561 gl
46 Line 360375E, 90300N - 90400N+gl 24 40 gl
47 Line 360375E, 90400N - 90500N+gl 25 558 gl

MT

count, rx_site, position, DAU, ref1, ref2, Cref1, Cref2, sensor_id
1 Line 360175E, 89400N - 89500N+gl
2 Line 360175E, 89500N - 89600N+gl
3 Line 360175E, 89600N - 89700N+gl
4 Line 360175E, 89700N - 89800N+gl

5 Line 360175E, 89800N - 89900N+gl
6 Line 360175E, 89900N - 90000N+gl
7 Line 360175E, 90000N - 90100N+gl
8 Line 360175E, 90100N - 90200N+gl
9 Line 360175E, 90200N - 90300N+gl
10 Line 360175E, 90300N - 90400N+gl
11 Line 360175E, 90400N - 90500N+gl
12 Line 360175E, 90500N, 360175E - 90500N, 360275E (Ey)+gl -13 294 2 2 2 2 gl
13 Line 360275E, 90500N - 90450N+gl
14 Line 360275E, 90450N - 90400N+gl
15 Line 360275E, 90400N (Hy)+bf
16 Line 360275E, 90400N (Hx)+bf
17 Line 360275E, 90400N - 90350N+gl
18 Line 360275E, 90350N - 90300N+gl
19 Line 360275E, 90300N - 90250N+gl
20 Line 360275E, 90250N - 90200N+gl
21 Line 360275E, 90200N - 90150N+gl
22 Line 360275E, 90150N - 90100N+gl
23 Line 360275E, 90100N - 90050N+gl
24 Line 360275E, 90050N - 90000N+gl
25 Line 360275E, 90000N - 89950N+gl
26 Line 360275E, 89950N - 89900N+gl
27 Line 360275E, 89900N - 89850N+gl
28 Line 360275E, 89850N - 89800N+gl
29 Line 360275E, 89800N - 89750N+gl
30 Line 360275E, 89750N - 89700N+gl
31 Line 360275E, 89700N - 89650N+gl
32 Line 360275E, 89650N - 89600N+gl
33 Line 360275E, 89600N - 89550N+gl
34 Line 360275E, 89550N - 89500N+gl
35 Line 360275E, 89500N (Hy)+bf
36 Line 360275E, 89500N (Hx)+bf
37 Line 360275E, 89500N - 89450N+gl
38 Line 360275E, 89450N - 89400N+gl
39 Line 360275E, 89400N, 360275E - 89400N, 360375E (Ey)+gl 15 11 2 2 2 2 gl
40 Line 360375E, 89400N - 89500N+gl
41 Line 360375E, 89500N - 89600N+gl
42 Line 360375E, 89600N - 89700N+gl
43 Line 360375E, 89700N - 89800N+gl
44 Line 360375E, 89800N - 89900N+gl
45 Line 360375E, 89900N - 90000N+gl
46 Line 360375E, 90000N - 90100N+gl

R11C

IP

count, rx_site, position, DAU, sensor_id
1 Line 348550E, 90400N - 90500N+gl -22 55 gl
2 Line 348550E, 90500N - 90600N+gl -21 141 gl
3 Line 348550E, 90600N - 90700N+gl -20 564 gl
4 Line 348550E, 90700N - 90800N+gl -19 36 gl
5 Line 348550E, 90800N - 90900N+gl -18 288 gl
6 Line 348550E, 90900N - 91000N+gl -17 66 gl
7 Line 348550E, 91000N - 91100N+gl -16 561 gl
8 Line 348550E, 91100N - 91200N+gl -15 82 gl
9 Line 348550E, 91200N - 91300N+gl -14 294 gl
10 Line 348550E, 91300N - 91400N+gl -13 107 gl
11 Line 348550E, 91400N - 91500N+gl -12 281 gl
12 Line 348550E, 91500N, 348550E - 91500N, 348650E (Ey)+gl -11 136 gl
13 Line 348650E, 91500N - 91450N+gl -10 80 gl
14 Line 348650E, 91450N - 91400N+gl -9 69 gl
15 Line 348650E, 91400N - 91350N+gl -8 550 gl
16 Line 348650E, 91350N - 91300N+gl -7 40 gl
17 Line 348650E, 91300N - 91250N+gl -6 144 gl
18 Line 348650E, 91250N - 91200N+gl -5 524 gl

19 Line 348650E, 91200N - 91150N+gl -4 129 gl
20 Line 348650E, 91150N - 91100N+gl -3 558 gl
21 Line 348650E, 91100N - 91050N+gl -2 44 gl
22 Line 348650E, 91050N - 91000N+gl -1 553 gl
23 (Tx) Line 348650E, 91375N - BC+cm 1 64 CMDF0006
24 Line 348650E, 91000N - 90950N+gl 2 23 gl
25 Line 348650E, 90950N - 90900N+gl 3 551 gl
26 Line 348650E, 90900N - 90850N+gl 4 570 gl
27 Line 348650E, 90850N - 90800N+gl 5 11 gl
28 Line 348650E, 90800N - 90750N+gl 6 100 gl
29 Line 348650E, 90750N - 90700N+gl 7 590 gl
30 Line 348650E, 90700N - 90650N+gl 8 151 gl
31 Line 348650E, 90650N - 90600N+gl 9 97 gl
32 Line 348650E, 90600N - 90550N+gl 10 563 gl
33 Line 348650E, 90550N - 90500N+gl 11 50 gl
34 Line 348650E, 90500N - 90450N+gl 12 295 gl
35 Line 348650E, 90450N - 90400N+gl 13 142 gl
36 Line 348650E, 90400N, 348650E - 90400N, 348750E (Ey)+gl 14 124 gl
37 Line 348750E, 90400N - 90500N+gl 15 115 gl
38 Line 348750E, 90500N - 90600N+gl 16 109 gl
39 Line 348750E, 90600N - 90700N+gl 17 596 gl
40 Line 348750E, 90700N - 90800N+gl 18 586 gl
41 Line 348750E, 90800N - 90900N+gl 19 48 gl
42 Line 348750E, 90900N - 91000N+gl 20 30 gl
43 Line 348750E, 91000N - 91100N+gl 21 59 gl
44 Line 348750E, 91100N - 91200N+gl 22 556 gl
45 Line 348750E, 91200N - 91300N+gl 23 121 gl
46 Line 348750E, 91300N - 91400N+gl 24 60 gl
47 Line 348750E, 91400N - 91500N+gl 25 93 gl

MT

count, rx_site, position, DAU, ref1, ref2, Cref1, Cref2, sensor_id
1 Line 348550E, 90400N - 90500N+gl
2 Line 348550E, 90500N - 90600N+gl
3 Line 348550E, 90600N - 90700N+gl
4 Line 348550E, 90700N - 90800N+gl
5 Line 348550E, 90800N - 90900N+gl
6 Line 348550E, 90900N - 91000N+gl
7 Line 348550E, 91000N - 91100N+gl
8 Line 348550E, 91100N - 91200N+gl
9 Line 348550E, 91200N - 91300N+gl
10 Line 348550E, 91300N - 91400N+gl
11 Line 348550E, 91400N - 91500N+gl
12 Line 348550E, 91500N, 348550E - 91500N, 348650E (Ey)+gl -13 136 2 2 2 2 gl
13 Line 348650E, 91500N - 91450N+gl
14 Line 348650E, 91450N - 91400N+gl
15 Line 348650E, 91400N - 91350N+gl
16 Line 348650E, 91400N (Hy)+bf
17 Line 348650E, 91400N (Hx)+bf
18 Line 348650E, 91350N - 91300N+gl
19 Line 348650E, 91300N - 91250N+gl
20 Line 348650E, 91250N - 91200N+gl
21 Line 348650E, 91200N - 91150N+gl
22 Line 348650E, 91150N - 91100N+gl
23 Line 348650E, 91100N - 91050N+gl
24 Line 348650E, 91050N - 91000N+gl
25 Line 348650E, 91000N - 90950N+gl
26 Line 348650E, 90950N - 90900N+gl
27 Line 348650E, 90900N - 90850N+gl
28 Line 348650E, 90850N - 90800N+gl
29 Line 348650E, 90800N - 90750N+gl
30 Line 348650E, 90750N - 90700N+gl
31 Line 348650E, 90700N - 90650N+gl
32 Line 348650E, 90650N - 90600N+gl
33 Line 348650E, 90600N - 90550N+gl
34 Line 348650E, 90550N - 90500N+gl

35 Line 348650E, 90500N - 90450N+gl
36 Line 348650E, 90500N (Hy)+bf
37 Line 348650E, 90500N (Hx)+bf
38 Line 348650E, 90450N - 90400N+gl
39 Line 348650E, 90400N, 348650E - 90400N, 348750E (Ey)+gl 15 124 2 2 2 2 gl
40 Line 348750E, 90400N - 90500N+gl
41 Line 348750E, 90500N - 90600N+gl
42 Line 348750E, 90600N - 90700N+gl
43 Line 348750E, 90700N - 90800N+gl
44 Line 348750E, 90800N - 90900N+gl
45 Line 348750E, 90900N - 91000N+gl
46 Line 348750E, 91000N - 91100N+gl
47 Line 348750E, 91100N - 91200N+gl
48 Line 348750E, 91200N - 91300N+gl
49 Line 348750E, 91300N - 91400N+gl
50 Line 348750E, 91400N - 91500N+gl

R11E

IP

count, rx_site, position, DAU, sensor_id
1 Line 349325E, 90200N - 90300N+gl -19 60 gl
2 Line 349325E, 90300N - 90400N+gl -18 136 gl
3 Line 349325E, 90400N - 90500N+gl -17 596 gl
4 Line 349325E, 90500N - 90600N+gl -16 55 gl
5 Line 349325E, 90600N - 90700N+gl -15 66 gl
6 Line 349325E, 90700N - 90800N+gl -14 59 gl
7 Line 349325E, 90800N - 90900N+gl -13 121 gl
8 Line 349325E, 90900N - 91000N+gl -12 23 gl
9 Line 349325E, 91000N - 91100N+gl -11 124 gl
10 Line 349325E, 91100N - 91200N+gl -10 48 gl
11 Line 349325E, 91200N - 91300N+gl -9 93 gl
12 Line 349325E, 91300N, 349325E - 91300N, 349425E (Ey)+gl -8 142 gl
13 Line 349425E, 91300N - 91250N+gl -7 590 gl
14 Line 349425E, 91250N - 91200N+gl -6 524 gl
15 Line 349425E, 91200N - 91150N+gl -5 561 gl
16 Line 349425E, 91150N - 91100N+gl -4 115 gl
17 Line 349425E, 91100N - 91050N+gl -3 281 gl
18 Line 349425E, 91050N - 91000N+gl -2 586 gl
19 Line 349425E, 91000N - 90950N+gl -1 26 gl
20 (Tx) Line 349425E, 90425N - BC+cm 1 64 CMDF0006
21 Line 349425E, 90950N - 90900N+gl 2 11 gl
22 Line 349425E, 90900N - 90850N+gl 3 14 gl
23 Line 349425E, 90850N - 90800N+gl 4 559 gl
24 Line 349425E, 90800N - 90750N+gl 5 552 gl
25 Line 349425E, 90750N - 90700N+gl 6 129 gl
26 Line 349425E, 90700N - 90650N+gl 7 36 gl
27 Line 349425E, 90650N - 90600N+gl 8 80 gl
28 Line 349425E, 90600N - 90550N+gl 9 40 gl
29 Line 349425E, 90550N - 90500N+gl 10 70 gl
30 Line 349425E, 90500N - 90450N+gl 11 564 gl
31 Line 349425E, 90450N - 90400N+gl 12 295 gl
32 Line 349425E, 90400N - 90350N+gl 13 69 gl
33 Line 349425E, 90350N - 90300N+gl 14 107 gl
34 Line 349425E, 90300N - 90250N+gl 15 82 gl
35 Line 349425E, 90250N - 90200N+gl 16 551 gl
36 Line 349425E, 90200N, 349425E - 90200N, 349525E (Ey)+gl 17 550 gl
37 Line 349525E, 90200N - 90300N+gl 18 294 gl
38 Line 349525E, 90300N - 90400N+gl 19 553 gl
39 Line 349525E, 90400N - 90500N+gl 20 556 gl
40 Line 349525E, 90500N - 90600N+gl 21 109 gl
41 Line 349525E, 90600N - 90700N+gl 22 563 gl
42 Line 349525E, 90700N - 90800N+gl 23 521 gl
43 Line 349525E, 90800N - 90900N+gl 24 144 gl
44 Line 349525E, 90900N - 91000N+gl 25 30 gl

45 Line 349525E, 91000N - 91100N+gl 26 558 gl
46 Line 349525E, 91100N - 91200N+gl 27 50 gl
47 Line 349525E, 91200N - 91300N+gl 28 100 gl

MT

count, rx_site, position, DAU, ref1, ref2, Cref1, Cref2, sensor_id
1 Line 349325E, 90200N - 90300N+gl
2 Line 349325E, 90300N - 90400N+gl
3 Line 349325E, 90400N - 90500N+gl
4 Line 349325E, 90500N - 90600N+gl
5 Line 349325E, 90600N - 90700N+gl
6 Line 349325E, 90700N - 90800N+gl
7 Line 349325E, 90800N - 90900N+gl
8 Line 349325E, 90900N - 91000N+gl
9 Line 349325E, 91000N - 91100N+gl
10 Line 349325E, 91100N - 91200N+gl
11 Line 349325E, 91200N - 91300N+gl
12 Line 349325E, 91300N, 349325E - 91300N, 349425E (Ey)+gl -10 142 2 2 2 2 gl
13 Line 349425E, 91300N - 91250N+gl
14 Line 349425E, 91250N - 91200N+gl
15 Line 349425E, 91200N - 91150N+gl
16 Line 349425E, 91200N (Hy)+bf
17 Line 349425E, 91200N (Hx)+bf
18 Line 349425E, 91150N - 91100N+gl
19 Line 349425E, 91100N - 91050N+gl
20 Line 349425E, 91050N - 91000N+gl
21 Line 349425E, 91000N - 90950N+gl
22 Line 349425E, 90950N - 90900N+gl
23 Line 349425E, 90900N - 90850N+gl
24 Line 349425E, 90850N - 90800N+gl
25 Line 349425E, 90800N - 90750N+gl
26 Line 349425E, 90750N - 90700N+gl
27 Line 349425E, 90700N - 90650N+gl
28 Line 349425E, 90650N - 90600N+gl
29 Line 349425E, 90600N - 90550N+gl
30 Line 349425E, 90550N - 90500N+gl
31 Line 349425E, 90500N - 90450N+gl
32 Line 349425E, 90450N - 90400N+gl
33 Line 349425E, 90400N - 90350N+gl
34 Line 349425E, 90350N - 90300N+gl
35 Line 349425E, 90300N - 90250N+gl
36 Line 349425E, 90300N (Hy)+bf
37 Line 349425E, 90300N (Hx)+bf
38 Line 349425E, 90250N - 90200N+gl
39 Line 349425E, 90200N, 349425E - 90200N, 349525E (Ey)+gl 18 550 2 2 2 2 gl
40 Line 349525E, 90200N - 90300N+gl
41 Line 349525E, 90300N - 90400N+gl
42 Line 349525E, 90400N - 90500N+gl
43 Line 349525E, 90500N - 90600N+gl
44 Line 349525E, 90600N - 90700N+gl
45 Line 349525E, 90700N - 90800N+gl
46 Line 349525E, 90800N - 90900N+gl
47 Line 349525E, 90900N - 91000N+gl
48 Line 349525E, 91000N - 91100N+gl
49 Line 349525E, 91100N - 91200N+gl
50 Line 349525E, 91200N - 91300N+gl

APPENDIX 6 – Receiver Locations

R4

Easting	Northing
360175	7789400
360175	7789500
360175	7789600
360175	7789700
360175	7789800
360175	7789900
360175	7790000
360175	7790100
360175	7790200
360175	7790300
360175	7790400
360175	7790500
360275	7789400
360275	7789450
360275	7789500
360275	7789550
360275	7789600
360275	7789650
360275	7789700
360275	7789750
360275	7789800
360275	7789850
360275	7789900
360275	7789950
360275	7790000
360275	7790050
360275	7790100
360275	7790150
360275	7790200
360275	7790250
360275	7790300
360275	7790350
360275	7790400
360275	7790450
360275	7790500
360375	7789400
360375	7789500
360375	7789600
360375	7789700
360375	7789800
360375	7789900
360375	7790000

360375	7790100
360375	7790200
360375	7790300
360375	7790400
360375	7790500

R11C

Easting	Northing
348550	7790400
348550	7790500
348550	7790600
348550	7790700
348550	7790800
348550	7790900
348550	7791000
348550	7791100
348550	7791200
348550	7791300
348550	7791400
348550	7791500
348750	7790400
348750	7790500
348750	7790600
348750	7790700
348750	7790800
348750	7790900
348750	7791000
348750	7791100
348750	7791200
348750	7791300
348750	7791400
348750	7791500
348650	7790400
348650	7790450
348650	7790500
348650	7790550
348650	7790600
348650	7790650
348650	7790700
348650	7790750
348650	7790800
348650	7790850
348650	7790900
348650	7790950
348650	7791000
348650	7791050

348650	7791100
348650	7791150
348650	7791200
348650	7791250
348650	7791300
348650	7791350
348650	7791400
348650	7791450
348650	7791500

R11E

Easting	Northing
349325	7790200
349325	7790300
349325	7790400
349325	7790500
349325	7790600
349325	7790700
349325	7790800
349325	7790900
349325	7791000
349325	7791100
349325	7791200
349325	7791300
349525	7790200
349525	7790300
349525	7790400
349525	7790500
349525	7790600
349525	7790700
349525	7790800
349525	7790900
349525	7791000
349525	7791100
349525	7791200
349525	7791300
349425	7790200
349425	7790250
349425	7790300
349425	7790350
349425	7790400
349425	7790450
349425	7790500
349425	7790550
349425	7790600
349425	7790650

349425	7790700
349425	7790750
349425	7790800
349425	7790850
349425	7790900
349425	7790950
349425	7791000
349425	7791050
349425	7791100
349425	7791150
349425	7791200
349425	7791250
349425	7791300

APPENDIX 7 – Transmitter Locations

R4

Easting	Northing
360275	7788450
360275	7788550
360275	7788650
360275	7788750
360275	7788850
360275	7788950
360275	7789050
360275	7789150
360275	7789250
360275	7789350
360275	7789425
360275	7789475
360275	7789525
360275	7789575
360275	7789625
360275	7789675
360275	7789725
360275	7789775
360275	7789825
360275	7789875
360275	7789925
360275	7789975
360275	7790025
360275	7790075
360275	7790125
360275	7790175
360275	7790225
360275	7790275
360275	7790325
360275	7790375
360275	7790425
360275	7790475
360275	7790550
360275	7790650
360275	7790750
360275	7790850
360275	7790950
360275	7791050
360275	7791150
360275	7791250
360275	7791350
360275	7791450

R11C

Easting	Northing
348650	7789450
348650	7789550
348650	7789650
348650	7789750
348650	7789850
348650	7789950
348650	7790050
348650	7790150
348650	7790250
348650	7790350
348650	7790425
348650	7790475
348650	7790525
348650	7790575
348650	7790625
348650	7790675
348650	7790725
348650	7790775
348650	7790825
348650	7790875
348650	7790925
348650	7790975
348650	7791025
348650	7791075
348650	7791125
348650	7791175
348650	7791225
348650	7791275
348650	7791325
348650	7791375
348650	7791425
348650	7791475
348650	7791550
348650	7791650
348650	7791750
348650	7791850
348650	7791950
348650	7792050
348650	7792150
348650	7792250
348650	7792350
348650	7792450

R11E

Easting	Northing
349425	7789250
349425	7789350
349425	7789450
349425	7789550
349425	7789650
349425	7789750
349425	7789850
349425	7789950
349425	7790050
349425	7790150
349425	7790225
349425	7790275
349425	7790325
349425	7790375
349425	7790425
349425	7790475
349425	7790525
349425	7790575
349425	7790625
349425	7790675
349425	7790725
349425	7790775
349425	7790825
349425	7790875
349425	7790925
349425	7790975
349425	7791025
349425	7791075
349425	7791125
349425	7791175
349425	7791225
349425	7791275
349425	7791350
349425	7791450
349425	7791550
349425	7791650
349425	7791750
349425	7791850
349425	7791950
349425	7792050
349425	7792150
349425	7792250

APPENDIX 8 – Short Note: MIMDAS Magnetotelluric Processing Scheme

The Basic Approach

We begin with the basic impedance relationship:

$$E_x = Z_{xx} H_x + Z_{xy} H_y \qquad \text{EQ. 1}$$

The classic magnetotelluric approach to processing without the use of remote reference stations involves averaging the cross and auto-spectra involving the two magnetic field terms;

$$\overline{E_x H_x^*} = Z_{xx} \overline{H_x H_x^*} + Z_{xy} \overline{H_y H_x^*}$$

$$\overline{E_x H_y^*} = Z_{xx} \overline{H_x H_y^*} + Z_{xy} \overline{H_y H_y^*} \qquad \text{EQ. 2}$$

In the notation above, * represents conjugation and the terms with bars represent the means of several repeated measurements. The two impedance terms can be estimated on the basis of the two equations in EQ. 2 above. A problem with this system of equations is that the auto-spectral terms do not average out noise. This leads to a bias in the calculated impedance terms.

The application of remote referencing, by using physically different measurements (remote references) oriented in the same directions, herein denoted $H_{x_r}^*$ and $H_{y_r}^*$ can be used to recover this bias and minimise noise. Multiplying EQ.1 by $H_{x_r}^*$ and $H_{y_r}^*$ (the remote references) provides the following set of equations:

$$\overline{E_x H_{x_r}^*} = Z_{xx} \overline{H_x H_{x_r}^*} + Z_{xy} \overline{H_y H_{x_r}^*}$$

$$\overline{E_x H_{y_r}^*} = Z_{xx} \overline{H_x H_{y_r}^*} + Z_{xy} \overline{H_y H_{y_r}^*} \qquad \text{EQ. 3}$$

This forces the impedance estimates to be based on components of the four magnetic field measurements that are spatially coherent, thus averaging out non-spatially coherent noise (such as instrument or wind vibration). The equations given in EQ. 3 above represent the standard approach to remote reference magnetotellurics and are the chosen methodology for the MIMDAS MT processing. For the non cross-referenced impedances the standard estimation approach (EQ. 2), which results in impedance bias due to noise in the H field data, but not due to noise in the E field data, is used.

In the MIMDAS processing scheme Fast Fourier Transforms (FFTs) are utilised, as opposed to other approaches such as cascade decimation, parametric time-domain, etc.

More Detail

In the acquisition of magnetotelluric data the MIMDAS system uses sampling rates that are integrally divisible by the power-line frequency. The advantages of this approach are;

- It facilitates time domain finite impulse response (FIR) filtering to attenuate power-line noise and provides a systematic way of dealing with power-line noise in the frequency domain.

- It tends to minimise leakage of power-line noise into adjacent frequencies of spectra.

Figure 1, below, illustrates the nature of the frequency domain filtering that the MIMDAS processing scheme employs. No averaging for the first three frequencies, short averages at moderate frequencies and longer averages at higher frequencies. The centre frequencies of the averages increment roughly by factors of $\sqrt{2}$, as do the window lengths. As suggested by Figure 1, a Hanning weighting scheme is used for the frequency domain smoothing. This scheme reduces the number of terms resulting in a 1024 point fft from 512 to 16. The scheme also means that for sampling rates $(2^n)(f_{pwr})$ of and 2n fft lengths, the resulting fft frequencies will always be part of the same set; i.e. they will overlay exactly for different sampling rates and fft lengths.

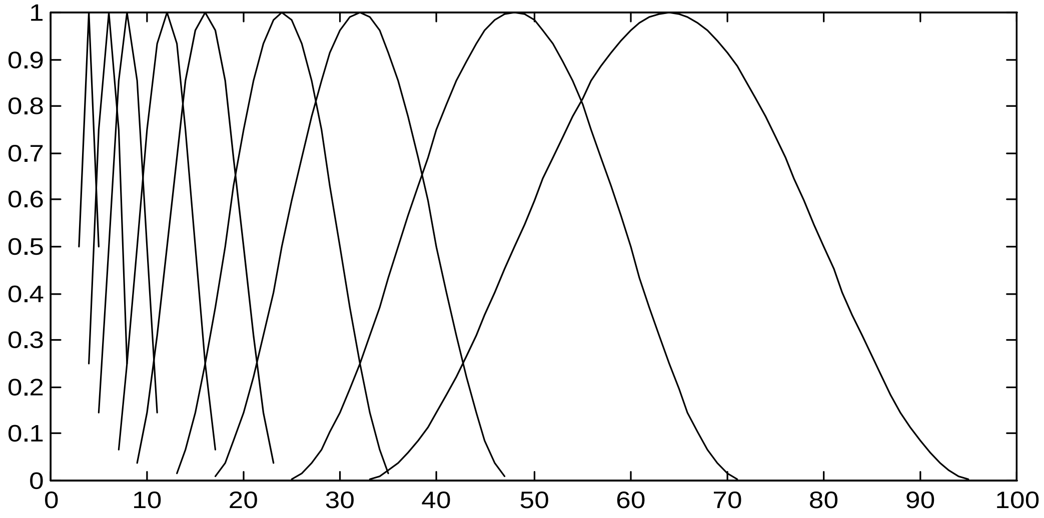

Figure 1 Illustration of frequency domain filtering at quasi-logarithmic spacing.

The table below details the averaging scheme specifically;

Centre Of Filter *(fft frequency number)*	**Filter Length**	**Filter Application Range** *(fft frequency number)*
1	1	1:1
2	1	2:2
3	1	3:3
4	3	3:5
6	5	4:8
8	7	5:11
12	11	7:17
16	15	9:23
24	23	13:35
32	31	17:47
$2^{(n-1)}+2^{n}$	$2^{(n-1)}+2^{n}-1$	$\left(2^{(n-2)}+2^{(n-1)}+1\right):\left(2^{(n-2)}+2^{(n+1)}-1\right)$
2^{n}	$2^{n}-1$	$\left(2^{(n-1)}+1\right):\left(2^{(n-1)}+2^{(n)}-1\right)$

APPENDIX 9 – Short Note: M.I.M. Chargeability Standard

M.I.M. Chargeability Standard

M.I.M. Exploration's standard for calculating chargeability is simply described as an estimate of the average decay voltage times 1000 and divided by the average charge voltage for a half-duty square wave response. This applies to all transmitted frequencies and essentially matches the Anaconda standard. M.I.M. chargeabilities primarily reflect two processing parameters: the starting time after turn-off (t_0) for which EM coupling is deemed to have dropped sufficiently, and the choice of any one of a range of symmetric (zero phase) moving average type filters designed to attenuate noise.

More specifically, M.I.M. chargeabilities are formed as illustrated in the diagram below, where:

V_{p0} is the average theoretical primary voltage for nominal filtering and averaging times

V_{s0} is the average theoretical secondary voltage for nominal filtering and averaging times

V_{p1} is the average theoretical primary voltage for specified filtering and averaging times

V_{s1} is the average theoretical secondary voltage for specified filtering and averaging times

V_{p0} is the average measured primary voltage for specified filtering and averaging times

V_{s0} is the average measured secondary voltage for specified filtering and averaging times

m_m is the un-normalised measured chargeability (volts/volt)

m_n is the normalised measured chargeability (milliVolts/volt)

Theoretical spectral parameters are (Halverson-Wait Model) r = 1.0 and k = 0.2, or (Cole-Cole Model) t = 1.0 and c = 0.2. These represent typical characteristics for most locations. Volume loading or Cole-Cole chargeability is not important in calculating the theoretical curves since they end up being ratioed in the normalisation process, but v = 0.01 is usually chosen.

Nominal filtering and averaging time specifications are:

- Filtering: a 3-tap Hanning window shaped moving average filter ([0.25, 0.5, 0.25])
- Averaging Start Time: corresponding to the second sample after the switch, regardless of sample rate and transmitted frequency, (turn-on for primary voltages and turn-off for secondary voltages) or equivalently 1.5f_s seconds after t=0, where f_s is the sampling rate (samples per second).
- Averaging Stop Time: corresponding to the second sample before the switch, regardless of sample rate and transmitted frequency, (turn-off for primary voltages and turn-on for secondary voltages) or equivalently 1.5f_s seconds before t=1/(4f_x), where f_s is the sampling rate (samples per second) and f_x is the transmitter frequency.

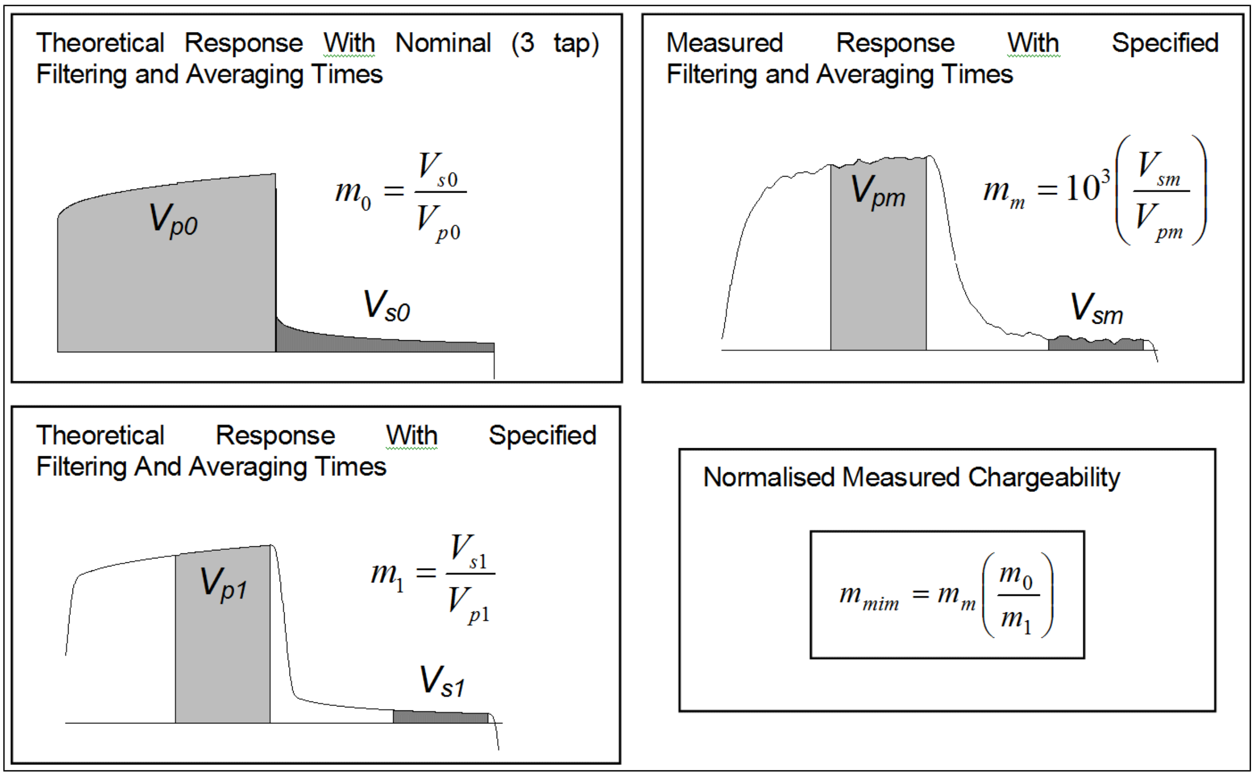

Specified averaging stop times are generally forced to correspond to the $(n_b+1)/2^{th}$ sample before the switch, where n_b is the moving average filter length, in order to avoid smearing the effects of the switching step into the chargeability calculation. Averaging start times are, of course, primarily chosen on the basis of EM coupling interference.

Conversion To Other IP Effect Measurements

With the exception of percent frequency effect (*PFE*), most common chargeability standards are related to M.I.M. chargeability by a constant multiplier. *PFE* exactly corresponds to 100 times the theoretical chargeability (*m*) of the Cole-Cole model when defined as:

$$PFE = 100\,x\,\frac{\left(\rho_a\left(f_{0_{Hz}}\right) - \rho_a\left(f_{\infty_{Hz}}\right)\right)}{\left(\rho_a\left(f_{0_{Hz}}\right)\right)}$$

Volume loading (v) is related to Cole-Cole chargeability (m_{cc}), and therefore *PFE* of the above definition accordingly, as follows[2]:

$$m_{cc} = \frac{9v}{2+3v} \text{ or, } \quad v = \frac{2m_{cc}}{9-3m_{cc}}$$

Other empirically derived conversion factors (presuming typical spectral values) are:

M.I.M. Chargeability (mV/V)	$\simeq$	**0.75***phase (milliradians)
M.I.M. Chargeability (mV/V)	$\simeq$	**0.60***Newmont Original M331[3] (milliseconds)
M.I.M. Chargeability (mV/V)	$\simeq$	**0.89***Newmont Second Standard[4] (milliseconds)
M.I.M. Chargeability (mV/V)	$\simeq$	**2.83***Volume Loading (percent)
Phase (milliradians)	$\simeq$	**1.34***M.I.M. Chargeability (mV/V)
Newmont Original (milliseconds)	$\simeq$	**1.67***M.I.M. Chargeability (mV/V)
Newmont Second (milliseconds)	$\simeq$	**1.12***M.I.M. Chargeability (mV/V)
Volume Loading (percent)	$\simeq$	**0.35***M.I.M. Chargeability (mV/V)

The reader should note that, for reasons to be discussed below and others, the conversion factors above imply more precision than is really meaningful. Using the M.I.M. chargeability (m_{mim}) to volume loading conversion along with the volume loading to Cole-Cole chargeability (m_{cc} - in millivolts per volt) given above, we have:

$$m_{cc} = \frac{31.5\, m_{mim}}{2+0.01\, m_{mim}} \simeq 15.8\, m_{mim} (\text{millivolts per volt})$$

and

$$PFE \simeq 1.58\, m_{mim} (\text{percent})$$

Spectral Effects and Different Transmitter Frequencies

Chargeabilities will vary for different pulse lengths and spectral values. In general, since M.I.M. chargeability is closely tied with phase (or perhaps more closely with the arctangent of phase), chargeabilities will tend to peak for spectral time constants that are equal to the transmitter frequency divided by 2π [5]. In other words, for $\tau = 8 \left(\tau = r^{(1/k)}\right)$ seconds the arctangent of the phase peaks at 0.02 seconds. Consequently, chargeabilities for that time constant and at transmitter frequencies of 25/512 (0.049Hz) and 25/2048 (0.012Hz) will lower than at 25/1024 Hz (0.024Hz).

Calculating chargeability ratios for different transmitter pulse lengths was a well established approach at Anaconda for gleaning useful time constant information. For transmitter frequencies

---

[2] see 'Induced Polarization As Practiced At The Anaconda Company - with insights for the present day', an internal MIM document by E.O.McAlister and M.O.Halverson, February 1997

[3] M331 (Newmont original standard) chargeability calculated as the area under the decay curve from 0 to 1.0 seconds divided by the maximum on-time voltage times 1000, for a 12 second period half-duty square wave input.

[4] A later Newmont standard calculated as the area under the decay curve from 0.45 to 1.1 seconds divide by the maximum on-time voltage *1870, for an 8 second period half-duty square wave input.

[5] see "Induced Polarization As Practiced At The Anaconda Co - with insights for the present day", MIMEX report by E.O. McAlister and M.O.Halverson, February, 1997

that are a factor of 4 or 8 different, chargeability ratios typically range from 0.5 to 1.5. Hence, differences in chargeabilities owing to changing transmitter frequencies tend to be a very diminished effect as compared with chargeability variations owing to Halverson-Wait volume loading or Cole-Cole chargeability. In other words, the differences in overall appearance of pseudosections for different pulse lengths are usually negligible.

By virtue of this time domain behaviour one should bear in mind that:

- For spectral character different than r = 1.0 and k = 0.2, the empirical conversion factors given above will not be correct. This is much the case for time-domain/time-domain conversions than time-domain/phase conversions.
- For spectral character different than r = 1.0 and k = 0.2, and averaging times different than the nominal, the normalization process is not exact - the normalized chargeabilities will not exactly reflect the true M.I.M. standard chargeabilities. This problem is worse for late start times (more than half way into the decay) and increasingly anomalous (either larger or smaller) time constants. Resulting errors in general will not exceed 10 percent.

Alternative Chargeability Calculations

Under some conditions there may be advantages to calculating chargeabilities based on alternative waveforms or duty-cycles. For example, in cases of severe EM coupling one might chose to make an impulse response based chargeability estimate (or less than 50% duty cycle) to allow chargeability calculation start times that are greater than one quarter period. An appropriate normalization scheme can be applied for most such alternative calculations that would still tend to keep us standardized on the half-duty, full area estimate.

16. Appendix IV. Mineral Title Expenditure Report for EL 27372 for the period ending 26 May 2018

17. Appendix V. Mineral Title Expenditure Report for EL 27292 for the period ending 26 May 2018.